5-24-2009

Evaluation of PBR in Breast Cancer

Stephany Shockley
Washington University in St. Louis

WASHINGTON UNIVERSITY IN ST. LOUIS

Division of Biology and Biomedical Sciences

Program in Chemical Biology

Dissertation Examination Committee:

Stephen M. Moerlein, Chair
Douglas F. Covey
J. William Harbour
Robert H. Mach
Michael J. Welch

EVALUATION OF THE PERIPHERAL BENZODIAZEPINE RECEPTOR AS A POSITRON EMISSION TOMOGRAPHY IMAGING TARGET FOR TUMOR AGGRESSION

By Stephany Elaine Shockley

A dissertation presented to the
Graduate School of Arts and Sciences
of Washington University in
partial fulfillment of the
requirements of the degree
of Doctor of Philosophy

August 2009

Saint Louis, Missouri

ABSTRACT OF THE DISSERTATION

Evaluation of the Peripheral Benzodiazepine Receptor as a Positron Emission Tomography Imaging Target for Tumor Aggression

By

Stephany Elaine Shockley

Doctor of Philosophy in Biology and Biomedical Sciences

(Chemical Biology)

Washington University in Saint Louis, 2009

Professor Stephen M. Moerlein, Advisor

The utility of Positron Emission Tomography (PET) in the detection of cancer began with the radiopharmaceutical 2-[^{18}F]fluoro-2-deoxyglucose (FDG) used for measuring altered cellular metabolism. Specific radioligands are being developed to allow non-invasive analysis of protein expression to further characterize tumors. One protein that has been identified as a promising target is the Peripheral Benzodiazepine Receptor (PBR). PBR expression is up-regulated in several cancers, and in many there has been a correlation drawn between increased malignancy and protein expression levels. Therefore, developing PET methodologies to apply for PBR imaging could be an important step in understanding individual tumors as we move toward an age of personalized medicine. This dissertation investigates the potential utility of two radioligands specific for PBR, and compares the radioligands to radiopharmaceuticals that map metabolism (FDG) and proliferation (3'-[^{18}F]fluoro-L-thymidine, FLT). The research has two specific aims: 1) to compare PBR expression with measures of cellular proliferation and aggression; 2) to directly compare radioligand localization *in vivo* to tumor sites in mouse

xenograft model studies. *In vitro* cell studies indicate a correlation between PBR expression and markers of aggression, but not proliferation. Using PET imaging and biodistribution, breast cancer xenografts with a breadth of PBR expression showed no significant uptake of PBR specific radioligands. However, radiopharmaceuticals targeting proliferation by metabolism and DNA synthesis showed greater differences in uptake between cell lines. The data obtained from these studies demonstrate a limitation to the translation of PBR imaging for personalized medicine, because the ubiquitous expression of the protein throughout the body creates challenges that will be difficult to overcome. Expression of PBR in non-target organs reduces the quantity of radiopharmaceutical that is available for tumor uptake, and the extent of non-tumor uptake of radiopharmaceuticals with affinity for PBR exceeds that of tumors. These results suggest that non-invasive imaging techniques to assay tumor PBR expression *in vivo* have limited potential for clinical applications.

ACKNOWLEDGEMENTS

During my graduate studies, I have been surrounded by many people in the Department of Radiological Sciences who have been instrumental in my accomplishments. There are far too many to acknowledge individually, however I would like to especially thank my fellow graduate students through the years as well as the post-docs who would visit our office. Peer support has been important in a way that I cannot describe for overcoming the numerous challenges which accompany the process of research and the PhD.

I would also like to thank my committee for all of their assistance. My advisor, Stephen Moerlein, and committee chair, Michael Welch, have been invaluable as resources when questions have arisen through the development of this research. Drs. Mach and Harbor have also provided valuable lab assistance.

Lastly, I would like to thank my friends and family for their encouragement and patience with me through these sometimes trying years.

TABLE OF CONTENTS

LIST OF FIGURES AND TABLES

LIST OF ABBREVIATIONS

% ID	% injected dose (of radioapharmaceutical)
% ID/cc	% injected dose (of radiopharmaceutical) per cm^3 tissue
% ID/g	% injected dose (of radiopharmaceutical) per gram tissue
ANC	Anion nucleotide carrier
BSA	Bovine serum albumin
CBR	Central benzodiazepine receptors
CNS	Central nervous system
CT	Computed Tomography
DAA1106	N-(2,5-dimethoxybenzyl)-N-(5-fluoro-2-phenoxyphenyl)acetamide
DMSO	Dimethyl sulfoxide
ECL	Enhanced chemiluminescence
ELISA	Enzyme linked immunosorbent assay (ELISA
[^{18}F]FDG	2-[^{18}F]fluoro-2-deoxyglucose
[^{18}F]FEDAA1106	N-(5-fluoro-2-phenoxyphenyl)-N-(2-[^{18}F]fluoroethyl-5-methoxybenzyl)acetamide
[^{18}F]FLT	3'-deoxy-3'-[^{18}F]fluorothymidine
[^{18}F]FMDAA1106	N-(5-fluoro-2-phenoxyphenyl)-N-(2-[^{18}F]fluoromethyl-5-methoxybenzyl)acetamide
fMRI	funtional MRI
GABA	γ-aminobutyric acid
GST	Glutathione S-transferase
HRP	Horse radish peroxidase
IBP	Isoquinoline binding protein
LOR	Line of response
MDR	Mitochondrial DBI receptor
MTS	3-(4,5-dimethylthiazol-2-yl)-5-(3-carboxymethoxyphenyl)-2-(4-sulfophenyl)-2H-tetrazolium, inner salt
MRI	Magnetic resonance imaging
MRS	Magnetic resonance spectroscopy
PBR	Peripheral benzodiazepine receptors
PET	Positron emission tomography
PBS	phosphate buffered saline PBS
PDT	Population doubling time
PK11195	1-(2-chlorophenyl)-N-methyl-N-(1-methylpropyl)-3-isoquinolinecarboxamide
PMS	Phenazine methosulfate
PMT	Photomultiplier tubes
Ro5-4864	4'-Chlorodiazepam,7-Chloro-1,3-dihydro-1-methyl-5-(p-chlorophenyl)-2H-1,4-benzodiazepin-2-one
ROI	Region of interest

SAR	Structure activity relationship
SCID	Severely compromised immunodeficient
siRNA	Small interfering RNA
SPECT	Single photon emission computed tomography
SUV	Standard uptake value
TK1	Thymidine kinase 1
TSPO	Translocator protein
TBST	Tris buffered saline with 0.05% Tween-20
VDAC	Voltage dependent anion channel

Chapter 1

Introduction

Identification of Benzodiazepine Receptors

Benzodiazepines are a class of drugs widely utilized for their anxiolytic, sedative, hypnotic and anticonvulsant effects.[1, 2] Beginning in the 1970s, there have been investigations aimed at better understanding the exact mechanisms by which these compounds mediate their actions, initially focusing on identifying their specific binding site.[3-7] Early data pointed to the glycine receptors in studies with tritiated strychnine.[3] However, γ-aminobutyric acid (GABA) association was hypothesized as an alternative, and this theory was supported by further studies.[7, 8]

In 1977, two groups simultaneously found a specific, discrete benzodiazepine binding site using synaptosomal preparations of brain homogenates.[5, 6, 9-11] Both groups reported results of binding studies using [^{3}H]diazepam (Valium®).[5, 6] They first measured the displacement of [^{3}H]diazepam in rat brain homogenates using several benzodiazepines, representing both potent and weak anxiolytic members of this class of compounds. They observed that there was a positive correlation between the displacement and predictors of therapeutic benefit. In other publications, Mohler *et al*. examined binding conditions[10] and the specific uptake and displacement in human brain homogenates.[11] Braestrup and Squires followed up with a paper that examined binding patterns and specificity, including peripheral tissues.[9] They noted that there was a fifteen-fold lower binding affinity in non-neuronal tissues, including kidney and liver, compared to the brain. They also observed a difference in the cellular localization, showing membrane binding in brain and mitochondrial binding in peripheral tissues. In displacement studies of [^{3}H]diazepam in homogenates with clonazepam (a potent anxiolytic drug) and Ro5-4864 (a benzodiazepine with no pharmacological effect), two pharmacologically distinct

benzodiazepine receptors were characterized. These two receptor types are referred to as the Central Benzodiazepine Receptors (CBR) and the Peripheral Benzodiazepine Receptors (PBR).

Benzodiazepine Receptor Pharmacology

CBRs and PBRs display distinct binding patterns. When Braestrup and Squires[9] performed binding displacement studies on brain homogenates using [^{3}H]diazepam (Figure 1A), clonazepam (Figure 1B) displayed potency, with an IC_{50} value of 5.0 nM, while Ro 5-4864 (Figure 1C) had little effect (IC_{50} value of 163 mM). When kidney, liver and lung homogenates were assayed, clonazepam potency was significantly reduced (IC_{50} values of 2.9 mM, 5.0 mM, and 7.9 mM, respectively) and Ro 5-4864 was much more potent (IC_{50} values of 4.7 nM, 4.1 nM, and 4.8 nM, respectively). Subsequently, Syapin and Skolnick utilized similar methods to investigate the potential of cultured glial cells, the C6 cell line, for the study of CBR.[12] They found that these cultured cells of neural origin unexpectedly had binding properties that mimicked kidney rather than cortex. In further investigations, PBR was found to be expressed within the central nervous system (CNS), including on glial cells and in the olfactory bulb. [13-17]

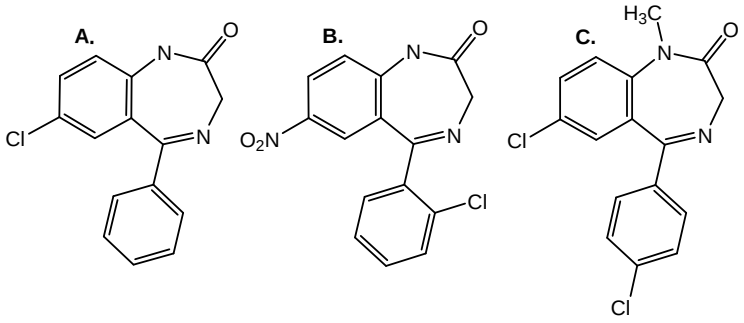

Figure 1: Structures of benzodiazepines utilized by Braestrup and Squires for receptor characterization.

Central Benzodiazepine Receptors

The identified relationship between the Central Benzodiazepine Receptor and the $GABA_A$ receptor has been extensively explored.[7, 18-25] To summarize, the $GABA_A$ receptor is a

ligand-gated ion channel and is composed of five subunits per channel to form an ion pore. CBR is a component of the $GABA_A$ complex, which includes chloride channels.[26] $GABA_A$ receptor subunits are classified as α, β, γ, δ, ε, θ, and ρ. The pentamer is composed of at least one α, at least one β, and at least one other subunit type. The α subunit is most influential for the benzodiazepine binding site. There are six isoforms (denoted by numerical subscript) of the α subunit, and it has been demonstrated that each isoform gives unique benzodiazepine pharmacology.[25, 27] Two subtypes of note are combinations of α_1,β_2, and γ_2 and α_2, β_3, and γ_2; with the former the sedative and anticonvulsant effects are seen with benzodiazepine binding, while the latter displays the anxiolytic effects.[27]

Peripheral Benzodiazepine Receptors

The peripheral benzodiazepine receptor has several alternative names in the literature. These include subtle variations such as the peripheral benzodiazepine binding site or peripheral-type benzodiazepine receptor, and attempts to rename the protein like omega (ω) receptor, mitochondrial DBI receptor (MDR) and most recently, the translocator protein (TSPO). These latter names reflect on the evolution of our understanding concerning this protein. For instance, the suggestion for renaming the benzodiazepine receptors the omega receptors (1 and 2 for CBR subtypes, and 3 for PBR) came after it was determined that other classes of compounds could bind at the site and the central nervous system contained both the GABA-associated CBR and PBR.[28] TSPO was proposed in 2006 because investigations into the roles played within the cell by PBR have yielded a list of direct and indirect involvements.[29] This work will refer to the protein by the historic name, PBR.

Ligands for PBR

The benzodiazepine Ro5-4864, utilized in the characterization of the benzodiazepine binding sites, was the first selective ligand. The isoquinoline carboxamide PK11195 (Figure 2), was developed and compared both *in vitro* and *in vivo*.[17, 30] Le Fur *et al.* found that PK11195, 1-(2-chlorophenyl)-N-methyl-N-(1-methylpropyl)-3-isoquinolinecarboxamide, could displace tritiated Ro5-4864 and matched the distribution pattern. They went on to characterize the ligand interactions, suggesting that PK11195 acts as an antagonist while Ro5-4864 is an agonist.[31]

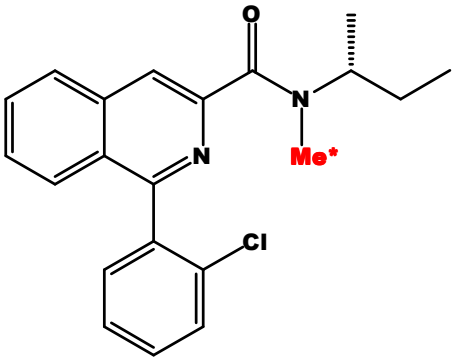

Figure 2: Structure of PBR ligand PK11195. The asterisk indicates the site of radiolabel with tritium or carbon-11.

PK11195 has emerged as the standard ligand for PBR. One important reason for this was the species variations in Ro5-4864 affinity while PK11195 had similar values across species.[32-34] Both ligands displayed a high affinity for rodent PBR, with K_D in the range of 15 nM.[17] However, Ro 5-4864 has greater variation of affinity between species,[33-36] rising to micromolar levels in human and bovine tissues,[32, 37] while the affinity of PK11195 remains below 20 nM in all species tested.[17, 32, 34, 36, 38]

Reconstitution studies in bacteria suggested an explanation for this occurrence. PK11195 binds only to an 18 kDa protein, referred to as the isoquinoline binding protein (IBP). However, Ro5-4864 was suggested to require both the 18 kDa protein and a 32 kDa protein (voltage dependent anion channel, VDAC) for binding. It was hypothesized that VDAC may have greater species variation, and this would explain the reduced affinity in some species. A third protein identified as a component in the multimer is the adenine nucleotide carrier (ANC) or

adenine nucleotide translocase (ANT), with a molecular weight of 30 kDa.[39, 40] In 1997, though, the necessity of VDAC was refuted.[41] Therefore sequence differences in IBP between species are now thought to explain the binding of Ro5-4864.[42]

Distribution and Roles of PBR

PBR is found in most tissues outside the CNS[43], and in low levels within non-neural tissues of the CNS.[12, 44, 45] Organs of expression include, but are not limited to kidney, adrenal and heart. Steroidogenic tissues have the highest expression levels.[17, 43, 46] PBR is found on macrophages and microglia.[47]

PBR is most commonly associated with the outer mitochondrial membrane[48], although it has also been isolated in the plasma membrane[49, 50] and nucleus.[51, 52] Figure 3[53] represents a simplified version of the complex as it is found *in vivo*. A variety of roles have been identified for PBR, including involvement in cell proliferation,[52, 54-58] cell respiration,[59] calcium influx[60] and steroid synthesis.[61-63]

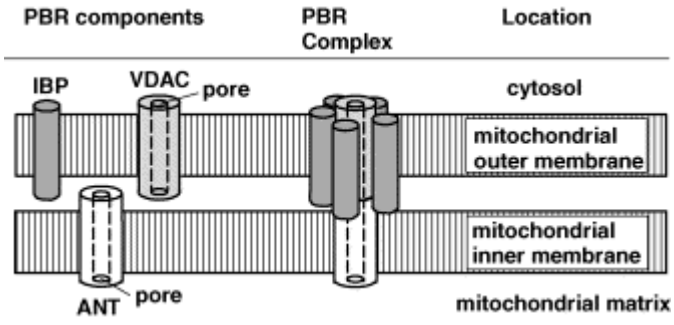

Fig. 3. The PBR complex and its protein components in the mitochondrial membrane. Figure reprinted with permission from Moshe Gavish, PhD at the Rappaport Institute, Isreal .

The 18 kDa isoquinoline binding protein has been further characterized. It has >80% sequence homology between species and is 169 amino acids.[64] The protein forms five alpha helices and inserts with the C-terminus extending into the cytoplasm while the N-terminus is

within the mitochondria.[65] Rather than exist as a trimer, with one of each subunit (IBP, ANC, VDAC), it has been suggested that multiple (2-6) IBP may be found together with ANC and VDAC.[66] It has been proposed that additional uncharacterized proteins associate to create the complete receptor structure required for each role.[64]

PBR Expression in Cancer

Investigations on the importance of PBR expression in cancer initially focused on cancers of the brain, in particular gliomas and astrocytomas. Several groups have shown that PBR levels are elevated, with ratios of 3- to 20-fold higher expression *in vitro* for tumor compared to normal brain tissue.[37, 67-72]

Peripheral benzodiazepine receptors have been shown to have elevated expression in different types of cancers, including brain cancers[37, 67-71, 73, 74], colon[75], breast[51], endometrial[76], ovary[77], prostate[78] and liver[79] cancers. It has been found that PBR expression is higher in more aggressive tumor tissues (breast, colon and prostate) and breast tumor cell lines compared to less aggressive phenotypes.[51, 80] Additionally, when low and high PBR expressing MDA-MB-231 (breast cancer) lines were compared, it was found that only the high PBR cells were able to grow and establish tumors in SCID mice.[81, 82]

In a study performed with colon cancer patients, it was found that stage III and IV tumors display similar, increased expression of PBR levels.[83] When investigators compared patient prognoses to expression levels, they found that PBR expression was an important factor in patient survival. Followed out to approximately 105 months, patients with high PBR expressing tumors had a 20% overall survival rate, compared to 80% when PBR

expression was low. Investigators have suggested that PBR overexpression contributes to tumor growth, though the specific role of PBR in cancer is not yet well understood.

An Overview of Imaging Today

Nuclear medicine techniques have developed to become cornerstones of modern medicine, but are still undergoing rapid advancement. Imaging can be utilized to gather data on physical structures of the body (anatomy) or measure cellular activities (physiology.) Computed tomography (CT) and magnetic resonance imaging (MRI) are utilized for visualizing anatomy. CT has improved in resolution and reduced acquisition time by expanding the detection field, and current clinical instruments have resolution capacities below 0.5 mm.[84] Similarly, MRI can provide high-resolution anatomical data.[85] Magnetic resonance spectroscopy (MRS) and functional MRI (fMRI) are being evaluated for their use in providing physiological data. Positron emission tomography (PET) and single photon emission computed tomography (SPECT) are widely used for a noninvasive analysis of physiology. SPECT isotopes typically are longer lived allowing for equilibrium at receptors. However SPECT instrumentation has less spatial resolution when compared to PET. The most commonly used PET isotopes require on-site production facilities. However, PET displays two very important properties: detection with PET is more sensitive and the resolution is better.[85-87] PET is considered to be the method of choice for functional imaging.

Today's clinical instruments are dual technology to incorporate the anatomical data with the functional data, such as PET/CT. By combining the information, the physiological data can be overlaid with the anatomy.[88] Utilizing these techniques, doctors are able to perform noninvasive tests toward the goal of characterizing a patient's disease.

Positron Emission Tomography

For PET studies, patients are injected with a radiopharmaceutical and imaged. The mechanism behind PET is outlined in Figure 4. The unstable nucleus of the radionuclide emits a

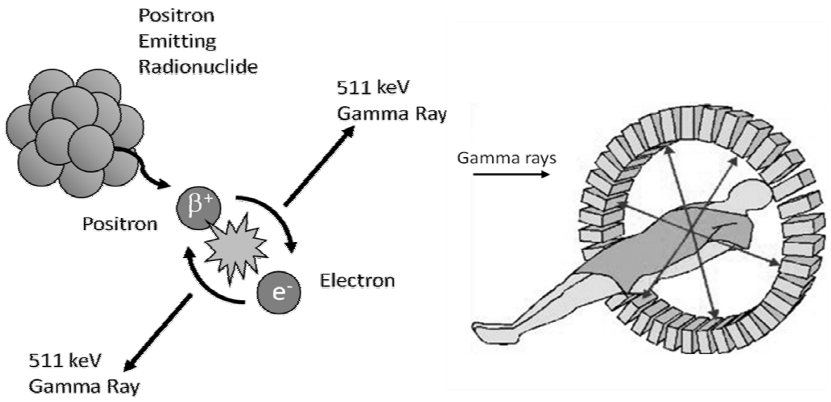

Figure 4: *A* cartoon diagram depicting the mechanism of PET. A positron is emitted from the unstable nucleus and annihilates to generate two gamma rays. The gamma rays are received by the coincidence detectors.

positron. This positron will travel a short, characteristic distance (positron range) within the tissue before an annihilation event occurs by a collision with an electron. Annihilation events result in the production of two 511 keV gamma rays approximately 180 degrees apart. The patient is surrounded by a ring of coincidence detectors, discrete scintillation crystals that absorb the photons and emit light. A line of response (LOR) forms when the two gamma rays are detected at the scintillation crystal within the narrow timeframe set as the window of coincidence, usually nanoseconds. The light emitted by the scintillation crystals is detected by the photomultiplier tubes (PMT) which converts light to photoelectrons, and amplifies the electric signal (Figure 5). Signal data is collected by computer and analyzed by algorithms to generate an image and capture the information from the study.

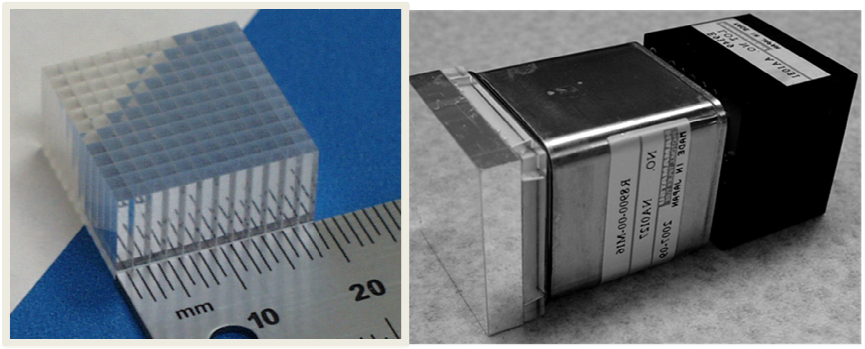

Figure 5: Images of a crystal array, demonstrating the arrangement of crystals. Crystals detect photons, resulting in light emissions. This light is transmitted into the photomultiplier tubes (PMT) that converts the light into photoelectrons and amplify the signal. Images were provided by Richard LaForest, PhD and Yuan Chan Tai, PhD at Washington University.

The first major change in PET instrumentation was in the advancements in scintillation crystals. Early instruments had sodium iodide (NaI-TI). These did not work well as the efficiency of detection for the 511 keV annihilation photons was poor. Sensitivity is measured as the percentage of the gamma rays that are actually detected. Second and third generation crystals generated from new scintillation materials have been utilized to better stop the gamma rays, improving the sensitivity.[88] This is an important improvement because high quality images requires sufficient signal detection for reconstruction, yet this must be balanced with minimal injected dose and absorbed radiation dose by the subject. Sensitivity and spatial resolution require optimization in scanner design. Sensitivity is maximized by surface area for detection. However the spatial resolution is improved by increasing the number of crystals[85], therefore reducing the surface area. Such refinements in instrumentation continue as the clinical and research applications for PET increase.

Small Animal PET

Small animal PET followed instrumentation for human imaging, but it has seen dramatic improvements. It provides an important tool for the development of radiotracers for translation into humans and also an opportunity to analyze animal models of human diseases. The spatial resolution of human scanners was insufficient for such applications. The smaller bodies and organs of the rodents being imaged required an increase in spatial resolution, without sacrificing the sensitivity.[89] Today there are scanners available with 1 mm resolution while retaining detector sensitivity.[90]

Radionuclides

A radiopharmaceutical is a compound given in trace quantities that has been labeled with a radionuclide. There are several radionuclides to choose for labeling tracers for PET. They fall into two broad categories involving covalent or ionic bonds. In the first category, such as carbon-11 and fluorine-18, the radionuclide is attached directly onto the substrate during the radiosynthesis. The other category of creating a radiopharmaceutical is utilized for metals such as copper-64 or gallium-68. Protein targeting moieties are coupled through a linker to a chelator prior to radiosynthesis. Metallic radionuclide is added, and by chelation the activity is incorporated into the molecule.

Today, the two most commonly used PET nuclides are fluorine-18 and carbon-11. Both are produced on a cyclotron and require on-site production. Carbon-11 has a half-life of 20.4 minutes, decays with emission of a positron (100%), and has maximum positron energy of 960 kEV.[91] It is produced by the $^{14}N(p,\alpha)^{11}C$ reaction on mixed target of N_2/0.5 % O_2. The bombardment generates $[^{11}C]CO_2$, which can be reduced to $[^{11}C]CH_4$ and iodinated for incorporation onto compounds as $[^{11}C]CH_3I$. At Washington University School of Medicine, the

reduction is carried out in the GE PETtrace® MeI Microlab. $[^{11}C]CO_2$ is first reduced to $[^{11}C]CH_4$ and run over an iodine column to make the final product, $[^{11}C]CH_3I$, that is transferred to reaction vessels for direct incorporation onto the substrate. Fluorine-18 has a half-life of 109.7 minutes, decays by emission of a positron (100%) with maximum positron energy of 634 keV. It can be produced by the $^{18}O(p,n)^{18}F$ reaction on isotopically enriched water ($[^{18}O]H_2O$).[91]

Fluorine-18 has properties that make it convenient to use in imaging; although both radionuclides can be used to provide useful clinical information. The longer half-life of fluorine-18 gives it a few advantages. First, radiosyntheses with fluorine-18 can be several hours long if there are reaction steps that make this necessary. When using carbon-11, syntheses must be constrained so that the isotope is incorporated and product is purified in one hour (three half-lives). Second, the use of a fluorinated radiotracer allows a longer imaging window and may be better for reaching equilibrium or maximizing target localization, depending on the tracer. Imaging sessions with fluorine-18 can extend pass two hours while carbon-11 should not be imaged past 90 minutes post-injection. However, the short half-life of $[^{11}C]$methylated tracers means that these can be used for imaging the subject successively on the same day.

Applying PET

PET provides a powerful tool for the detection and characterization of cancer. The non-invasive technique allows for ease in repetitive testing, for example as tumor response is monitored during therapy.[92, 93] A major advantage to imaging a tumor to supplement a biopsy is the limitation of biopsy from the small sample size excised. If heterogeneity is present within a tumor, imaging provides a quantifiable analysis of the whole tumor.[87] To this end, many approaches can be taken. Tracers can be designed as analogs to target a metabolic pathway, to mimic ligands and bind specific proteins, or as markers of an indicative cellular process, such as

DNA or protein synthesis.[88] The potential for ligand-targeted radiopharmaceuticals is especially broad. Proteins involved in angiogenesis[94], hypoxia[94], proliferation[95], and metastatic potential[96] are among those under investigation as cancer imaging agents. These target methods have been employed in oncological imaging with PET.

The most widely used tracer is [^{18}F]FDG, 2-[^{18}F]fluoro-2-deoxyglucose (Figure 6). [^{18}F]FDG is a fluorinated analog to glucose, and is a measure of glucose utilization. Tumor metabolism of glucose is altered from normal cells as tumor cells are rapidly dividing and therefore consuming more nutrients. [^{18}F]FDG is phosphorylated by hexokinase and trapped within the cell.[97]

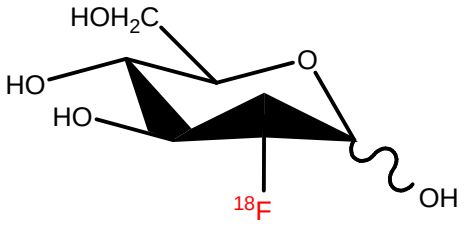

Figure 6: [^{18}F]FDG, 2-[^{18}F]fluoro-2-deoxyglucose

A second option for imaging tumors is to target DNA synthesis. This can be done by identifying cellular elements important in synthesis of the building blocks, nucleotides. Thymidine Kinase 1 (TK1) emerged as a promising target based on two ideas. Thymidine is the only nucleotide that is exclusive to DNA, and TK1 has been shown to be upregulated in cancer tissues.[98] Thymidine has been labeled with both carbon-11 and fluorine-18 as a substrate for TK1 imaging.[99, 100] When labeled with carbon-11, metabolism was found to be rapid.[101, 102] When labeled as an analog with fluorine-18 as 3'-deoxy-3'-[^{18}F]fluorothymidine (FLT) (Figure 7) however, the PET tracer displayed more promising characteristics, and has become the major means for imaging DNA synthesis.[99]

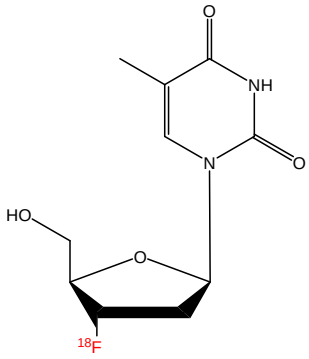

Figure 7: [^{18}F]FLT, 3'-deoxy-3'-[^{18}F]fluorothymidine

Glucose metabolism and DNA synthesis have been developed for PET imaging and provided a great deal of insight. However, problems have been observed.[88, 97] For one, [^{18}F]FDG also localizes to sites of inflammation.[103] Additionally, the relatively high glucose consumption of the brain makes tumor localization and tumor-to-background signal poor. Both [^{18}F]FDG and [^{18}F]FLT also localize to non-tumor sites in the body that have cells that are dividing rapidly, such as the gastrointestinal tract.

Ligand-specific protein interactions provide a third option for looking at proliferation. Several proteins have been identified whose increased expression correlates with tumor proliferation. As noted earlier, PBR is one such protein. An advantage to this approach is the potential of specific radiotracer uptake.[104]

Many factors must be considered in radiopharmaceutical design.[105] These compounds must possess adequate localization properties to ensure that *in vivo* distribution mimics *in vitro* uptake. Metabolic stability is very important so that the tracer is delivered intact to the cells. Secondly, the radiotracer must be able to cross the cell membrane if the target protein is intracellular. If the target is in the brain, the radiopharmaceutical must be lipophilic enough to cross the blood-brain barrier. Ligand-specific interactions present additional challenges for optimal target to non-target localization. The radioligand should have nanomolar affinity for the receptor, and to avoid receptor saturation and distribution to non-target tissues, the specific activity of the radiotracer should be as high as possible.

Peripheral Benzodiazepine Receptor Specific Ligands

Brain imaging has been the focus of PBR ligand development. Bergstrom *et al* labeled Ro5-4864 with carbon-11 and imaged patients with gliomas. As it had been shown that this ligand had reduced affinity in human tissues[32], it is not surprising that they found no uptake

above background.[106] PK11195, however, gave different results. When tritiated and analyzed by *in vivo* autoradiography, PK11195 localized to the tumor.[74, 107] Carbon-11 labeled PK11195 was then considered as a glioma imaging agent in two human studies.[108, 109] The investigators found a two-fold increase in tumor uptake compared to normal brain tissue. Pappata *et al* additionally demonstrated that the uptake was specific by giving a patient a blocking dose of PK11195 in a second imaging session. Tumor uptake was reduced and tracer was more evenly distributed, as one would expect when sites for selective uptake are blocked.[109]

In the mid-1990's a series of studies were published that brought attention to the potential utility of PBR. The first was a comparison study that measured [^{18}F]FDG uptake *in vivo* by PET and [^{3}H]PK11195 *in vitro* on excised tissue samples by autoradiography. They observed a different behavior in treated versus untreated tumor. If the patient had undergone therapy, there was no correlation between the glucose and PBR specific ligand. However, when untreated, glucose uptake correlated with PBR ligand binding.[110] In another experiment, an *in vitro* binding study was performed on patient samples representing a range of glioma grade, and binding of [^{3}H]PK11195 was found to be elevated in high grade tumors.[71, 111] Investigations of neuroinflammatory diseases such as Alzheimer's Disease[112] and Multiple Sclerosis[113] were also performed with PET and [^{11}C]PK11195. Distribution was heterogeneous and indicated that the tracer was localizing to sites of inflammation within the brain. These data encouraged the development of novel ligands for PBR in nuclear imaging.

In the last decade several new compounds have been synthesized.[114, 115] PK11195 and Ro5-4864 have been used as a lead compounds in the synthesis of these derivatives. Preclinical evaluations of these ligands continue since PBR is a protein marker and imaging target in cancer and inflammation. To date, PK11195 remains the standard to which all others are compared.[116]

The class of ligands phenoxyphenyl-acetamide derivatives appears to hold great potential. In 1999, Taisho Pharmaceutical Company published a report identifying ligand DAA1106, N-(2,5-dimethoxybenzyl)-N-(5-fluoro-2-phenoxyphenyl)acetamide, which displayed selectivity and increased affinity for PBR.[117] They found that the compound inhibited [^{3}H]PK11195 and [^{3}H]Ro5-4864 binding at PBR with concentrations of less than one nanomolar, while flunitrazam binding to CBR was not affected. Additionally, they used [^{3}H]DAA1106 to characterize binding, calculating affinity mitochondrial values of 0.12±0.03 nM.[118] Autoradiography in rat brain demonstrated that [^{3}H]DAA1106 corresponded to [^{3}H]PK11195 localization, and DAA1106 behaves as a receptor antagonist.[119]

To create a PET tracer, [^{11}C]DAA1106 (Figure 8) was synthesized by *O*-methylation with [^{11}C]CH_3I and characterized.[120] In biodistribution data, the tracer showed uptake in PBR-expressing tissues, including lung and adrenals. Permeability of the blood-brain barrier was found to exceed that of [^{11}C]PK11195. The radiotracer remained intact in brain. However, in serum the radiotracer was rapidly metabolized, and only 20% of the tracer was intact at 15 minutes post-injection.

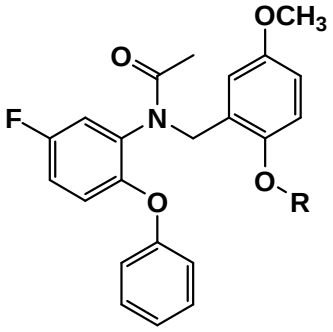

[^{11}C]DAA1106 R=$^{11}CH_3$
[^{18}F]FMDAA1106 R=$CH_2{}^{18}F$
[^{18}F]FEDAA1106 R=$C_2H_4{}^{18}F$

Figure 8: Structures of PET analogs of DAA1106

The ligand [^{11}C]DAA1106 has been examined in animal models as well as non-human primate models and human patients with neuroinflammation. Four rat models of brain injury to simulate neuroinflammation were used to look at DAA1106 distribution. [^{11}C]DAA1106 uptake was detected at the sites of injury.[121-124] In two of these studies, uptake of [^{11}C]DAA1106 was compared to [^{11}C]PK11195, and found to be better at localizing to the site of injury.[122, 123] Brain uptake in normal monkey was measured by PET, and specific uptake was seen in the occipital

cortex. Comparing [^{11}C]DAA1106 and [^{11}C]PK11195, DAA1106 was four times higher at 30 minutes post injection in the occipital cortex, and displaced when a blocking dose was administered. [124] Finally, in a small study early stage Alzheimer's Disease patients were compared to age matched controls. [^{11}C]DAA1106 uptake was increased in several regions, suggesting that the ligand may provide a sensitive measure of neuroinflammation.

Fluorinated derivatives were developed to utilize the improved radionuclide properties of fluorine-18. [^{18}F]FMDAA1106, N-(5-fluoro-2-phenoxyphenyl)-N-(2-[^{18}F]fluoromethyl-5-methoxybenzyl)acetamide, and [^{18}F]FEDAA1106, N-(5-fluoro-2-phenoxyphenyl)-N-(2-[^{18}F]fluoroethyl-5-methoxybenzyl)acetamide, (Figure 8) were derived from DAA1106 to create longer-lived tracers.[125] [^{18}F]FEDAA1106 displayed improved specificity for PBR and was not metabolized in rat brain. [^{18}F]FMDAA1106 bound similarly to DAA1106 but was metabolized in the brain. The authors studied these tracers in further detail using biodistribution and PET in normal monkey brain.[126] [^{18}F]FMDAA1106 defluorinated over the course of the study, while [^{18}F]FEDAA1106 did not. [^{18}F]FEDAA1106 displayed improved stability in mouse serum, with almost 40% intact at 15 minutes, while [^{18}F]FMDAA1106 was rapidly metabolized. Metabolite analysis with monkey plasma showed that [^{18}F]FEDAA1106 was more stable than mouse serum (56% vs. 30% at 30 minutes). In the biodistribution study, uptake was greater in PBR-expressing organs, with highest uptake in the lungs as seen with [^{11}C]DAA1106. The longer lived half-life, coupled with the increased affinity for PBR and metabolic stability suggest that [^{18}F]FEDAA1106 may be a useful, improved PET ligand for PBR.

Summary

The Peripheral Benzodiazepine Receptor presents an interesting target for characterization of tumors and inflammation. In recent years understanding of PBR has evolved and encouraged the development of radiopharmaceuticals for non-invasive detection of this biomarker. While PBR upregulation has been noted throughout the body, to date the focus of imaging applications has concerned applications in the CNS.

This dissertation will examine the potential of imaging PBR sites in locations outside of the CNS. The investigation will examine cell culture studies using proliferation and malignancy, and evaluate potential correlations with PBR expression. *In vivo* localization of radioligands specific to PBR will be evaluated in rodents and compared to established biomarkers for tumor metabolism and DNA synthesis. The study examines PBR expression in tumors and concludes with a comprehensive evaluation of the utility of PBR as a target site for oncological PET imaging.

BIBLIOGRAPHY

1. Kelly, D., Anxiety and drug therapy. *Proc R Soc Med* **1973,** 66, (3), 252-5.

2. Hoffman, E. J.; Mathew, S. J., Anxiety disorders: a comprehensive review of pharmacotherapies. *Mt Sinai J Med* **2008,** 75, (3), 248-62.

3. Young, A. B.; Zukin, S. R.; Snyder, S. H., Interaction of benzodiazepines with central nervous glycine receptors: possible mechanism of action. *Proc Natl Acad Sci U S A* **1974,** 71, (6), 2246-50.

4. Costa, E.; Guidotti, A.; Mao, C. C.; Suria, A., New concepts on the mechanism of action of benzodiazepines. *Life Sci* **1975,** 17, (2), 167-85.

5. Squires, R. F.; Brastrup, C., Benzodiazepine receptors in rat brain. *Nature* **1977,** 266, (5604), 732-4.

6. Mohler, H.; Okada, T., Benzodiazepine receptor: demonstration in the central nervous system. *Science* **1977,** 198, (4319), 849-51.

7. Costa, E.; Guidotti, A., Molecular mechanisms in the receptor action of benzodiazepines. *Annual Review of Pharmacology and Toxicology* **1979,** 19, 531-45.

8. Costa, E.; Guidotti, A.; Mao, C. C., Evidence for involvement of GABA in the action of benzodiazepines: studies on rat cerebellum. *Adv Biochem Psychopharmacol* **1975**, (14), 113-30.

9. Braestrup, C.; Squires, R. F., Specific benzodiazepine receptors in rat brain characterized by high-affinity [3H]-diazepam binding. *Proceedings of the National Academy of Sciences of the United States of America* **1977,** 74, (9), 3805-9.

10. Mohler, H.; Okada, T., Properties of 3H-diazepam binding to benzodiazepine receptors in rat cerebral cortex. *Life Sci* **1977,** 20, (12), 2101-10.

11. Mohler, H.; Okada, T.; Heitz, P.; Ulrich, J., Biochemical identification of the site of action of benzodiazepines in human brain by 3H-diazepam binding. *Life Sci* **1978,** 22, (11), 985-95.

12. Syapin, P. J.; Skolnick, P., Characterization of benzodiazepine binding sites in cultured cells of neural origin. *Journal of Neurochemistry* **1979,** 32, (3), 1047-51.

13. Marangos, P. J.; Patel, J.; Boulenger, J. P.; Clark-Rosenberg, R., Characterization of peripheral-type benzodiazepine binding sites in brain using [3H]Ro 5-4864. *Mol Pharmacol* **1982,** 22, (1), 26-32.

14. Schoemaker, H.; Boles, R. G.; Horst, W. D.; Yamamura, H. I., Specific high-affinity binding sites for [3H]Ro 5-4864 in rat brain and kidney. *J Pharmacol Exp Ther* **1983,** 225, (1), 61-9.

15. Talwar, D.; Sher, P. K., Benzodiazepine receptor development in murine glial cultures. *Dev Neurosci* **1987,** 9, (3), 183-9.

16. Doble, A.; Malgouris, C.; Daniel, M.; Daniel, N.; Imbault, F.; Basbaum, A.; Uzan, A.; Gueremy, C.; Le Fur, G., Labelling of peripheral-type benzodiazepine binding sites in human

brain with [3H]PK 11195: anatomical and subcellular distribution. *Brain Res Bull* **1987,** 18, (1), 49-61.

17. Le Fur, G.; Perrier, M. L.; Vaucher, N.; Imbault, F.; Flamier, A.; Benavides, J.; Uzan, A.; Renault, C.; Dubroeucq, M. C.; Gueremy, C., Peripheral benzodiazepine binding sites: effect of PK 11195, 1-(2-chlorophenyl)-N-methyl-N-(1-methylpropyl)-3-isoquinolinecarboxamide. I. In vitro studies. *Life Sciences* **1983,** 32, (16), 1839-47.

18. Kozhechkin, S. N., Benzodiazepines are synergic with gamma-aminobutyric acid. Microiontophoretic evidence. *Ann Ist Super Sanita* **1978,** 14, (1), 139-46.

19. Tallman, J. F.; Thomas, J. W.; Gallager, D. W., GABAergic modulation of benzodiazepine binding site sensitivity. *Nature* **1978,** 274, (5669), 383-5.

20. Bertilsson, L., Mechanism of action of benzodiazepines - the GABA hypothesis. *Acta Psychiatr Scand Suppl* **1978**, (274), 19-26.

21. Gallager, D. W.; Mallorga, P.; Thomas, J. W.; Tallman, J. F., GABA-benzodiazepine interactions: physiological, pharmacological and developmental aspects. *Fed Proc* **1980,** 39, (12), 3043-9.

22. Haefely, W. E., Central actions of benzodiazepines: general introduction. *Br J Psychiatry* **1978,** 133, 231-8.

23. Meldrum, B., Pharmacology of GABA. *Clin Neuropharmacol* **1982,** 5, (3), 293-316.

24. Olsen, R. W., GABA-benzodiazepine-barbiturate receptor interactions. *J Neurochem* **1981,** 37, (1), 1-13.

25. Barnard, E. A.; Skolnick, P.; Olsen, R. W.; Mohler, H.; Sieghart, W.; Biggio, G.; Braestrup, C.; Bateson, A. N.; Langer, S. Z., International Union of Pharmacology. XV. Subtypes of gamma-aminobutyric acidA receptors: classification on the basis of subunit structure and receptor function. *Pharmacol Rev* **1998,** 50, (2), 291-313.

26. Macdonald, R. L.; Olsen, R. W., GABAA receptor channels. *Annu Rev Neurosci* **1994,** 17, 569-602.

27. Mohler, H., GABA(A) receptor diversity and pharmacology. *Cell Tissue Res* **2006,** 326, (2), 505-16.

28. Langer, S. Z.; Arbilla, S., Limitations of the benzodiazepine receptor nomenclature: a proposal for a pharmacological classification as omega receptor subtypes. *Fundam Clin Pharmacol* **1988,** 2, (3), 159-70.

29. Papadopoulos, V.; Baraldi, M.; Guilarte, T. R.; Knudsen, T. B.; Lacapere, J. J.; Lindemann, P.; Norenberg, M. D.; Nutt, D.; Weizman, A.; Zhang, M. R.; Gavish, M., Translocator protein (18kDa): new nomenclature for the peripheral-type benzodiazepine receptor based on its structure and molecular function. *Trends Pharmacol Sci* **2006,** 27, (8), 402-9.

30. Le Fur, G.; Guilloux, F.; Rufat, P.; Benavides, J.; Uzan, A.; Renault, C.; Dubroeucq, M. C.; Gueremy, C., Peripheral benzodiazepine binding sites: effect of PK 11195, 1-(2-chlorophenyl)-N-

methyl-(1-methylpropyl)-3 isoquinolinecarboxamide. II. In vivo studies. *Life Sciences* **1983,** 32, (16), 1849-56.

31. Le Fur, G.; Vaucher, N.; Perrier, M. L.; Flamier, A.; Benavides, J.; Renault, C.; Dubroeucq, M. C.; Gueremy, C.; Uzan, A., Differentiation between two ligands for peripheral benzodiazepine binding sites, [3H]RO5-4864 and [3H]PK 11195, by thermodynamic studies. *Life Sci* **1983,** 33, (5), 449-57.

32. Awad, M.; Gavish, M., Binding of [3H]Ro 5-4864 and [3H]PK 11195 to cerebral cortex and peripheral tissues of various species: species differences and heterogeneity in peripheral benzodiazepine binding sites. *Journal of Neurochemistry* **1987,** 49, (5), 1407-14.

33. Eshleman, A. J.; Murray, T. F., Differential binding properties of the peripheral-type benzodiazepine ligands [3H]PK 11195 and [3H]Ro 5-4864 in trout and mouse brain membranes. *Journal of Neurochemistry* **1989,** 53, (2), 494-502.

34. Gavish, M.; Katz, Y.; Bar-Ami, S.; Weizman, R., Biochemical, physiological, and pathological aspects of the peripheral benzodiazepine receptor. *Journal of Neurochemistry* **1992,** 58, (5), 1589-601.

35. Basile, A. S.; Klein, D. C.; Skolnick, P., Characterization of benzodiazepine receptors in the bovine pineal gland: evidence for the presence of an atypical binding site. *Molecular Brain Research* **1986,** 1, (2), 127-35.

36. Awad, M.; Gavish, M., Peripheral-type benzodiazepine receptors in human cerebral cortex, kidney, and colon. *Life Sciences* **1991,** 49, (16), 1155-61.

37. Broaddus, W. C.; Bennett, J. P., Jr., Peripheral-type benzodiazepine receptors in human glioblastomas: pharmacologic characterization and photoaffinity labeling of ligand recognition site. *Brain research* **1990,** 518, (1-2), 199-208.

38. Escubedo, E.; Camins, A.; Tresserra, F.; Adzet, T.; Camarasa, J., Peripheral-type benzodiazepine receptors in human prostate. *Pharmacology* **1993,** 46, (2), 115-20.

39. Garnier, M.; Dimchev, A. B.; Boujrad, N.; Price, J. M.; Musto, N. A.; Papadopoulos, V., In vitro reconstitution of a functional peripheral-type benzodiazepine receptor from mouse Leydig tumor cells. *Molecular Pharmacology* **1994,** 45, (2), 201-11.

40. McEnery, M. W.; Snowman, A. M.; Trifiletti, R. R.; Snyder, S. H., Isolation of the mitochondrial benzodiazepine receptor: association with the voltage-dependent anion channel and the adenine nucleotide carrier. *Proceedings of the National Academy of Sciences of the United States of America* **1992,** 89, (8), 3170-4.

41. Joseph-Liauzun, E.; Farges, R.; Delmas, P.; Ferrara, P.; Loison, G., The Mr 18,000 subunit of the peripheral-type benzodiazepine receptor exhibits both benzodiazepine and isoquinoline carboxamide binding sites in the absence of the voltage-dependent anion channel or of the adenine nucleotide carrier. *J Biol Chem* **1997,** 272, (44), 28102-6.

42. Parola, A. L.; Stump, D. G.; Pepperl, D. J.; Krueger, K. E.; Regan, J. W.; Laird, H. E., 2nd, Cloning and expression of a pharmacologically unique bovine peripheral-type benzodiazepine receptor isoquinoline binding protein. *J Biol Chem* **1991,** 266, (21), 14082-7.

43. Anholt, R. R. H.; De Souza, E. B.; Oster-Granite, M. L.; Snyder, S. H., Peripheral-type benzodiazepine receptors: autoradiographic localization in whole-body sections of neonatal rats. *Journal of Pharmacology and Experimental Therapeutics* **1985,** 233, (2), 517-26.

44. Schoemaker, H.; Bliss, M.; Yamamura, H. I., Specific high-affinity saturable binding of [3H] R05-4864 to benzodiazepine binding sites in the rat cerebral cortex. *European Journal of Pharmacology* **1981,** 71, (1), 173-5.

45. Marangos, P.; Patel, J.; Boulenger, J.; Clark-Rosenberg, R., Characterization of peripheral-type benzodiazepine binding sites in brain using [3H]Ro 5-4864. *Molecular Pharmacology* **1982,** 22, (1), 26-32.

46. De Souza, E.; Anholt, R.; Murphy, K.; Snyder, S.; Kuhar, M., Peripheral-type benzodiazepine receptors in endocrine organs: autoradiographic localization in rat pituitary, adrenal, and testis. *Endocrinology* **1985,** 116, (2), 567-573.

47. Benavides, J.; Dubois, A.; Gotti, B.; Bourdiol, F.; Scatton, B., Cellular distribution of omega 3 (peripheral type benzodiazepine) binding sites in the normal and ischaemic rat brain: an autoradiographic study with the photoaffinity ligand [3H]PK 14105. *Neurosci Lett* **1990,** 114, (1), 32-8.

48. Anholt, R. R. H.; Pedersen, P. L.; DeSouza, E. B.; Snyder, S. H., The peripheral-type benzodiazepine receptor. Localization to the mitochondrial outer membrane. *Journal of Biological Chemistry* **1986,** 261, (2), 576-83.

49. O'Beirne, G. B.; Woods, M. J.; Williams, D. C., Two subcellular locations for peripheral-type benzodiazepine acceptors in rat liver. *European journal of biochemistry / FEBS* **1990,** 188, (1), 131-8.

50. Olson, J. M. M.; Ciliax, B. J.; Mancini, W. R.; Young, A. B., Presence of peripheral-type benzodiazepine binding sites on human erythrocyte membranes. *European Journal of Pharmacology* **1988,** 152, (1-2), 47-53.

51. Hardwick, M.; Fertikh, D.; Culty, M.; Li, H.; Vidic, B.; Papadopoulos, V., Peripheral-type benzodiazepine receptor (PBR) in human breast cancer: correlation of breast cancer cell aggressive phenotype with PBR expression, nuclear localization, and PBR-mediated cell proliferation and nuclear transport of cholesterol. *Cancer Research* **1999,** 59, (4), 831-842.

52. Brown, R. C.; Degenhardt, B.; Kotoula, M.; Papadopoulous, V., Location-dependent role of the human glioma cell peripheral-type benzodiazepine receptor in proliferation and steroid biosynthesis. *Cancer Letters* **2000,** 156, (2), 125-32.

53. Veenman, L.; Levin, E.; Weisinger, G.; Leschiner, S.; Spanier, I.; Snyder, S. H.; Weizman, A.; Gavish, M., Peripheral-type benzodiazepine receptor density and in vitro tumorigenicity of glioma cell lines. *Biochem Pharmacol* **2004,** 68, (4), 689-98.

54. Wang, J.; Morgan, J.; Spector, S., Benzodiazepines that bind at peripheral sites inhibit cell proliferation. *Proceedings of the National Academy of Sciences of the United States of America* **1984,** 81, (3), 753-756.

55. Carmel, I.; Fuad, F.; Leschiner, S.; Scheruebl, H.; Weisinger, G.; Gavish, M., Peripheral-type benzodiazepine receptors in the regulation of proliferation of MCF-7 human breast carcinoma cell line. *Biochemical Pharmacology* **1999,** 58, 273-78.

56. Beinlich, A.; Strohmeier, R.; Kaufmann, M.; Kuhl, H., Relation of cell proliferation to expression of peripheral benzodiazepine receptors in human breast cancer cell lines. *Biochemical Pharmacology* **2000,** 60, (3), 397-402.

57. Beinlich, A.; Strohmeier, R.; Kaufmann, M.; Kuhl, H., Specific binding of benzodiazepines to human breast cancer cell lines. *Life Sciences* **1999,** 65, (20), 2099-2108.

58. Li, W.; Hardwick, M.; Rosenthal, D.; Culty, M.; Papadopoulos, V., Peripheral-type benzodiazepine receptor overexpression and knockdown in human breast cancer cells indicate its prominent role in tumor cell proliferation. *Biochemical Pharmacology* **2007,** 73, (4), 491-503.

59. Hirsch, J.; Beyer, C.; Malkowitz, L.; Beer, B.; Blume, A. J., Mitochondrial benzodiazepine receptors mediate inhibition of mitochondrial respiratory control. *Molecular Pharmacology* **1989,** 35, (1), 157-63.

60. Python, C.; Rossier, M.; Vallotton, M.; Capponi, A., Peripheral-type benzodiazepines inhibit calcium channels and aldosterone production in adrenal glomerulosa cells. *Endocrinology* **1993,** 132, (4), 1489-96.

61. Krueger, K.; Papadopoulos, V., Peripheral-type benzodiazepine receptors mediate translocation of cholesterol from outer to inner mitochondrial membranes in adrenocortical cells. *Journal of Biological Chemistry* **1990,** 265, (25), 15015-22.

62. Papadopoulos, V.; Brown, A., Role of peripheral-type benzodiazepine receptor and the polypeptide diazepam binding inhibitor in steroidogenesis. *Journal of Steroid Biochemistry and Molecular Biology* **1995,** 53, (1-6), 103-10.

63. Papadopoulos, V.; Widmaier, E.; Amri, H.; Zilz, A.; Li, H.; Culty, M.; Castello, R.; Philip, G.; Sridaran, R.; Drieu, K., In vivo studies on the role of the peripheral benzodiazepine receptor (PBR) in steroidogenesis. *Endocrine Research* **1998,** 24, (3-4), 479-87.

64. Papadopoulos, V., Structure and function of the peripheral-type benzodiazepine receptor in steroidogenic cells. *Proceedings of the Society for Experimental Biology and Medicine* **1998,** 217, (2), 130-42.

65. Culty, M.; Li, H.; Boujrad, N.; Amri, H.; Vidic, B.; Bernassau, J. M.; Reversat, J. L.; Papadopoulos, V., In vitro studies on the role of the peripheral-type benzodiazepine receptor in steroidogenesis. *J Steroid Biochem Mol Biol* **1999,** 69, (1-6), 123-30.

66. Papadopoulos, V.; Boujrad, N.; Ikonomovic, M. D.; Ferrara, P.; Vidic, B., Topography of the Leydig cell mitochondrial peripheral-type benzodiazepine receptor. *Mol Cell Endocrinol* **1994,** 104, (1), R5-9.

67. Black, K. L.; Ikezaki, K.; Toga, A. W., Imaging of brain tumors using peripheral benzodiazepine receptor ligands. *Journal of Neurosurgery* **1989,** 71, (1), 113-8.

68. Ferrarese, C.; Appollonio, I.; Frigo, M.; Gaini, S. M.; Piolti, R.; Frattola, L., Benzodiazepine receptors and diazepam-binding inhibitor in human cerebral tumors. *Annals of Neurology* **1989,** 26, (4), 564-8.

69. Black, K. L.; Ikezaki, K.; Santori, E.; Becker, D. P.; Vinters, H. V., Specific high-affinity binding of peripheral benzodiazepine receptor ligands to brain tumors in rat and man. *Cancer* **1990,** 65, (1), 93-7.

70. Takada, A.; Mitsuka, S.; Diksic, M.; Yamamoto, Y. L., Autoradiographic study of peripheral benzodiazepine receptors in animal brain tumor models and human gliomas. *European Journal of Pharmacology* **1992,** 228, (2-3), 131-9.

71. Miyazawa, N.; Hamel, E.; Diksic, M., Assessment of the peripheral benzodiazepine receptors in human gliomas by two methods. *Journal of Neuro-oncology* **1998,** 38, (1), 19-26.

72. Cornu, P.; Benavides, J.; Scatton, B.; Hauw, J.; Philippon, J., Increase in omega 3 (peripheral-type benzodiazepine) binding site densities in different types of human brain tumours. A quantitative autoradiography study. *Acta Neurochirurgica* **1992,** 119, (1-4), 146-52.

73. Miettinen, H.; Kononen, J.; Haapasalo, H.; Hel.acte.en, P.; Sallinen, P.; Harjuntausta, T.; Helin, H.; Alho, H., Expression of peripheral-type benzodiazepine receptor and diazepam binding inhibitor in human astrocytomas: relationship to cell proliferation. *Cancer Research* **1995,** 55, (12), 2691-5.

74. Starosta-Rubinstein, S.; Ciliax, B. J.; Penney, J. B.; McKeever, P.; Young, A. B., Imaging of a glioma using peripheral benzodiazepine receptor ligands. *Proceedings of the National Academy of Sciences of the United States of America* **1987,** 84, (3), 891-5.

75. Katz, Y.; Eitan, A.; Gavish, M., Increase in peripheral benzodiazepine binding sites in colonic adenocarcinoma. *Oncology* **1990,** 47, (2), 139-42.

76. Batra, S.; Iosif, C., Peripheral benzodiazepine receptor in human endomentrium and endometrial carcinoma. *Anticancer Research* **2000,** 20, 463-6.

77. Katz, Y.; Ben-Baruch, G.; Kloog, Y.; Menczer, J.; Gavish, M., Increased density of peripheral benzodiazepine-binding sites in ovarian carcinomas as compared with benign ovarian tumours and normal ovaries. *Clinical Science* **1990,** 78, (2), 155-8.

78. Batra, S.; Alenfall, J., Characterization of peripheral benzodiazepine receptors in rat prostatic adenocarcinoma. *Prostate* **1994,** 24, (5), 269-78.

79. Venturini, I.; Zeneroli, M. L.; Corsi, L.; Avallone, R.; Farina, F.; Alho, H.; Baraldi, C.; Ferrarese, C.; Pecora, N.; Frigo, M.; Ardizzone, G.; Arrigo, A.; Pellicci, R.; Baraldi, M., Up-regulation of peripheral benzodiazepine receptor system in hepatocellular carcinoma. *Life Sciences* **1998,** 63, (14), 1269-1280.

80. Han, Z.; Slack, R.; Li, W.; Papadopoulos, V., Expression of peripheral benzodiazepine receptor (PBR) in human tumors: relationship to breast, colorectal, and prostate tumor progression. *Journal of Receptors and Signal Transduction* **2003,** 23, (2&3), 225-38.

81. Hardwick, M.; Rone, J.; Han, Z.; Haddad, B.; Papadopoulos, V., Peripheral-type benzodiazepine receptor levels correlate with the ability of human breast cancer MDA-MB-231 cell line to grow in SCID mice. *International Journal of Cancer* **2001,** 94, (3), 322-7.

82. Sanger, N.; Strohmeier, R.; Kaufmann, M.; Kuhl, H., Cell cycle-related expression and ligand binding of peripheral benzodiazepine receptor in human breast cancer cell lines. *European Journal of Cancer* **2000,** 36, (16), 2157-2163.

83. Maaser, K.; Grabowski, P.; Sutter, A. P.; Hoepfner, M.; Foss, H.-D.; Stein, H.; Berger, G.; Gavish, M.; Zeitz, M.; Scheruebl, H., Overexpression of the peripheral benzodiazepine receptor is a relevant prognostic factor in stage III colorectal cancer. *Clinical Cancer Research* **2002,** 8, (10), 3205-3209.

84. Rogalla, P.; Kloeters, C.; Hein, P. A., CT technology overview: 64-slice and beyond. *Radiol Clin North Am* **2009,** 47, (1), 1-11.

85. Pichler, B. J.; Wehrl, H. F.; Judenhofer, M. S., Latest advances in molecular imaging instrumentation. *J Nucl Med* **2008,** 49 Suppl 2, 5S-23S.

86. Rahmim, A.; Zaidi, H., PET versus SPECT: strengths, limitations and challenges. *Nucl Med Commun* **2008,** 29, (3), 193-207.

87. Van Den Bossche, B.; Van de Wiele, C., Receptor imaging in oncology by means of nuclear medicine: current status. *J Clin Oncol* **2004,** 22, (17), 3593-607.

88. Mittra, E.; Quon, A., Positron emission tomography/computed tomography: the current technology and applications. *Radiol Clin North Am* **2009,** 47, (1), 147-60.

89. Myers, R.; Hume, S., Small animal PET. *Eur Neuropsychopharmacol* **2002,** 12, (6), 545-55.

90. Rowland, D. J.; Cherry, S. R., Small-animal preclinical nuclear medicine instrumentation and methodology. *Semin Nucl Med* **2008,** 38, (3), 209-22.

91. Shirley, V. S., *Table of Isotopes* Eighth ed.; 1996; Vol. 1.

92. Pio, B. S.; Park, C. K.; Pietras, R.; Hsueh, W. A.; Satyamurthy, N.; Pegram, M. D.; Czernin, J.; Phelps, M. E.; Silverman, D. H., Usefulness of 3'-[F-18]fluoro-3'-deoxythymidine with positron emission tomography in predicting breast cancer response to therapy. *Mol Imaging Biol* **2006,** 8, (1), 36-42.

93. Mankoff, D. A.; Eary, J. F., Proliferation imaging to measure early cancer response to targeted therapy. *Clin Cancer Res* **2008,** 14, (22), 7159-60.

94. Charnley, N.; Donaldson, S.; Price, P., Imaging angiogenesis. *Methods Mol Biol* **2009,** 467, 25-51.

95. Mankoff, D. A.; Shields, A. F.; Krohn, K. A., PET imaging of cellular proliferation. *Radiol Clin North Am* **2005,** 43, (1), 153-67.

96. Winnard, P. T., Jr.; Pathak, A. P.; Dhara, S.; Cho, S. Y.; Raman, V.; Pomper, M. G., Molecular imaging of metastatic potential. *J Nucl Med* **2008,** 49 Suppl 2, 96S-112S.

97. Fass, L., Imaging and cancer: a review. *Mol Oncol* **2008,** 2, (2), 115-52.

98. Broet, P.; Romain, S.; Daver, A.; Ricolleau, G.; Quillien, V.; Rallet, A.; Asselain, B.; Martin, P. M.; Spyratos, F., Thymidine kinase as a proliferative marker: clinical relevance in 1,692 primary breast cancer patients. *J Clin Oncol* **2001,** 19, (11), 2778-87.

99. Shields, A. F.; Grierson, J. R.; Dohmen, B. M.; Machulla, H. J.; Stayanoff, J. C.; Lawhorn-Crews, J. M.; Obradovich, J. E.; Muzik, O.; Mangner, T. J., Imaging proliferation in vivo with [F-18]FLT and positron emission tomography. *Nat Med* **1998,** 4, (11), 1334-6.

100. Christman, D.; Crawford, E. J.; Friedkin, M.; Wolf, A. P., Detection of DNA synthesis in intact organisms with positron-emitting (methyl- 11 C)thymidine. *Proc Natl Acad Sci U S A* **1972,** 69, (4), 988-92.

101. Shields, A. F.; Grierson, J. R.; Kozawa, S. M.; Zheng, M., Development of labeled thymidine analogs for imaging tumor proliferation. *Nucl Med Biol* **1996,** 23, (1), 17-22.

102. Shields, A. F.; Mankoff, D.; Graham, M. M.; Zheng, M.; Kozawa, S. M.; Link, J. M.; Krohn, K. A., Analysis of 2-carbon-11-thymidine blood metabolites in PET imaging. *J Nucl Med* **1996,** 37, (2), 290-6.

103. van Waarde, A.; Elsinga, P. H., Proliferation markers for the differential diagnosis of tumor and inflammation. *Curr Pharm Des* **2008,** 14, (31), 3326-339.

104. Haubner, R.; Wester, H. J., Radiolabeled tracers for imaging of tumor angiogenesis and evaluation of anti-angiogenic therapies. *Curr Pharm Des* **2004,** 10, (13), 1439-55.

105. Kilbourn, M. R.; Zalutsky, M. R., Research and clinical potential of receptor based radiopharmaceuticals. *J Nucl Med* **1985,** 26, (6), 655-62.

106. Bergstrom, M.; Mosskin, M.; Ericson, K.; Ehrin, E.; Thorell, J. O.; von Holst, H.; Noren, G.; Persson, A.; Halldin, C.; Stone-Elander, S., Peripheral benzodiazepine binding sites in human gliomas evaluated with positron emission tomography. *Acta radiologica. Supplementum* **1986,** 369, 409-11.

107. Dubois, A.; Benavides, J.; Peny, B.; Duverger, D.; Fage, D.; Gotti, B.; MacKenzie, E. T.; Scatton, B., Imaging of primary and remote ischaemic and excitotoxic brain lesions. An autoradiographic study of peripheral type benzodiazepine binding sites in the rat and cat. *Brain Res* **1988,** 445, (1), 77-90.

108. Junck, L.; Olson, J. M.; Ciliax, B. J.; Koeppe, R. A.; Watkins, G. L.; Jewett, D. M.; McKeever, P. E.; Wieland, D. M.; Kilbourn, M. R.; Starosta-Rubinstein, S., PET imaging of human gliomas with ligands for the peripheral benzodiazepine binding site. *Annals of Neurology* **1989,** 26, (6), 752-8.

109. Pappata, S.; Cornu, P.; Samson, Y.; Prenant, C.; Benavides, J.; Scatton, B.; Crouzel, C.; Hauw, J.; Syrota, A., PET study of carbon-11-PK 11195 binding to peripheral type benzodiazepine sites in glioblastoma: a case report. *Journal of Nuclear Medicine* **1991,** 32, (8), 1608-10.

110. Ferrarese, C.; Pierpaoli, C.; Linfante, I.; Bobo, R.; Guthrie, B.; Kufta, C.; Duhaney, M.; Melisi, J.; Fulham, M., Peripheral benzodiazepine receptors and glucose metabolism in human gliomas. *Journal of Neuro-oncology* **1994,** 22, (1), 15-22.

111. Miettinen, H.; Kononen, J.; Haapasalo, H.; Helén, P.; Sallinen, P.; Harjuntausta, T.; Helin, H.; Alho, H., Expression of peripheral-type benzodiazepine receptor and diazepam binding inhibitor in human astrocytomas: relationship to cell proliferation. *Cancer Research* **1995,** 55, (12), 2691-2695.

112. Groom, G. N.; Junck, L.; Foster, N. L.; Frey, K. A.; Kuhl, D. E., PET of peripheral benzodiazepine binding sites in the microgliosis of Alzheimer's disease. *J Nucl Med* **1995,** 36, (12), 2207-10.

113. Vowinckel, E.; Reutens, D.; Becher, B.; Verge, G.; Evans, A.; Owens, T.; Antel, J. P., PK11195 binding to the peripheral benzodiazepine receptor as a marker of microglia activation in multiple sclerosis and experimental autoimmune encephalomyelitis. *J Neurosci Res* **1997,** 50, (2), 345-53.

114. Chauveau, F.; Boutin, H.; Van Camp, N.; Dolle, F.; Tavitian, B., Nuclear imaging of neuroinflammation: a comprehensive review of [11C]PK11195 challengers. *Eur J Nucl Med Mol Imaging* **2008,** 35, (12), 2304-19.

115. James, M. L.; Selleri, S.; Kassiou, M., Development of ligands for the peripheral benzodiazepine receptor. *Curr Med Chem* **2006,** 13, (17), 1991-2001.

116. Doorduin, J.; de Vries, E. F.; Dierckx, R. A.; Klein, H. C., PET imaging of the peripheral benzodiazepine receptor: monitoring disease progression and therapy response in neurodegenerative disorders. *Curr Pharm Des* **2008,** 14, (31), 3297-315.

117. Okuyama, S.; Chaki, S.; Yoshikawa, R.; Ogawa, S.; Suzuki, Y.; Okubo, T.; Nakazato, A.; Nagamine, M.; Tomisawa, K., Neuropharmacological profile of peripheral benzodiazepine receptor agonists, DAA1097 and DAA1106. *Life Sci* **1999,** 64, (16), 1455-64.

118. Chaki, S.; Funakoshi, T.; Yoshikawa, R.; Okuyama, S.; Okubo, T.; Nakazato, A.; Nagamine, M.; Tomisawa, K., Binding characteristics of [3H]DAA1106, a novel and selective ligand for peripheral benzodiazepine receptors. *Eur J Pharmacol* **1999,** 371, (2-3), 197-204.

119. Culty, M.; Silver, P.; Nakazato, A.; Gazouli, M.; Li, H.; Muramatsu, M.; Okuyama, S.; Papadopoulos, V., Peripheral Benzodiazepine Receptor Binding Properties and Effects on Steroid Sythesis of Two New Phenoxyphenyl-Acetamide Derivatives, DAA1097 and DAA1106. *Drug Development Research* **2001,** 52, 475-484.

120. Zhang, M. R.; Kida, T.; Noguchi, J.; Furutsuka, K.; Maeda, J.; Suhara, T.; Suzuki, K., [(11)C]DAA1106: radiosynthesis and in vivo binding to peripheral benzodiazepine receptors in mouse brain. *Nucl Med Biol* **2003,** 30, (5), 513-9.

121. Maeda, J.; Higuchi, M.; Inaji, M.; Ji, B.; Haneda, E.; Okauchi, T.; Zhang, M. R.; Suzuki, K.; Suhara, T., Phase-dependent roles of reactive microglia and astrocytes in nervous system injury as delineated by imaging of peripheral benzodiazepine receptor. *Brain Res* **2007,** 1157, 100-11.

122. Venneti, S.; Lopresti, B. J.; Wang, G.; Slagel, S. L.; Mason, N. S.; Mathis, C. A.; Fischer, M. L.; Larsen, N. J.; Mortimer, A. D.; Hastings, T. G.; Smith, A. D.; Zigmond, M. J.; Suhara, T.; Higuchi, M.; Wiley, C. A., A comparison of the high-affinity peripheral benzodiazepine receptor ligands DAA1106 and (R)-PK11195 in rat models of neuroinflammation: implications for PET imaging of microglial activation. *J Neurochem* **2007,** 102, (6), 2118-31.

123. Venneti, S.; Wagner, A. K.; Wang, G.; Slagel, S. L.; Chen, X.; Lopresti, B. J.; Mathis, C. A.; Wiley, C. A., The high affinity peripheral benzodiazepine receptor ligand DAA1106 binds specifically to microglia in a rat model of traumatic brain injury: implications for PET imaging. *Exp Neurol* **2007,** 207, (1), 118-27.

124. Maeda, J.; Suhara, T.; Zhang, M. R.; Okauchi, T.; Yasuno, F.; Ikoma, Y.; Inaji, M.; Nagai, Y.; Takano, A.; Obayashi, S.; Suzuki, K., Novel peripheral benzodiazepine receptor ligand [11C]DAA1106 for PET: an imaging tool for glial cells in the brain. *Synapse* **2004,** 52, (4), 283-91.

125. Zhang, M. R.; Maeda, J.; Furutsuka, K.; Yoshida, Y.; Ogawa, M.; Suhara, T.; Suzuki, K., [18F]FMDAA1106 and [18F]FEDAA1106: two positron-emitter labeled ligands for peripheral benzodiazepine receptor (PBR). *Bioorg Med Chem Lett* **2003,** 13, (2), 201-4.

126. Zhang, M.-R.; Maeda, J.; Ogawa, M.; Noguchi, J.; Ito, T.; Yoshida, Y.; Okauchi, T.; Obayashi, S.; Suhara, T.; Suzuki, K., Development of a New Radioligand, N-(5-Fluoro-2-phenoxyphenyl)-N-(2-[18F]fluoroethyl-5-methoxybenzyl)acetamide, for PET Imaging of Peripheral Benzodiazepine Receptor in Primate Brain. *Journal of Medicinal Chemistry* **2004,** 47, (9), 2228-2235.

Chapter 2

Cellular Expression of Peripheral Benzodiazepine Receptors:

Comparison to Proliferation and Malignancy

Introduction

The Peripheral Benzodiazepine Receptor (PBR, or TSPO and ω3 alternatively) was identified in 1977.[1] It has been characterized as a complex containing three primary components: the isoquinoline binding protein (IBP), voltage dependent anion channel (VDAC) and the anion nucleotide carrier (ANC).[2] PBR has been found to have higher expression in steroidogenic tissues, with moderate to low expression in several other organs.[3-5] Tumor cells from several types of tissues have also been examined and noted to express PBR.[6-9] The protein is normally found at the mitochondrial membrane.[4] However, it has been seen that the protein also localizes to the nuclear membrane in malignant cancer cell lines.[7, 10]

Several roles have been attributed to PBR, including proliferation[7, 11] and apoptosis,[12-14] although tissue type may in part dictate the action of the protein. Studies on tumor lines suggest an important role for PBR in tumor development, but the precise involvement has not been determined. One trend seen in literature is a correlation between PBR expression and proliferation.[15] Studies with antibodies against markers like Ki-67 (MIB-1), a known tumor proliferation marker,[16] or glucose utilization by [^{18}F]FDG demonstrate a relationship correlating PBR and proliferation.[18]

PBR has also been correlated to malignancy. For instance, several investigations have suggested that PBR could serve as a biomarker for glioma tumor grade differentiation.[9, 17, 19, 20] In an *in vitro* study with glioma cell lines, Veenman *et al.* found a positive correlation for colony size in a soft agar assay, a method to determine survival, and [^{3}H]PK11195 specific binding.[21]

Several conflicting reports are found in breast cancer literature. In a study on patient biopsy samples, PBR expression correlated with Ki-67.[22] They found that lymph node negative patients had a poorer prognosis when PBR levels were higher, and suggested that perhaps the

protein could be a prognostic biomarker. In cultured cells, [^{3}H]PK11195 uptake was measured and compared to several cell characteristics.[7] They analyzed cell proliferation in the presence of several concentrations of PK11195, as well as performing *in vitro* assays of aggression. Their data suggest a positive correlation between PBR expression and invasion potential. In this paper, they also looked at metastatic patient samples compared to normal breast tissue expression of PBR. Tumor samples had greater quantities of PBR, and perinuclear localization was not found in normal tissue samples.

However, a later reference from the same group resulted in different data. Two clones were created of MDA-MB-231, a breast cancer cell line characterized as a high PBR expressor. One clone was a "low" expressor and the other was a "high" expressor.[23] Scatchard analysis using [^{3}H]PK11195 show a B_{max} that is approximately doubled in the "high" expressor compared to the low expressor. *In vitro* proliferation was measured as was chemoinvasive potential, and these characteristics were found to be similar in both cell lines. However, the "high" expressor clone was able to form tumors in SCID mice whereas the "low" expressor clone could not. Analysis revealed that they were of the same genetic linage, and chromosomal abnormalities were shared. No conclusive explanation for the capacity to form tumors was given, but the suggestion is made that a minimum PBR level may be required for PBR to act in cell proliferation.

In order to better understand the cells we implant, cell characterization became necessary. For each cell line, a variety of properties were assessed *in vitro*. These *in vitro* measurements include proliferation studies, measures of aggression such as motility and survival, and determination of PBR expression.

Cell lines used in the studies described below include: MCF-7, MDA-MB-468 and MDA-MB-231. These are all breast cancer cell lines that were purchased from ATCC (Manassas, VA). MDA-MB-435, is a cell line that was classified as a human breast cancer line when these studies began, but is now identified as a melanoma cell line.[24] MDA-MB-435 was provided by Dr. Janet Price at MD Anderson (Houston, Texas), and used with her permission. MCF-7 (ER-) clone was given by Dr. Antonio Rosato at University of Padua, Italy, and used with his permission. MDA-BGL2 is a clone of MDA-MB-231 which has been selected for its potential to form metastases; this cell line was used with permission of Dr. Kathy Weilbaecher, at Washington University.

Quantifying PBR expression

Western Blot

Western blot analysis was the first method applied to analyze the expression of PBR in cells. Cells were grown in T-75 flasks (BD Falcon), and maintained at 5% CO_2. Media was removed from the cells, and cells were washed twice with phosphate buffered saline (PBS). Collection by scraping was followed by centrifugation at 2000g for five minutes. Supernatant was removed and lysis buffer was added. Lysis buffer was made by diluting 10X Lysis Buffer (Cell Signaling Technology) to 1X with MQ water and 7X protease inhibitor, from Complete Mini Protease Inhibitor Cocktail Tablets (Roche) dissolved in MQ water. 100 μL of lysis buffer was added to each microfuge tube of cells and placed on ice for 15 minutes before centrifugation at 16,000g for 10 minutes at 4°C. Supernatant was removed and analyzed by BCA Assay (Pierce Biotechnology) for protein concentration.

BioRad Mini Protean Cell was used with a BioRad Ready Gel (12% Tris-HCl, 30 μL per well). The molecular weight standards used were the Dual Color Precision Plus Protein Standards (BioRad). 10 μg total protein were added to each lane in 25 μL. 10X Tris/Glycine/SDS

Buffer (BioRad) and 10X Tris/Glycine Buffer (BioRad) were diluted to make running buffer and transfer buffer. Following transfer to PVDF, the blot was blocked with 5% milk in Tris Buffered saline with 0.05% Tween-20 (TBST). Rabbit anti-PBR (Santa Cruz) diluted 1:1000 in TBST was incubated overnight at 4°C, washed, and the blot was probed with Goat anti-rabbit IgG,

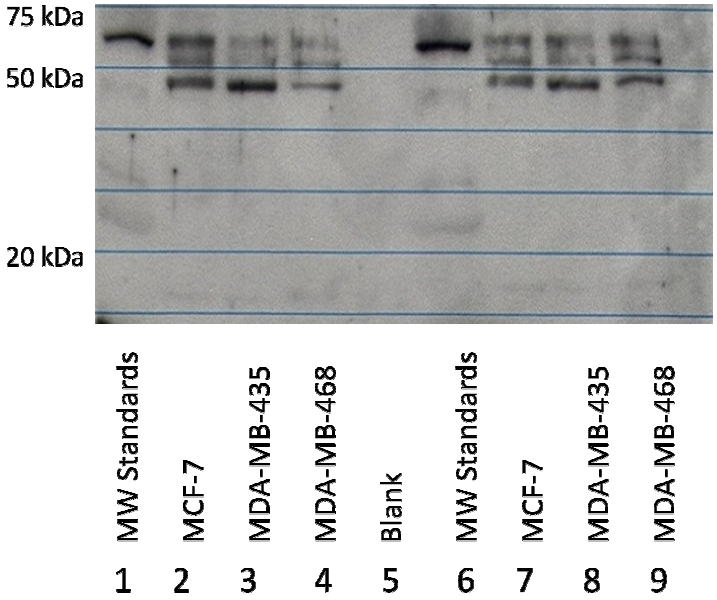

Figure 1: Western Blot on cultured cell lines with the Santa Cruz anti-PBR antibody. Bands are seen at 75, 62, and 50 kDa. The monomer (18 kDa) is not present in significant quantities.

Dylight™647 (Pierce Biotechnology) at 2:15,000 in TBST at room temperature (RT) for one hour. The blot was developed with ECL (Amersham). Overnight exposure is shown below in Figure 1.

The standard protein ladder (lanes 1 and 6), MCF-7 (lanes 2 and 7), MDA-MB-435 (lanes 3 and 8) and MDA-MB-468 (lanes 4 and 9) are shown in Figure 1. There is very little monomer present at 18kDa (IBP). Bands are seen at 50, 62 and 75 kDa. These may be attributed to the trimer (~80 kDa), or all may be IBP multimers. However, there was not a control protein so this experiment was repeated with additional cell lines and recombinant PBR Control Protein (Trevigen). Unfortunately, after initial success with the Santa Cruz anti-PBR antibody, I was unable to reproduce the data despite many attempts to do so. The standard protein was

detected at approximately 20 kDa, which is the predicted weight for the GST-tagged recombinant protein, but no bands were visible in sample lanes.

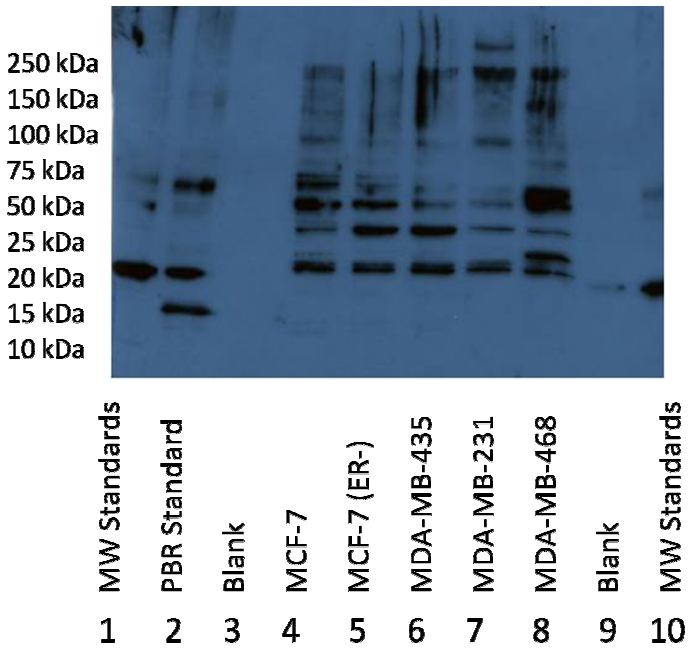

Figure 2: Western blot on cultured cell homogenates with the Trevigen anti-PBR antibody. Streaking was seen in lanes sporadically and increased with film exposure.

Another rabbit anti-PBR antibody was purchased (Trevigen) and used to probe for PBR. With this antibody, multiple bands are detected in the samples (lanes 4-8 below), but there was variable streaking in samples that would become more intense with extended exposures (Figure 2). Efforts were made to resolve the issue, but it could not be prevented. Therefore, we concluded that another method would be required to measure PBR expression.

ELISA

The enzyme linked immunosorbent assay (ELISA) is an alternative method to quantify proteins. It is a plate-based assay. There are two options when using ELISA, the direct or in the indirect ELISA.

In indirect ELISA the antigen, the protein of interest, is coated on the wells of the 96-well plate. After one hour wells are rinsed and blocked with a 2% bovine serum albumin (BSA) solution. Primary antibody is incubated at 37°C for 1.5 hours followed by secondary antibody conjugated to horse radish peroxidase (HRP) for one hour incubation at 37°C. Washing well to ensure that all unbound antibodies are removed, HRP substrate is incubated at RT for 20 minutes. Reaction is stopped with the addition of acid. Plates are read at 490 nm.

The method described above was utilized with both the Santa Cruz Biotechnology anti-PBR and Trevigen anti-PBR as the primary antibody. The secondary antibody was a donkey anti-rabbit IgG, conjugated to HRP (Amersham Biosciences). Substrate was SigmaFast® o-phenylene diamine dihydroxychloride tablet (Sigma) dissolved in water.

The antigen was the Trevigen recombinant protein with a GST tag, suspended at a concentration of 9.80×10^{-6} M (0.2 mg/mL). Antigen was diluted to measure the absorbance with a standards curve. Dilutions ranged from 78 picomoles in 100 µL to 40 femtomoles in 100 µL. For wells in which the 40 fmoles was added (2 µg protein), this would be equivalent to 20 pmoles PBR in a total of 1 mg protein.

Figure 3 shows a standard curve. Little difference is seen in absorbance below 20 fmoles PBR/ 2 µg total protein (10 pmoles/mg protein). Literature quantifies the expression of MDA-MB-231 cells, PBR positive controls to be approximately 10 pmoles/mg protein.[23] Since the cell lines that are accepted as high expressing positive control cells are at threshold for detection of differences in absorbance, this method will not be useful for measuring a range of PBR expression.

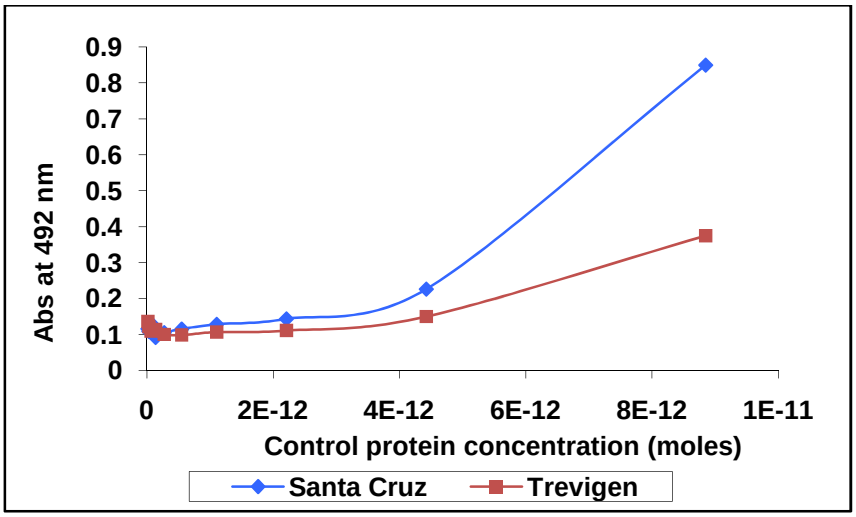

Figure 3: Sample data from a standards curve for the indirect ELISA using Trevigen recombinant PBR to determine assay sensitivity.

In direct or "sandwich" ELISA, a primary antibody is coated on the wells of the 96-well plate (TPP) and allowed to incubate overnight at 4°C to allow complete binding. The next day, wells are rinsed and blocked with a 2% BSA solution. Antigen, the recombinant PBR, is added followed by 2.5 hour incubation with an anti-PBR primary antibody from a different species. By doing this, cross reactions between any unbound antibody on the surface of the well will be avoided. Secondary antibody conjugated to HRP incubated for two hours at 37°C. Washing well to ensure that all unbound antibodies are removed, HRP substrate is incubated at RT for 30 minutes. Reaction is stopped with the addition of acid. Plates are read at 490 nm.

The technique was executed as described above. The coating antibody was a chicken anti-PBR antibody (GenWay Biotech). Both the Santa Cruz and Trevigen anti-PBR were used for detection with the same Amersham secondary as above. Trevigen recombinant control PBR protein was diluted at the same concentrations for the direct ELISA.

Useful data could not be generated with the sandwich ELISA method. With this method equal absorbance was seen at all concentrations. When conditions were tested to determine

the reason why the absorbance did not vary, data shown in Figure 4 provided an explanation. The conditions are described with abbreviations, and the order indicates the above sequence of primary/PBR standard/primary/secondary. In the red bars, the GenWay antibody was coated followed by PBR protein (P) or not (N), Trevigen antibody and secondary. Orange equals GenWay, PBR protein, Trevigen antibody and no (N) secondary. Green bars are GenWay antibody, PBR protein (P) or not (N), Santa Cruz anti-PBR, and secondary. In blue, it is GenWay, PBR protein, Santa Cruz anti-PBR and no (N) secondary. What is shown is that there is very little difference whether the PBR control protein is added to bind the Trevigen or Santa Cruz anti-PBR antibody. When BSA is coated onto the plate in the place of GenWay and when Trevigen or Santa Cruz is substituted by a BSA solution, absorbance is equal to the blank. We conclude that the two primary antibodies are interacting, and thus the absorbance is equal regardless of the PBR added.

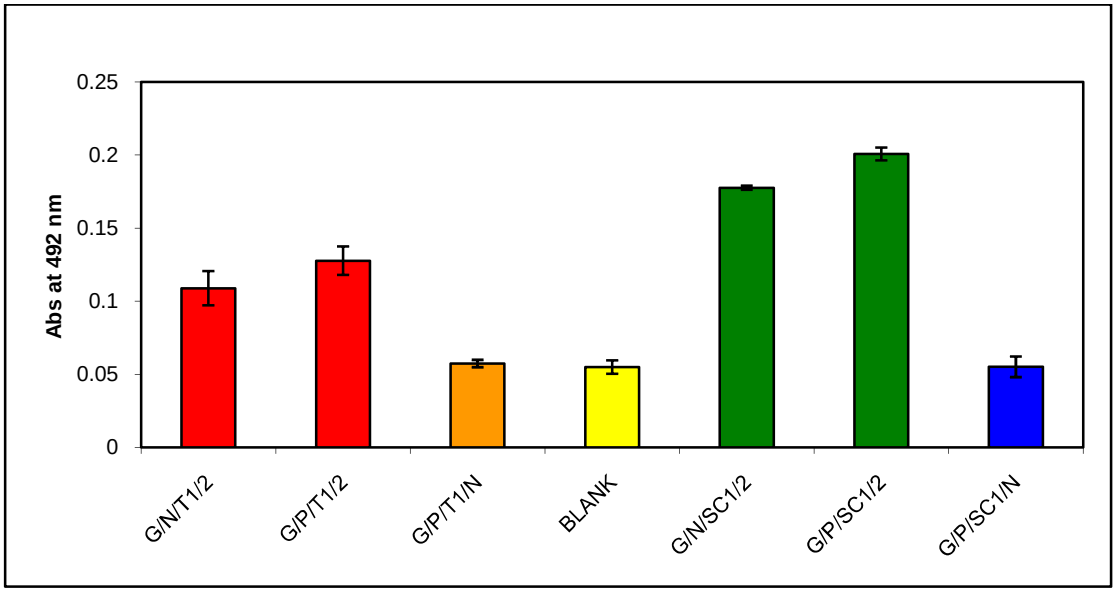

Figure 4: Direct or sandwich ELISA data demonstrating that the antibodies are interacting. In the red, using the Trevigen anti-PBR, absorbance is similar when PBR recombinant protein is not added to bind the coating antibody. In orange, the absence of secondary antibody reduces the absorbance to blank absorbance. In green, the same observation of unchanged absorbance is seen when no PBR standard protein has been added, while the absence of secondary reduces absorbance.

Comparison of [^{11}C]PK11195 Uptake

At this point, studies had begun measuring the *in vitro* cellular uptake of the radiopharmaceutical [^{11}C]PK11195. This assay is more applicable for comparison to *in vivo* studies, since it requires the uptake of the radiopharmaceutical. Therefore, with the difficulties encountered in attempts with the above techniques to quantify PBR expression, we pursued this assay to measure PBR levels.

Radiopharmaceutical synthesis: (R)-N-desmethyl PK11195 (ABX GmbH, Germany) is methylated by [^{11}C]CH_3I produced on the GE PETtrace MeI MicroLab in a method based on Camsonne et al.[25] Substrate was dissolved in DMSO (250 µL) with 15% KOH (3 µL) added prior to [^{11}C]CH_3I delivery. After [^{11}C]CH_3I has been trapped, the reaction mixture is heated at 90°C (3 minutes). Preparative reverse phase HPLC separation is performed with a mobile phase of actonitrile/ammonium formate buffer. The radioligand was reformulated in 10% ethanol in normal saline. Overall synthesis time is 60 minutes from the end of bombardment, and batch yields were 0.26 to 0.54 GBq (10-20 mCi), with radiochemical purity greater than 99% and specific activity exceeding 37 TBq/mmol (1,350 Ci/mmol).

Cell uptake studies: Cells were grown in 6-well plates (Co-star) to be at 70-80% confluency. Media was changed before the addition of the radiopharmaceutical. For blocking, 200 ng of cold N-methyl-PK11195 (ABX GmbH, Germany) was added thirty minutes prior to the addition of the radiopharmaceutical. A solution of [^{11}C]PK11195 was added to each well. Cells were incubated for 0, 10, 30, and 60 minutes. After removing the media, cells were washed and lysed. Media, washes and cell lysates were counted by gamma counter to determine the percent uptake for the cells. BCA Protein Assay (Pierce Biotechnology) was performed to normalize for protein levels. Data was normalized to %ID/g representing the fraction of the total radioactivity added to the media that was bound per gram of protein.

Figure 5 shows averaged data from several studies (n=3). The amount of uptake in the presence of 200 ng cold PK11195 was subtracted from normal uptake conditions to calculate the net %ID/g protein. Distinct uptake of [^{11}C]PK11195 is seen for the MDA-MB-435 while the uptake by MDA-MB-468 could be catagorized as moderate. MCF-7 displays little selective uptake, in agreement with data from literature.[7]

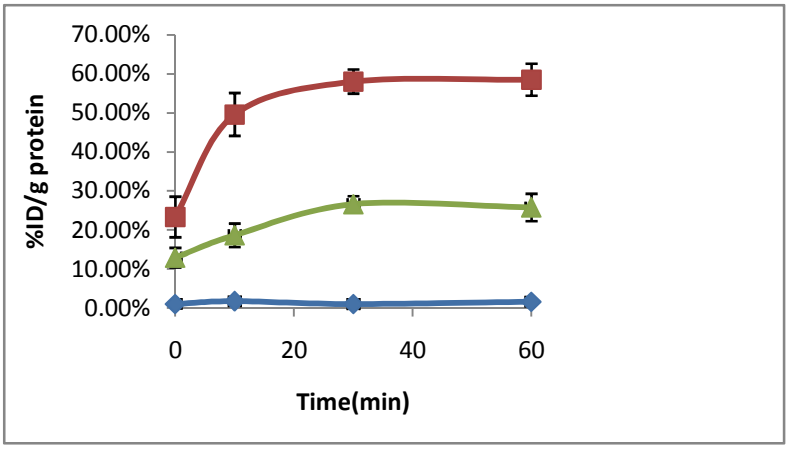

Figure 5: Net Uptake for [^{11}C]PK11195 in cultured cells showing differential uptake of the PBR ligand *in vitro*. The trends seen correspond to literature

Measuring Proliferation Potential

PBR has been suggested to play a significant role in proliferation due to observed correlations of PBR expression and proliferation. Support for this hypothesis is that when the cell line MCF-7, which has very little natural expression of PBR, was stably transfected with PBR, there was a five-fold increase the binding of [^{3}H]PK11195, and proliferation was increased. When siRNA targeting PBR was introduced in MDA-MB-231 cells, a significant reduction in [^{3}H]PK11195 binding and proliferation measured by BrdU were observed.[11] In these studies, we wanted to evaluate our cell lines and establish proliferation parameters.

Cell Counts Method

This is a very straightforward method to determine the proliferation potential for each cell line. Cells were harvested from a T-75 flask using Trypsin/EDTA (Washington University Tissue Culture Support Center), and counted using a hemocytometer. Cells were resuspended in fresh media for addition to a 24-well plate (Costar). Cells were plated at three densities: $1x10^5$ cells/mL, $5x10^4$ cells/mL, and $1x10^4$ cells/mL in total volume of 1 mL. Each day three wells were washed with PBS and trypsinized from each density. Using 1:1 trypan blue, each sample was counted twice. The six values were averaged for the growth curve. Data are plotted as shown in Figure 6. A line is drawn where the proliferation is linear, and proliferation rate was calculated by determining the population doubling time (PDT) as shown as follows:

$$r = 3.32 [\log (Nf) – \log (Ni)] / (Tf - Ti)$$

$$PDT = 1/r$$

A. MDA-BGL2

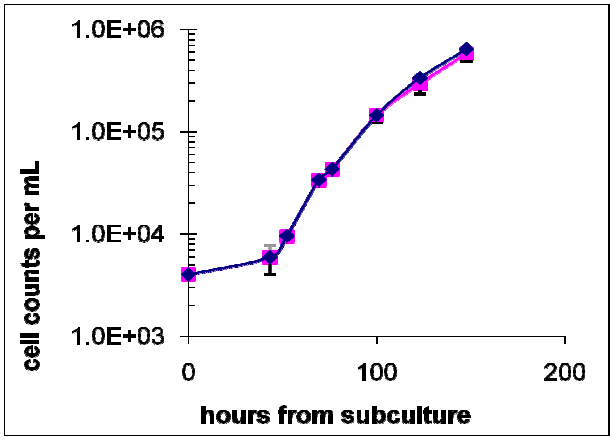

B. MDA-MB-435

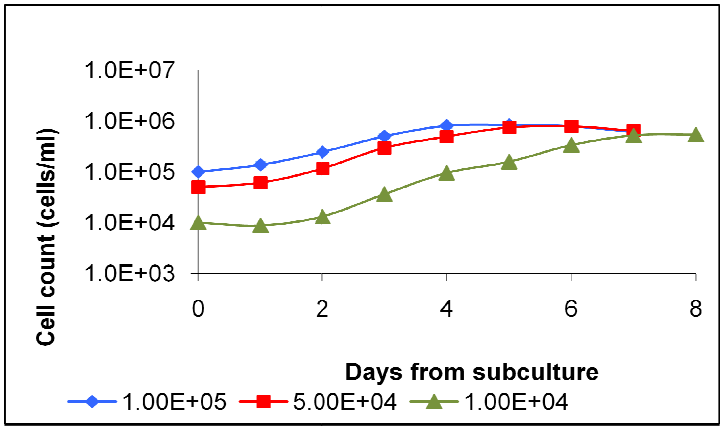

C. MDA-MB-468

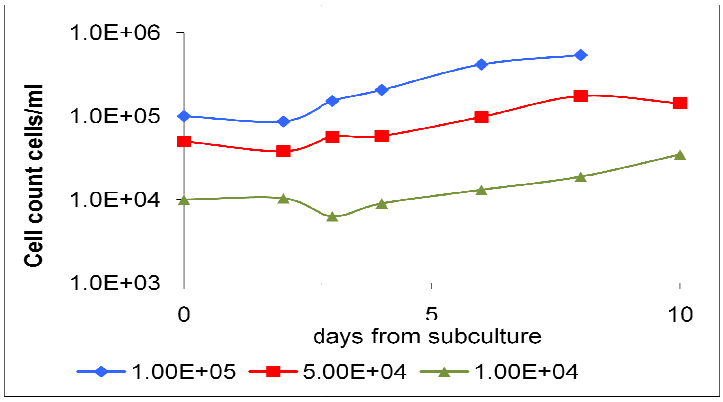

Figure 6: Proliferation curves generated by cell counting with a hemocytometer for selected cell lines showing fast (MDA-BGL2) and slow proliferation (MDA-MB-468).

MTS Assay

A second method was used to confirm the data on proliferation. Cell counts in log-phase growth are very low, leading to less certainty in the values obtained. In the ideal, in each 1 mm^2 area on the hemocytometer, there would be between 20 to 50 cells. For my studies, the number of cells in the 1 mm^2 area was typically below the ideal threshold for the first three to four days after the subculturing to the 24 well plates.

The MTS Assay kit that was used was the Promega Cell Titer® Aqueous non-radioactive cell proliferation assay kit. There are two solutions, a tetrazolium compound 3-(4,5-dimethylthiazol-2-yl)-5-(3-carboxymethoxyphenyl)-2-(4-sulfophenyl)-2H-tetrazolium, inner salt (MTS) and an electron coupling reagent, phenazine methosulfate or PMS. After opening, the two reagents can be combined and stored at -20°C for a year, thawing in the water bath when in use. MTS is reduced by cells to form a formazan product. The absorbance of the formazan product at 490nm can be measured in 96-well assay plates. The extent of MTS reduction is proportional to the number of cells present within a range of linearity (Figure 7).

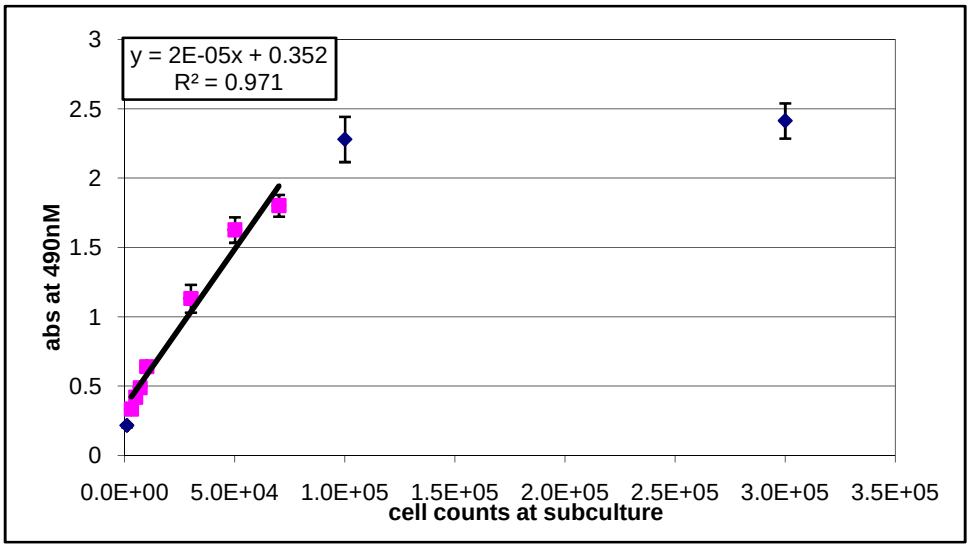

Figure 7: Standards curve for MTS with MDA-MB-435 cells. The line drawn indicates the linear data that can be used to quantify the number of cells present in each well of the 96-well plate. The equation is displayed.

When using the MTS assay, on the day that cells are subcultured into the 96-well plates, a standards curve must be made. As shown in Figure 7, a typical curve would have points below the linear region and a plateau at the upper limits of the cell densities. The cells are subcultured at the lower limits of detection so they will grow into the linear zone. When cells are dividing in log phase growth, apply the equation shown above to calculate population doubling time.

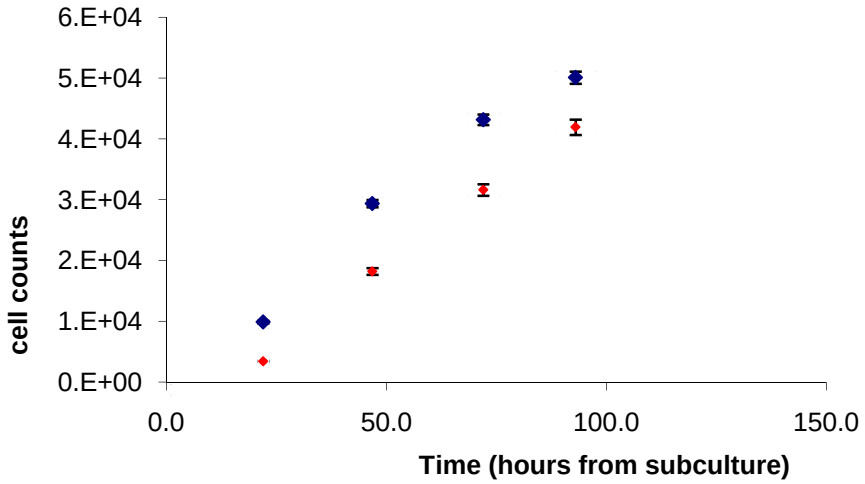

Figure 8: Sample MTS Data Curve for MDA-MB-435 over the linear range of growth as determined by the standard curve.

Figure 8 shows a sample data set for the MDA-MB-435 cell line. The shortcoming of the MTS method is in the narrow window for calculating data. As shown in Figure 8, the time for viable cell count approximation is less than an order of magnitude, and the line does not form a true exponential shape in growth.

Results and Summary of Measuring Proliferation Potential

Data is reported in Table 1. Both methods have short-comings, but the MTS assay is slightly better for the determination of PDT. This is because its range of utility, though narrow, more closely corresponds to the early time points when cells would be most rapidly dividing. In

contrast, the small number of cells in the hemocytometer 1 mm square is at or below the threshold for confidence.

Table 1: Maximum population doubling time (in hours) as determined by the two methods.

	MCF-7 (ER-)	MDA-MB-435	MDA-MB-468	MDA-BGL2 (MDA-MB-231)	MDA-MB-231	MCF-7 (ER+)
MTS Assay	14	16	33	13.7	30	39
Cell Counts	17	18	47	9	41	42.5

Defining Cell Aggression

How do you define aggressive when describing a tumor? Historically, the PET view has been centered on [^{18}F]FDG which, as a glucose analog, will localize to a tumor due to elevated metabolism. Radiopharmaceutical development has moved from this simplistic view to embrace a more descriptive characterization, such as antibodies targeting proteins important in establishing tumor vasculature. From a molecular biology perspective, there are an infinite number of ways to characterize aggression.

My focus was on motility and survival. Motility, distinct from chemoinvasive potential, addresses the simple migration of the cells to an unoccupied space. Chemoinvasion is the capacity of the cell to penetrate a cellular barrier such as the extracellular matrix. Another way to describe survival would be heartiness. Some cell lines may not form tumors quickly, but are able to survive unfavorable conditions. With assistance from personnel in Dr. Harbour's lab, I performed "wound-healing" assays to measure motility and soft agar assays to measure survival.

Migration Assay

The "wound-healing" assay was performed using 60 mm dishes that had been previously marked with 2 mm circles to provide reference points. Cells were grown in the dishes to approximately 80-90% confluency. "Wounds" were made using a cell scraper. Media and any floating cells were removed. Pictures were quickly taken using a microscope and fresh media was added. The dishes were kept in the appropriate incubator (5% CO_2 or no CO_2) at 37°C between handling. At 24 hour intervals, out to 72 hours post-wounding, images were taken on a Nikon Eclipse E600 microscope with digital camera DXM1200F. Analysis was performed using ImageJ (NIH) to quantify the amount of wound tract that had been filled in by new cells, quantifying the open "wound tract" in pixels each day and calculating the % "wound tract" filled at each time point by comparison to image taken immediately after creating the "wound".

Migration Results and Summary

Figures 9 and 10 show the data from the wound-healing experiments. In Figure 9, the data is graphed for comparison. In Figure 10, a visual comparison is provided for the cell lines. As shown in Figure 9, the cell lines migrate into the "wound tract" at different rates. The PBR positive control cells, MDA-MB-231 (Figure 10A) and clone MDA-BGL2, have similar rapid response and quickly move into the void space. MDA-MB-435 (Figure 10B) moves at a consistent rate into the tract and has mostly "healed" in 72 hours. MDA-MB-468 (Figure 10C) and MCF-7 (Figure 10D) cells do not display significant "healing" response in 72 hours.

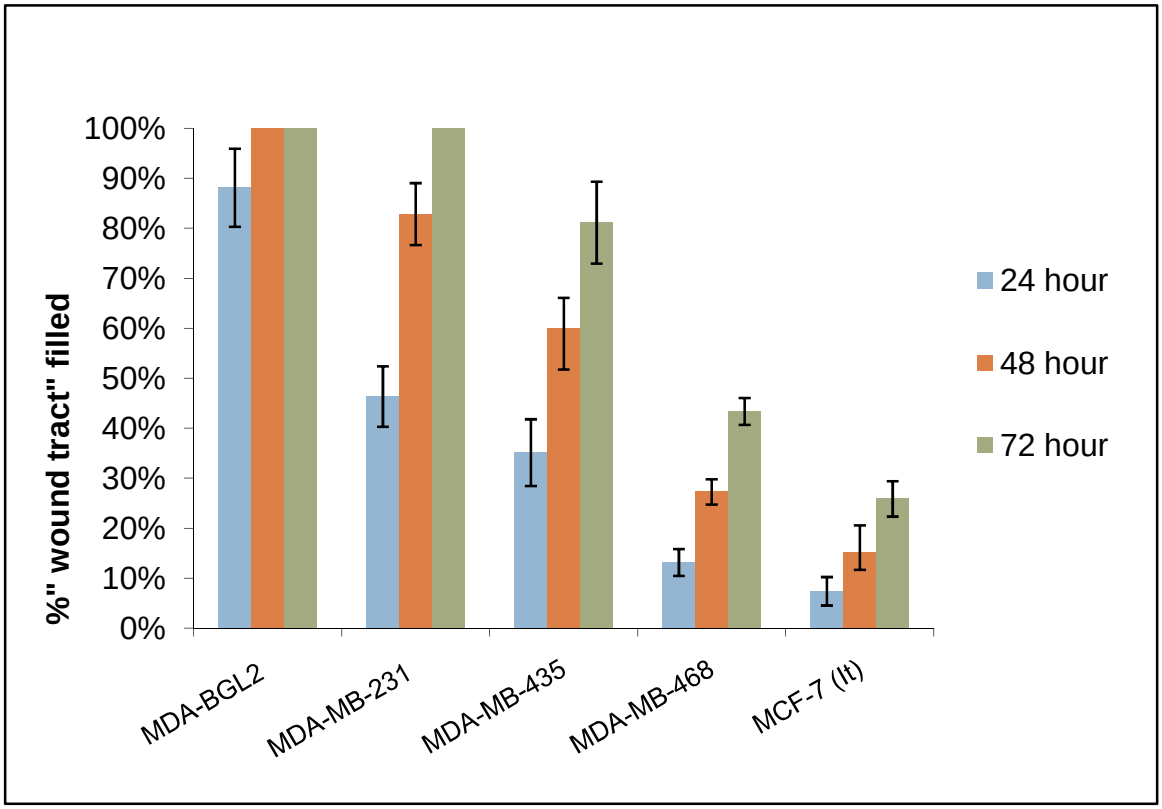

Figure 9: Data for *in vitro* wound-healing demonstrating the different responses for each cell line when a "wound" was created.

A. MDA-MB-231

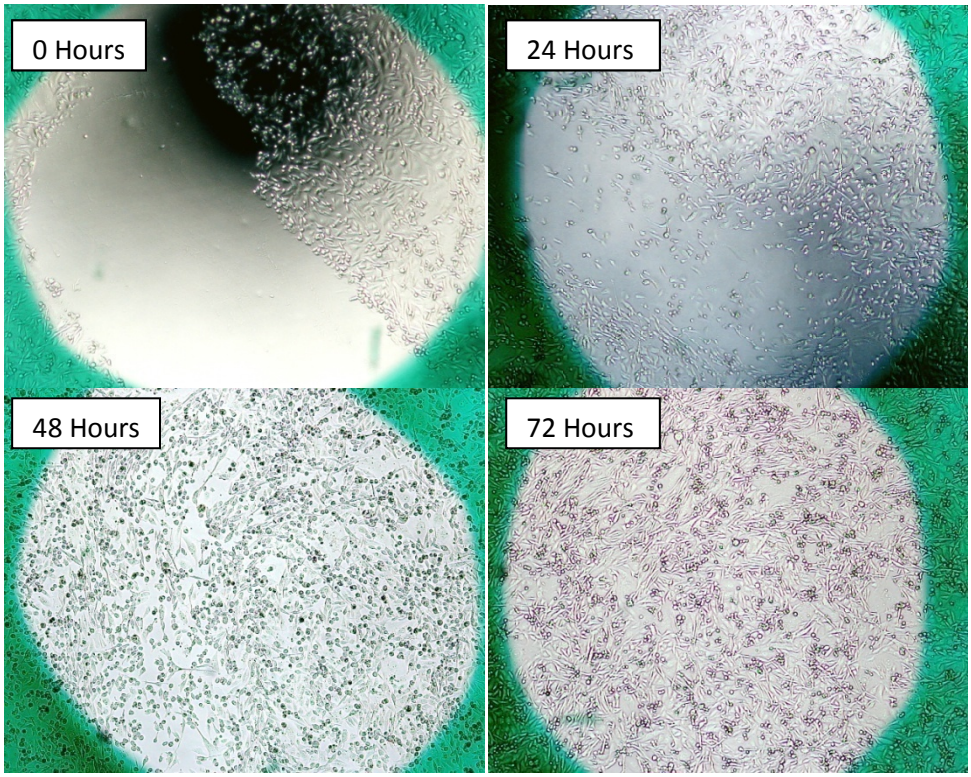

B. MDA-MB-435

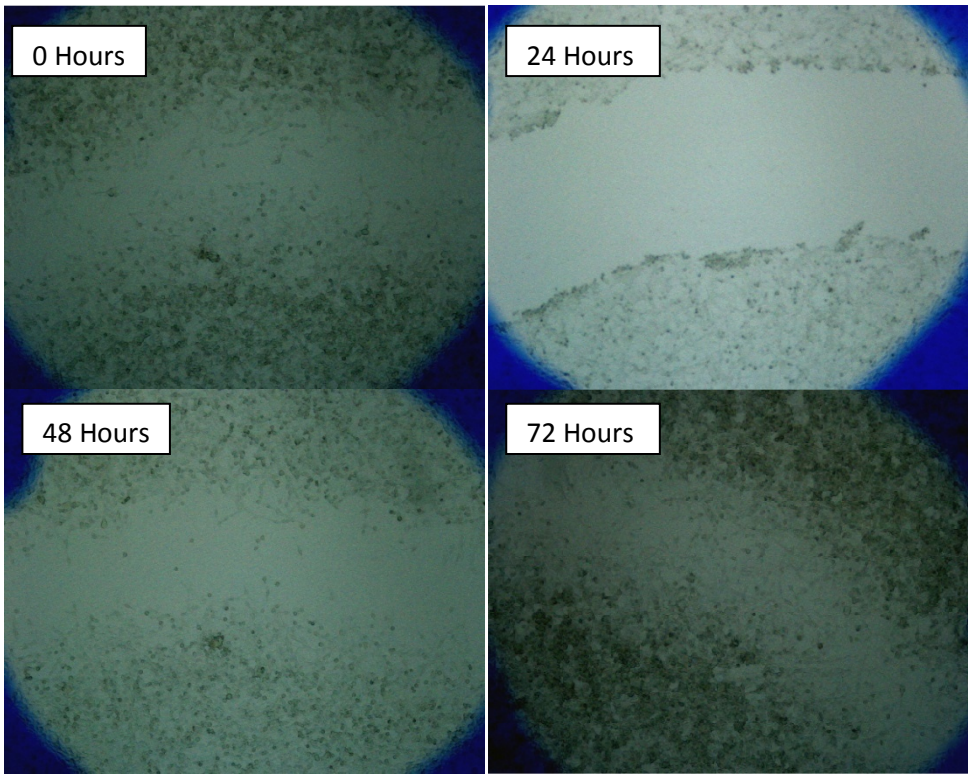

C. MDA-MB-468

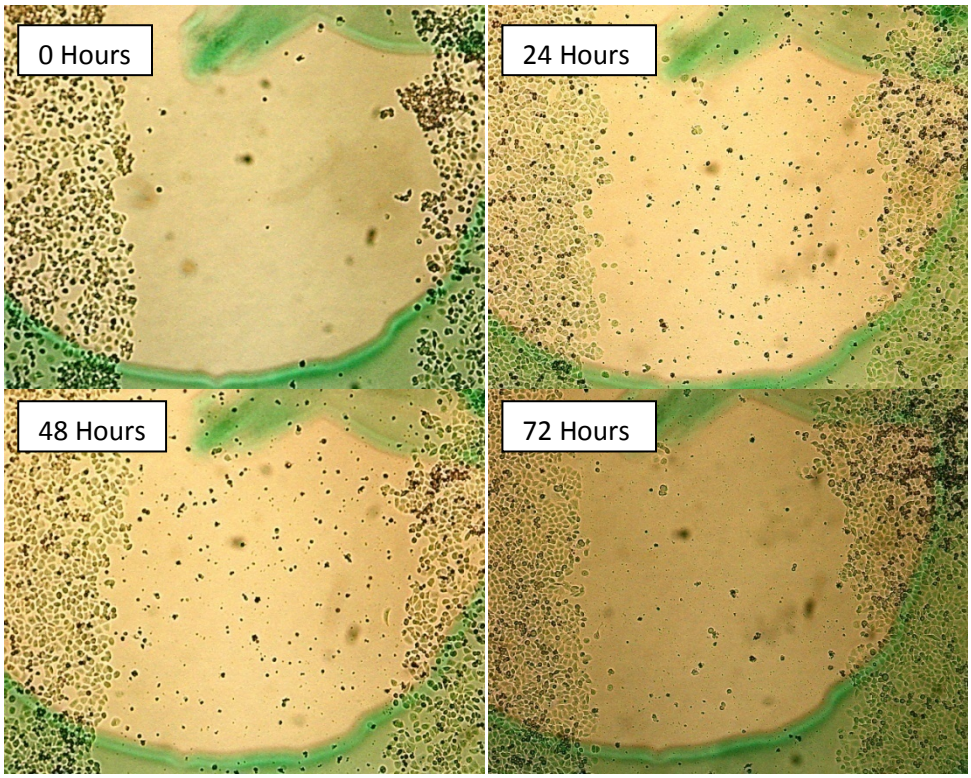

D. MCF-7

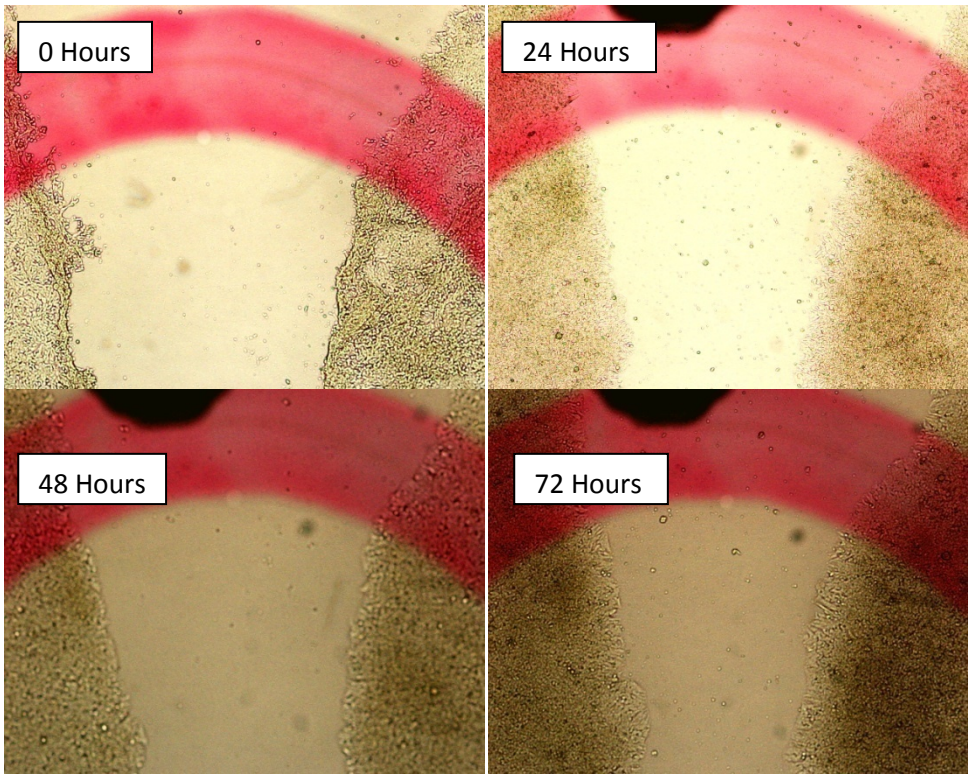

Figure 10: Selected wounds from cell lines representing high to low rate of "healing" in the wound tract over a 72 hour period. A. MDA-MB-231, B. MDA-MB-435, C. MDA-MB-468, and D. MCF-7.

Cell Survival

The soft agar assay measures the capacity of the cells to survive and grow in the absence of a growth surface. The capacity for anchorage-independent growth is a marker that a cell has undergone malignant transformation. For this assay, cells were cultured to be in log phase growth. On the first day of setting up the experiment, a twelve-well plate (TPP) was prepared by adding 1 mL of 0.8% agar (Invitrogen Ultra Pure L.M.P. Agarose) in sterile PBS (Cellgro) and media. A stock solution of 3% agar was made in PBS, and diluted to 0.8% with media. The plate was moved to 4°C for 10 minutes to allow the agar to set, and returned to RT. On the following day, cells were harvested and counted. Cells were suspended in a 0.3% agar solution (3% PBS stock solution diluted with media) to concentrations of $5x10^5$, $1x10^5$, and $5x10^4$. This cell dispersion was added to the 12-well plate on top of the 0.8% agar. The plate was moved to 4°C to allow the agar to set and returned to RT. The 12-well plates were incubated for 14 days. To visualize colonies, crystal violet solution (Sigma) was added. Colonies were counted under a microscope, with the standard of 350 μm as the minimum diameter for a colony to be counted.

Results and Summary of Anchorage-Independent Growth

Figure 11 shows data comparing the cell lines in the soft agar assay. The cell line MDA-MB-435 had an average of 416±51, followed by MDA-BGL2 with 312±54 colonies in each well. MDA-MB-468 and MCF-7 (ER-) had fewer colonies at 99±29 and 80±36, respectfully. Therefore the MDA-MB-231 clone MBA-BGL2 and MDA-MB-435 have greater malignancy as measured by anchorage-dependent growth.

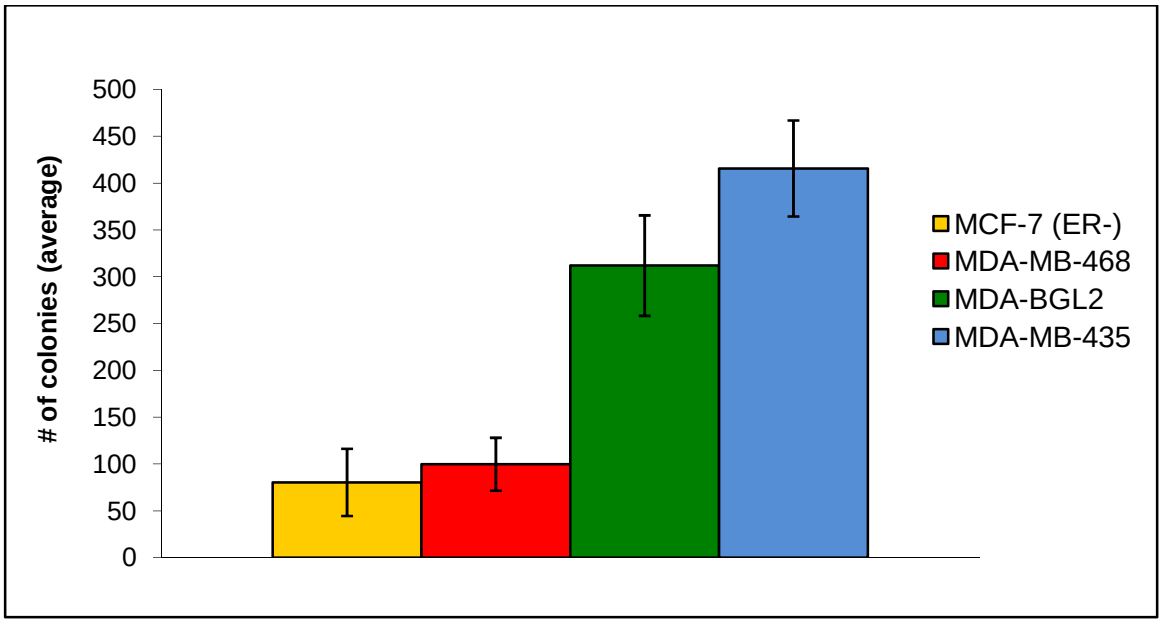

Figure 11: Anchorage-independent growth data using the soft agar assay. Two groups are seen the low colony counts for MCF-7 (ER-) and MDA-MB-468, while the MDA-BGL2 and MDA-MB-435 were able to form a greater number of colonies over the two week incubation.

Data Summary

Data for the assays performed in this chapter is in summarized in Table 2. As shown in Table 2, different levels of uptake were seen for [^{11}C]PK11195 uptake *in vitro* for the cell cultures. Two PBR positive control cell lines, MDA-MB-231 and the clone MDA-BGL2, were also used. When PBR levels are compared against proliferation, there is a no correlation. Though the cell line MDA-MB-231 does not display rapid proliferation, the MDA-MB-231 clone MDA-BGL2 does. MDA-MB-435 had the highest uptake of [^{11}C]PK11195 at 58.5% ID/g protein and a PDT of 16 hours by MTS. MDA-MB-468 had a longer PDT of 33 hours and moderate uptake of [^{11}C]PK11195 (26.8% ID/g). Meanwhile, MCF-7 (ER+) had a population doubling time that was only slightly longer than MDA-MB-468 (39 hours) with a much lower uptake of [^{11}C]PK11195 at 1.62 % ID/g protein, in keeping with reported data for MCF-7. Within these cell lines, there is no association of PBR and population doubling time.

Table 2: Summary of Data

	MCF-7 (ER-)	MDA-MB-435	MDA-MB-468	MDA-BGL2 (MDA-MB-231)	MDA-MB-231	MCF-7 (ER+)
%ID/g [^{11}C]PK11195	--	58.5	26.8	--	--	1.62
MTS Assay	14	16	33	13.7	30	39
Cell Counts	17	18	47	9	41	42.5
"Wound- Healing" (at 72 hrs)	26%	80%	40%	100%	100%	--
Soft Agar Assay (colonies)	80 ± 36	416 ± 51	100 ± 29	312 ± 53	--	--

When PBR levels are compared to the data for aggression, there is a positive correlation. Both of the PBR positive control cell lines had completely "healed" at 72 hours, and in fact both had done so in less than 48 hours. This effect could be due to rapid proliferation in the MDA-BGL2 cells. However, the observation of nearly identical "healing" in the MDA-MB-231 line with a reduced proliferation rate and the lack of similar behavior in MCF-7 cells with high proliferation eliminates that concern. MDA-MB-435 had the highest [^{11}C]PK11195 uptake, and has the highest values for amount of "wound tract" that "healed" and average quantity of colonies that formed in the anchorage-independent growth assay. MDA-MB-468 had a moderate uptake of [^{11}C]PK11195, and displayed reduced capacity to "heal" and form colonies compared to both MDA-MB-435 and MDA-BGL2. MCF-7 is a low PBR expressing cell line and displays reduced "healing" and colony formation.

Chapter Summary

In this chapter, human breast cancer cell lines were characterized for their PBR expression, proliferation and aggression. Using [^{11}C]PK11195 in whole cell uptake assays, there were significant differences in the specific uptake of the radiopharmaceutical. Population doubling time was calculated by the cell counting method and the MTS assay. To characterize aggression *in vitro* the "wound-healing" assay measured the migration of cells, and the soft agar assay probed the capacity of the cells to grow in an anchorage-independent environment.

Comparing the data for expression to the data for proliferation, there was no discernable trend. Cell lines with similar population doubling times had different levels of PBR expression. Two clones of a positive control, the MDA-MB-231 cell line have significant variation in PDT, indicating that PBR is not important in proliferation.

However, there is a positive correlation for PBR expression and aggression. In the positive control cell lines, there was rapid "wound-healing" and formation of colonies. In MDA-MB-435 cells, which displayed elevated expression of PBR, there was migration and pronounced capacity to grow in the soft agar assay. For the MDA-MB-468, moderate PBR expressing cell line, there is partial "healing" in the "wound tract" and a reduced number of colonies. For the ER negative clone of the non-aggressive tumor cell line MCF-7, there is limited migration into the "wound tract" and colony formation.

The data is in agreement with literature. In fact, molecular biologists have conducted more thorough exams of cell lines, measuring cell characteristics with a litany of tests. To condense the findings, PBR is found at elevated levels in neoplastic tissues and there is a correlation between the expression of PBR and malignancy *in vitro* and *ex vivo.* Higher PBR levels would suggest a poor prognosis, so PBR may be a useful biomarker in characterizing

tumors although this has only been explored *in vivo* for gliomas and astrocytomas. Tumors located outside of the CNS have not been investigated *in vivo*. The next chapter will describe our experiments designed to investigate PBR radioligand distribution and compare it to the localization of two PET radiopharmaceuticals widely used *in vivo* tumor imaging.

BIBLIOGRAPHY

1. Braestrup, C.; Squires, R. F., Specific benzodiazepine receptors in rat brain characterized by high-affinity [3H]-diazepam binding. *Proceedings of the National Academy of Sciences of the United States of America* **1977,** 74, (9), 3805-9.

2. McEnery, M. W.; Snowman, A. M.; Trifiletti, R. R.; Snyder, S. H., Isolation of the mitochondrial benzodiazepine receptor: association with the voltage-dependent anion channel and the adenine nucleotide carrier. *Proceedings of the National Academy of Sciences of the United States of America* **1992,** 89, (8), 3170-4.

3. Benavides, J.; Dubois, A.; Gotti, B.; Bourdiol, F.; Scatton, B., Cellular distribution of omega 3 (peripheral type benzodiazepine) binding sites in the normal and ischaemic rat brain: an autoradiographic study with the photoaffinity ligand [3H]PK 14105. *Neurosci Lett* **1990,** 114, (1), 32-8.

4. Anholt, R. R. H.; De Souza, E. B.; Oster-Granite, M. L.; Snyder, S. H., Peripheral-type benzodiazepine receptors: autoradiographic localization in whole-body sections of neonatal rats. *Journal of Pharmacology and Experimental Therapeutics* **1985,** 233, (2), 517-26.

5. De Souza, E. B.; Anholt, R. R. H.; Murphy, K. M. M.; Snyder, S. H.; Kuhar, M. J., Peripheral-type benzodiazepine receptors in endocrine organs: autoradiographic localization in rat pituitary, adrenal, and testis. *Endocrinology* **1985,** 116, (2), 567-73.

6. Han, Z.; Slack, R.; Li, W.; Papadopoulos, V., Expression of peripheral benzodiazepine receptor (PBR) in human tumors: relationship to breast, colorectal, and prostate tumor progression. *Journal of Receptors and Signal Transduction* **2003,** 23, (2&3), 225-38.

7. Hardwick, M.; Fertikh, D.; Culty, M.; Li, H.; Vidic, B.; Papadopoulos, V., Peripheral-type benzodiazepine receptor (PBR) in human breast cancer: correlation of breast cancer cell aggressive phenotype with PBR expression, nuclear localization, and PBR-mediated cell proliferation and nuclear transport of cholesterol. *Cancer Res* **1999,** 59, (4), 831-42.

8. Broaddus, W. C.; Bennett, J. P., Jr., Peripheral-type benzodiazepine receptors in human glioblastomas: pharmacologic characterization and photoaffinity labeling of ligand recognition site. *Brain research* **1990,** 518, (1-2), 199-208.

9. Miyazawa, N.; Hamel, E.; Diksic, M., Assessment of the peripheral benzodiazepine receptors in human gliomas by two methods. *Journal of Neuro-oncology* **1998,** 38, (1), 19-26.

10. Brown, R. C.; Degenhardt, B.; Kotoula, M.; Papadopoulous, V., Location-dependent role of the human glioma cell peripheral-type benzodiazepine receptor in proliferation and steroid biosynthesis. *Cancer Letters* **2000,** 156, (2), 125-32.

11. Li, W.; Hardwick, M. J.; Rosenthal, D.; Culty, M.; Papadopoulos, V., Peripheral-type benzodiazepine receptor overexpression and knockdown in human breast cancer cells indicate its prominent role in tumor cell proliferation. *Biochem Pharmacol* **2007,** 73, (4), 491-503.

12. Papadopoulos, V.; Amri, H.; Li, H.; Yao, Z.; Brown, R. C.; Vidic, B.; Culty, M., Structure, function and regulation of the mitochondrial peripheral-type benzodiazepine receptor. *Therapie* **2001,** 56, (5), 549-56.

13. Papadopoulos, V.; Dharmarajan, A. M.; Li, H.; Culty, M.; Lemay, M.; Sridaran, R., Mitochondrial peripheral-type benzodiazepine receptor expression. Correlation with gonadotropin-releasing hormone (GnRH) agonist-induced apoptosis in the corpus luteum. *Biochem Pharmacol* **1999,** 58, (9), 1389-93.

14. Papadopoulos, V.; Baraldi, M.; Guilarte, T. R.; Knudsen, T. B.; Lacapere, J. J.; Lindemann, P.; Norenberg, M. D.; Nutt, D.; Weizman, A.; Zhang, M. R.; Gavish, M., Translocator protein (18kDa): new nomenclature for the peripheral-type benzodiazepine receptor based on its structure and molecular function. *Trends Pharmacol Sci* **2006,** 27, (8), 402-9.

15. Miettinen, H.; Kononen, J.; Haapasalo, H.; Helén, P.; Sallinen, P.; Harjuntausta, T.; Helin, H.; Alho, H., Expression of peripheral-type benzodiazepine receptor and diazepam binding inhibitor in human astrocytomas: relationship to cell proliferation. *Cancer Research* **1995,** 55, (12), 2691-2695.

16. Vlodavsky, E.; Soustiel, J. F., Immunohistochemical expression of peripheral benzodiazepine receptors in human astrocytomas and its correlation with grade of malignancy, proliferation, apoptosis and survival. *J Neurooncol* **2007,** 81, (1), 1-7.

17. Takada, A.; Mitsuka, S.; Diksic, M.; Yamamoto, Y. L., Autoradiographic study of peripheral benzodiazepine receptors in animal brain tumor models and human gliomas. *European Journal of Pharmacology* **1992,** 228, (2-3), 131-9.

18. Ferrarese, C.; Pierpaoli, C.; Linfante, I.; Bobo, R.; Guthrie, B.; Kufta, C.; Duhaney, M.; Melisi, J.; Fulham, M., Peripheral benzodiazepine receptors and glucose metabolism in human gliomas. *Journal of Neuro-oncology* **1994,** 22, (1), 15-22.

19. Black, K. L.; Ikezaki, K.; Toga, A. W., Imaging of brain tumors using peripheral benzodiazepine receptor ligands. *Journal of Neurosurgery* **1989,** 71, (1), 113-8.

20. Cornu, P.; Benavides, J.; Scatton, B.; Hauw, J.; Philippon, J., Increase in omega 3 (peripheral-type benzodiazepine) binding site densities in different types of human brain tumours. A quantitative autoradiography study. *Acta Neurochirurgica* **1992,** 119, (1-4), 146-52.

21. Veenman, L.; Levin, E.; Weisinger, G.; Leschiner, S.; Spanier, I.; Snyder, S. H.; Weizman, A.; Gavish, M., Peripheral-type benzodiazepine receptor density and in vitro tumorigenicity of glioma cell lines. *Biochem Pharmacol* **2004,** 68, (4), 689-98.

22. Galiegue, S.; Casellas, P.; Kramar, A.; Tinel, N.; Simony-Lafontaine, J., Immunohistochemical assessment of the peripheral benzodiazepine receptor in breast cancer and its relationship with survival. *Clinical Cancer Research* **2004**, 10, (6), 2058-64.

23. Hardwick, M.; Rone, J.; Han, Z.; Haddad, B.; Papadopoulos, V., Peripheral-type benzodiazepine receptor levels correlate with the ability of human breast cancer MDA-MB-231 cell line to grow in SCID mice. *International Journal of Cancer* **2001,** 94, (3), 322-7.

24. Rae, J. M.; Creighton, C. J.; Meck, J. M.; Haddad, B. R.; Johnson, M. D., MDA-MB-435 cells are derived from M14 melanoma cells--a loss for breast cancer, but a boon for melanoma research. *Breast Cancer Res Treat* **2007,** 104, (1), 13-9.

25. Camsonne, R.; Crouzel, C.; Comar, D.; Maziere, M.; Prenent, C.; Sastre, J.; Moulin, M.; Syrota,A, Synthesis of N-(^{11}C) methyl, N-(methyl-1 propyl), (chloro-2 phenyl)-1 isoquinoline carboxamide-3 (PK11195): A new ligand for peripheral benzodiazepine receptors. *Journal of Labelled Compounds and Radiophamaceuticals* **1984**, 21, (10), 985-91.

Chapter 3

Animal Studies Targeting PBR

Introduction

PET imaging provides a non-invasive tool for the characterization of tumors. PET tracer [^{18}F]FDG, 2-[18F]fluoro-2-deoxyglucose, measures the metabolism of the cell by glucose utilization, while [^{18}F]FLT, 3'-deoxy-3'-[18F]fluorothymidine, is an analog for thymidine and substrate for Thymidine Kinase 1, a biomarker for proliferation.[1] In recent years, several additional proteins have been identified as potential biomarkers for tumor characterization.

One of these is the Peripheral Benzodiazepine Receptor[2], which has been characterized as both a marker for proliferation and malignancy.[3-6] The ligand [^{11}C]PK11195, 4'-chlorodiazepam,7-chloro-1,3-dihydro-1-methyl-5-(p-chlorophenyl)-2H-1,4-benzodiazepin-2-one, (Figure 1A) has been utilized for PET imaging of neuroinflammation and gliomas.[4, 7-10] Other ligands have been developed as derivatives of PBR specific Ro5-4864 and PK11195. Several promising compounds have been synthesized, including DAA1106 analog [^{18}F]FEDAA1106 (Figure 1B). However, while PBR was found to be upregulated in brain and peripheral tumors, imaging has not addressed tumors located outside of the central nervous system.

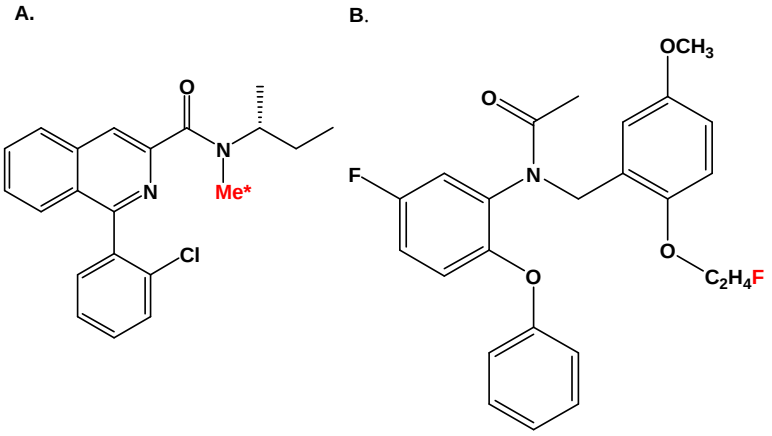

Figure 1: Chemical structures of [^{11}C]PK11195 (A) and [^{18}F]FEDAA1106 (B), specific ligands for PBR. Site of radiolabel is indicated.

The overexpression of PBR is not found in all types of cancer[11], but is nonetheless found in cancer of many tissue types. These include colon[12], breast[3, 6, 13], prostate[14], and liver[15]

carcinomas. The application of imaging would add valuable information by allowing the characterization of the whole, heterogeneous tumor rather that the small biopsy sample. In colon cancer, advanced stages had elevated PBR levels compared to lower grade tumors. Additionally, patients with low PBR expressing tumors had a much greater (80% versus 20%) chance of survival when followed approximately ten years after diagnosis.[16] Several investigations have demonstrated that breast tumor biopsies have higher expression of PBR over normal breast tissue.[3, 6, 11] Such examples demonstrate the potential value of PET imaging of PBR for better characterizing individual tumors.

Therefore, we conducted experiments designed to consider the protein PBR as a biomarker. In breast tumor-bearing animals, radiotracer uptake was measured by small animal imaging and *ex vivo* biodistribution studies. Tumor-implanted rodents were imaged in a three-day sequence for direct comparisons of radiotracer distribution and tumor localization. We ask the question: can PBR ligands differentially localize to tumor sites?

I. Preliminary Comparison of Radiopharmaceuticals *In Vivo*

Our first study exploring the potential for PBR as a PET biomarker was a straightforward examination of tumor-bearing mice.

A) Tumor-bearing mice. Nu/Nu female mice had breast cancer cells implanted in the mammary fat pad. Cell lines that were used included: MDA-MB-468 (a breast cancer cell line identified to express PBR[3]), MDA-MB-435 (a cell line that is now classified as a melanoma but was thought to be of breast tissue origin prior to genetic analysis)[17], and MDA-MB-231 (a breast cancer cell line that is considered to be a positive control for PBR).

B) Radiopharmaceuticals: [^{18}F]FDG, a glucose analog; [^{18}F]FLT, a fluorinated derivative of thymidine; [^{11}C]PK11195, an isoquinoline that was identified for its high affinity for the peripheral benzodiazepine receptor and widely accepted standard ligand for PBR.

a. Radiosynthesis of [^{18}F]FDG: [^{18}F]FDG was synthesized on the Coincidence FDG Synthesis Module in high specific activity.

b. Radiosynthesis of [^{18}F]FLT: 5'-O-(4,4'-dimethoxytrityl)-2,3'-anhydrothymidine (ABX, GmbH, Germany) is fluorinated by [^{18}F]fluoride produced by the ^{18}O(p,n)^{18}F reaction through proton irradiation of enriched ^{18}O water. Overall synthesis time is 110 minutes from the end of bombardment, and had radiochemical purity greater than 99% and specific activity exceeding 74 TBq/mmol (2,000 Ci/mmol).

c. Radiosynthesis of [^{11}C]PK11195: (R)-N-desmethyl PK11195 (ABX GmbH, Germany) is methylated by [^{11}C]CH_3I produced on the GE PETtrace MeI MicroLab in a method based on Camsonne et al. Substrate was dissolved in DMSO (250 μL) with 15% KOH (3 μL) added prior to [^{11}C]CH_3I delivery. After [^{11}C]CH_3I has been trapped, the reaction mixture is heated at 90°C (3 minutes). Reverse phase HPLC preparative separation is used with ACN/ ammonium formate buffer mobile phase. Product was reformulated in 10% ethanol in normal saline. Overall synthesis time is 60 minutes from the end of bombardment, and batch yields were 0.26 to 0.54 GBq (10-20 mCi) with radiochemical purity greater than 99% and specific activity exceeding 37 TBq/mmol (1,350 Ci/mmol).

C) Imaging and biodistribution studies. All animal experiments were conducted in compliance with the Guidelines for Care and Use of Research Animals established by Washington University's Animal Studies Committee. Tumor-bearing mice were monitored to observe tumor development. CT co-registration was performed (ImTek microCAT II, Knoxville, TN, USA) to obtain a full anatomical image. PET imaging studies were performed on a microPET

Focus scanner or on a microPET F120 (Concorde Microsystems, Knoxville, TN, USA). Radiopharmaceutical was given by tail vein injection and animals were imaged at one hour post-injection. For imaging, mice were anesthetized under oxygen with isofluorane.

In biodistribution studies, blood, tumor and organs of interest are collected after an animal has been killed by cervical dislocation while anesthetized. Each is individually counted in a γ counter and later weighed. Uptake is reported as % injected dose (% ID/organ) and % injected dose per gram tissue (% ID/g) for each sample by comparison to known samples.

Results:

Figure 2 shows two breast cancer tumor models which were analyzed with [^{18}F]FDG. Post-PET biodistribution data supports observations seen in the images, with greatest uptake in the heart. MDA-MB-435 tumors had approximately 3% ID/g localize to the tumor tissue, while MDA-MB-231 had slightly more radiopharmaceutical localization (3.7% ID/g).

In Figure 3, [^{18}F]FLT localization for a selected MDA-MB-231 tumor-bearing mouse is shown. As the images indicate, when compared to FDG, FLT is more equally distributed throughout the upper torso, and liver uptake has more than doubled. Tumor localization (3% ID/g) as determined by post-PET biodistribution experiments is similar to [^{18}F]FDG.

In Figure 4 [^{11}C]PK11195 localization is shown. Despite elevated uptake in the chest, tumors located in the mammary fat pad (under the front limbs) are still distinguished. Biodistribution *ex vivo* confirms radiopharmaceutical localization imaged *in vivo.*

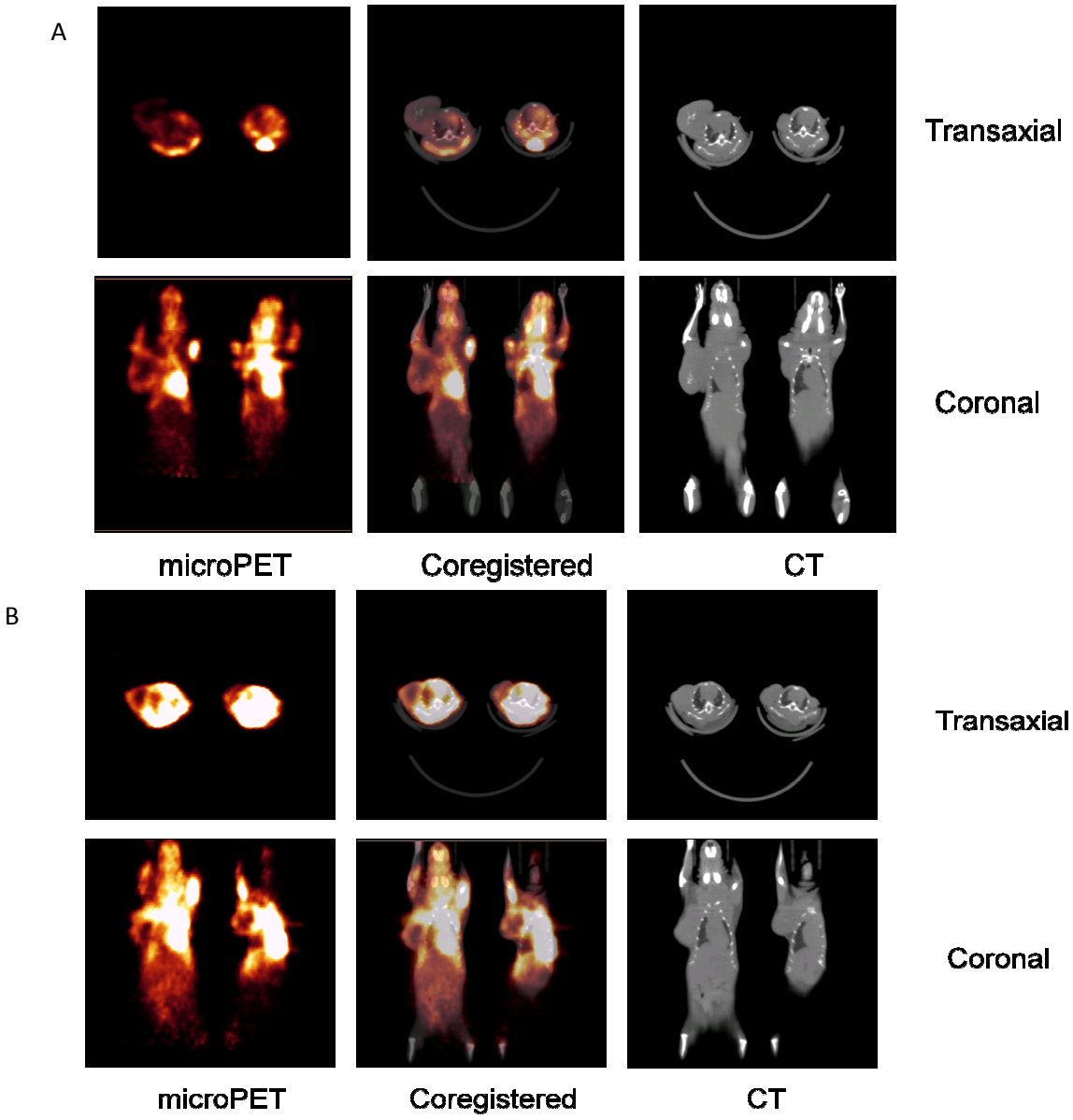

Figure 2: AMIRA Co-registered images from mice implanted in the mammary fat pad imaged with [^{18}F]FDG. In A, MDA-MB-231 and in B, MDA-MB-435 tumor-bearing mice show good radiotracer localization to the tumor, as well as high uptake in the heart.

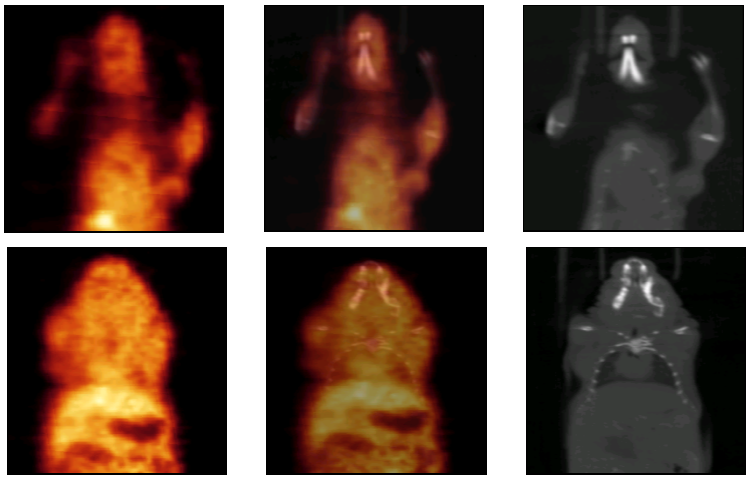

Figure 3: Co-registered images of a MDA-MB-231 tumor-bearing mouse with [^{18}F]FLT. Both right and left tumors, in the mammary fat pad, can be visualized. Liver uptake of FLT is greater than FDG.

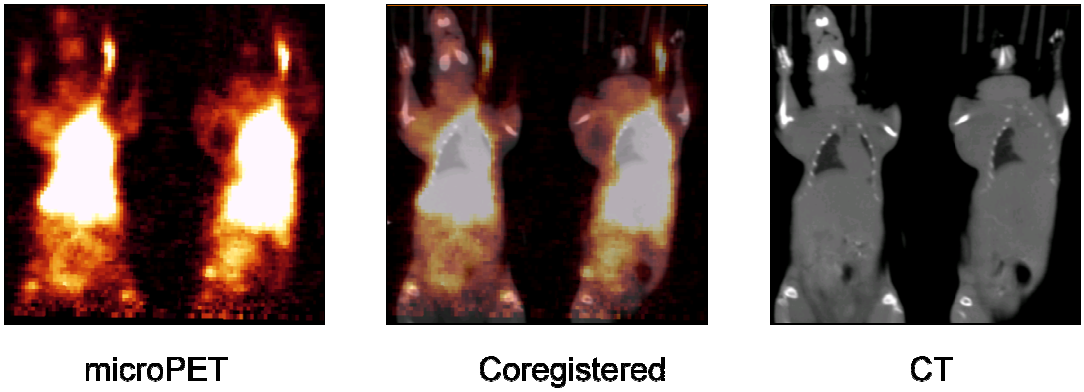

Figure 4: MDA-MB-435 tumor-bearing mice, implanted at the mammary fat pad, imaged with [^{11}C]PK11195 at 60 minutes post-injection. Both tumors display significant radioligand uptake, as do the lungs and heart.

Summary of Part I

Using small animal imaging followed immediately by *ex vivo* biodistribution, we compared the localization of biomarkers FDG and FLT to the PBR ligand PK11195, with favorable results. This provides preliminary evidence for the utility of PBR as an imaging target with PET.

However, these preliminary studies were unable to compare uptake of tracers within a single tumor. Therefore, a study using tumors as their own internal controls was done.

II. *In vivo* comparison of radiopharmaceutical uptake

Study Methods:

A) Tumor cell lines selected for implant. Based on the *in vitro* uptake data for [^{11}C]PK11195 shown in the last chapter, cell lines differential in expressed levels of PBR in the rank order of MCF-7 < MDA-MB-468 < MDA-MB-435. MDA-MB-231 clone MDA-BGL2 was used to provide a PBR positive control, as MDA-MB-231 is recognized as a high expressing cell line. When these cells were implanted in nude mice, all developed into tumors. However, the rate of tumor development for imaging varied among the cell lines.

B) Radiopharmaceuticals used. As in the previous studies, three tracers were compared: [^{18}F]FDG, [^{18}F]FLT, and [^{11}C]PK11195.

a. Radiosynthesis of [^{18}F]FDG: [^{18}F]FDG was synthesized on the Coincidence FDG Synthesis Module in high specific activity.

b. Radiosynthesis of [^{18}F]FLT: 5'-O-(4,4'-dimethoxytrityl)-2,3'-anhydrothymidine (ABX, GmbH, Germany) is fluorinated by [^{18}F]fluoride produced by the ^{18}O(p,n)^{18}F reaction through proton irradiation of enriched ^{18}O water. Overall synthesis time is 110 minutes from the end of bombardment, and had radiochemical purity greater than 99% and specific activity exceeding 74 TBq/mmol (2,000 Ci/mmol).

c. Radiosynthesis of [^{11}C]PK11195: (R)-N-desmethyl PK11195 (ABX GmbH, Germany) is methylated by [^{11}C]CH_3I produced on the GE PETtrace MeI MicroLab in a method based on Camsonne et al. Substrate was dissolved in DMSO (250 μL) with 15% KOH (3 μL) added prior to [^{11}C]CH_3I delivery. After [^{11}C]CH_3I has been trapped, the reaction mixture is heated at 90°C (3

minutes). Reverse phase HPLC preparative separation is used with ACN/ ammonium formate buffer mobile phase. Product was reformulated in 10% ethanol in normal saline. Overall synthesis time is 60 minutes from the end of bombardment, and batch yields were 0.37 to 0.74 GBq (10-20 mCi) with radiochemical purity greater than 99% and specific activity exceeding 50 TBq/mmol (1,350 Ci/mmol).

C) Imaging and biodistribution studies. All animal experiments were conducted in compliance with the Guidelines for Care and Use of Research Animals established by Washington University's Animal Studies Committee. Ten Nu/Nu mice were implanted for each cell line with bilateral mammary fat pad injections. The mice were monitored to observe tumor development. Tumors were allowed to form until they reached a size ranging from 100 to 350 microliters. On the day of the study with FDG, CT was performed (ImTek microCAT II, Knoxville, TN, USA) to obtain a full anatomical image. PET imaging studies were performed on a microPET Focus scanner or on a microPET F120 (Concorde Microsystems, Knoxville, TN, USA). Radiopharmaceutical was given by tail vein injection or via catheter. For imaging mice were anesthetized under oxygen with isofluorane.

The animals were then imaged in a three day sequence with [^{18}F]FDG, [^{18}F]FLT and [^{11}C]PK11195. Day 1 was either [^{18}F]FDG or [^{18}F]FLT, and Day 2 was the other radiopharmaceutical. For both tracers, imaging was at one hour post injection. On the third day, [^{11}C]PK11195 was administered and imaged at twenty minutes post injection. If tumors grew at a rate allowing two imaging courses, half of the mice (those with the larger tumors) were killed for an immediate post-PET biodistribution study. For the second imaging course, all imaged mice were used in a post-PET biodistribution study.

In biodistribution studies, blood, tumor and organs of interest are sampled after an animal has been killed via cervical dislocation. Each is individually counted in a γ counter and later weighed. Uptake is reported as % injected dose (% ID) and % injected dose per gram tissue (% ID/g) for each sample by comparison to standard samples.

PET data were analyzed with ASIPro® PET data analysis software (Concorde) to draw regions of interest and measure radiopharmaceutical localization. Data is reported as standard uptake value (SUV). Where post-PET biodistribution studies were performed with [^{11}C]PK11195, data was compared to ASIPro results for correlation between *ex vivo* and *in vivo* measurements.

Results:

Table 1 summarizes the data obtained, and Figure 5 shows representative images. Several points can be made about the trends seen. First, the relative uptake of radiopharmaceuticals is approximately the same for [^{18}F]FDG and [^{18}F]FLT, while [^{11}C]PK11195 displays significantly lower tumor uptake (uptake is at or below 1% ID/cc in ASIPro analysis). Biodistribution data confirms that noninvasive *in vivo* measurements by ASIPro are as expected based on *ex vivo* data. FDG and FLT uptake *in vivo* as determined noninvasively by imaging is less than uptake measurements *ex vivo* due to the intrinsic limitations of the PET technique. However, the image data correlates well with the dissection data, and demonstrates significantly higher uptake for the metabolic/proliferation markers compared to PK11195. [^{11}C]PK11195 uptake does not indicate that tumor cells that express PBR would be detectable *in vivo* using [^{11}C]PK11195.

Table 1: Data summarizing the tumor localization of [^{18}F]FDG, [^{18}F]FLT, and [^{11}C]PK11195 in tumor-bearing mice.

Tumor Uptake	MCF-7	MCF-7 (2nd)	MDA-435	MDA-435 (2nd)	MDA-468	MDA-468 (2nd)	MDA-BGL2	MDA-231
FDG %ID/cc	3.62 ± 0.97	2.78 ± 0.96	3.51 ± 1.37	2.89 ± 1.07	3.15 ± 0.80	1.84 ± 0.70	3.63 ± 0.42	1.20 ± 0.65
FLT %ID/cc	3.88 ± 0.77	3.81 ± 0.51	2.99 ± 0.77	2.76 ± 0.58	4.38 ± 0.80	3.78 ± 0.98	2.50 ± 0.11	3.82 ± 1.26
PK %ID/cc	0.56 ± 0.23	0.52 ± 0.22	0.50 ± 0.19	0.41 ± 0.18	0.43 ± 0.30	1.19 ± 0.23	0.92 ± 0.18	0.71 ± 0.22
Biodistribution % ID/g	0.83 ± 0.20	1.39 ± 0.55	2.01 ± 0.84	ND	ND	ND	1.42 ± 0.28	ND
Biodistribution % ID	0.76 ± 0.62	1.05 ± 0.25	1.10 ± 0.72	ND	ND	ND	1.87 ± 0.27	ND

When the [^{18}F]FDG and [^{18}F]FLT data are considered, it is noted that when tumors that are imaged in a second tracer study, there is a uniform reduction of radiopharmaceutical uptake. This effect may be due to therapeutic of radiation exposure in the first study with CT and small animal PET, or due to reduction of metabolism and cellular processes in larger, established tumors compared to newly-formed tumors that are still in the process of establishing a microenvironment.

The pattern of uptake of [^{18}F]FDG and [^{18}F]FLT is also noteworthy considering that the MDA-MB-468 and MDA-MB-231 took a longer time to develop compared to the MCF-7 cells,

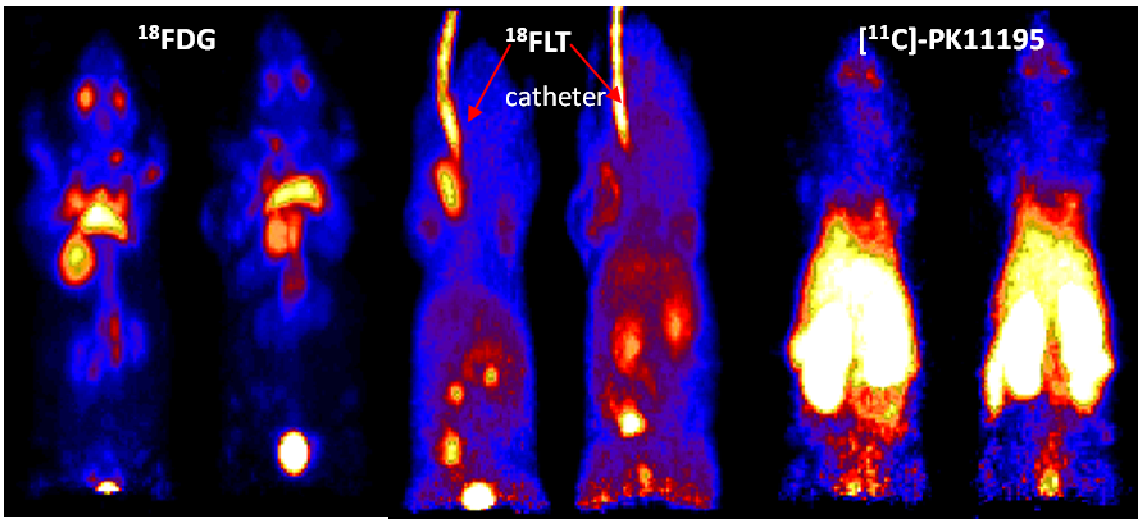

Figure 5: ASIPro images of the same MDA-MB-435 tumor bearing mice with [^{18}F]FDG, [^{18}F]FLT and [^{11}C]PK11195 imaged on three consecutive days. FLT and FDG localize to the site of the tumor significantly more than PK11195. Biodistribution data confirms that the tumor uptake of PK11195 is reduced when compared to FDG and FLT.

which rapidly established themselves after implant. Cells that are able to establish tumors quickly had more glucose metabolism, and [^{18}F]FDG uptake, the MDA-MB-468, which was slow to establish primary tumor, showed more TK1 activity and [^{11}C]PK11195 uptake.

Summary of Part II

The poor uptake of [^{11}C]PK11195 was disappointing and unexpected based on data collected in the preliminary studies. With these studies, the post-injection imaging time for PK11195 was shortened by necessity, due to half-life of carbon-11 and limited benefit to extending sessions beyond 60 minutes. Time-activity curves used to analyze whole body distribution, demonstrated that tumor-to-background ratios did not further improve after approximately twenty minutes.

III. **Validation of the Method**

Our tumor model was validated. Due to the fact that brain cancers, specifically gliomas and astrocytomas, have been characterized as overexpressing PBR, glial cell lines were reviewed to select a model. After consideration, the 9L line was selected. It is utilized in the lab of a collaborator and known to grow outside the CNS. With this tumor line, we used the previous studies as a template with the goal of validating the methodology.

For this study, mice were imaged on two sequential days with [^{18}F]FDG and [^{18}F]FLT, for two hours post injection, with the radiotracer not administered on the first day given on the second. On the third day, [^{11}C]PK11195 was produced and administered. Mice were imaged for up to one hour post injection.

In concurrent biodistribution studies, blood, tumor and organs of interest were collected after an animal has been killed. *Ex vivo* time-points for all three radiopharmaceuticals were at 5, 30, and 60 minutes post-injection. For [^{11}C]PK11195, a blocking dose of unlabeled PK11195 at 5 mg/kg was given at 30 minutes pre-injection to demonstrate specific, ligand-mediated uptake.

Results

Biodistribution data is presented in Table 2, and imaging data with 3 tumor-bearing mice is summarized in Figure 6. The ASIPro (Concorde) analyzed image data are presented as %ID/cc and SUV. For %ID/cc, regions of interest (ROIs) were drawn on axial slices to quantitate radiopharmaceutical localization. Data is generated as nCi/cc, and adjusted by correction for the total amount of activity injected. Standard uptake value, SUV, is used to normalize data to body size and provides a useful evaluation tool for uptake. An SUV of 1 would equal

homogenous distribution or no distinguishable uptake over background. Therefore, an SUV of less than one would indicate poor localization and greater than one would indicate that the tumor could be targeted. SUV is calculated by multiplying the %ID/cc by the mass of the subject.

Table 2a: Biodistribution data of tumor uptake in 9L xenograft (%ID/g) for [^{18}F]FDG, [^{18}F]FLT and [^{11}C]PK11195.

Radiopharmaceutical	5 minutes	30 minutes	30 minutes (+ block)	60 minutes
FDG %ID/g	4.01±0.74	2.39±0.39	NA	3.11±0.79
FLT %ID/g	6.64±0.89	9.09±0.68	NA	7.03±1.15
PK11195 %ID/g	1.52±0.52	2.70±1.84	2.97±0.78	3.50±0.92

Table 2b: Biodistribution data of tumor uptake in 9L xenografts (%ID/ tumor) for [^{18}F]FDG, [^{18}F]FLT and [^{11}C]PK11195.

Radiopharmaceutical	5 minutes	30 minutes	30 minutes block	60 minutes
FDG %ID/tumor	0.90±0.51	0.47±0.51	NA	0.64±0.12
FLT %ID/tumor	2.07±1.037	3.02±0.84	NA	2.49±1.34
PK11195 %ID/tumor	0.40±0.31	0.99±0.88	0.73±0.40	1.57±1.10

The FDG data from the *ex vivo* biodistribution analysis show rapid tumor localization and provide an example of metabolic variation within tumors. However, due to the location and growth of the tumors, the [^{18}F]FDG *in vivo* data is higher than tumor localization *ex vivo*. Tumors cells were implanted subcutaneously at the nape, the typical site for our imaging studies of this tumor line. Unfortunately for these studies, the tumors grew upward towards and onto the skull to varying degrees. The normal brain uptake of [^{18}F]FDG is high due to the tissue metabolism

and is the reason for the continued increase of radiopharmaceutical and the extent of localization for *in vivo* data. The proximity of the tumor to the brain resulted in significant spillover from adjacent tissue. This spillover effect is responsible for the lack of correlation between *in vivo* and *ex vivo* data because the *ex vivo* analysis allows for clear delineation of tumor versus brain.

A. [^{18}F]FDG

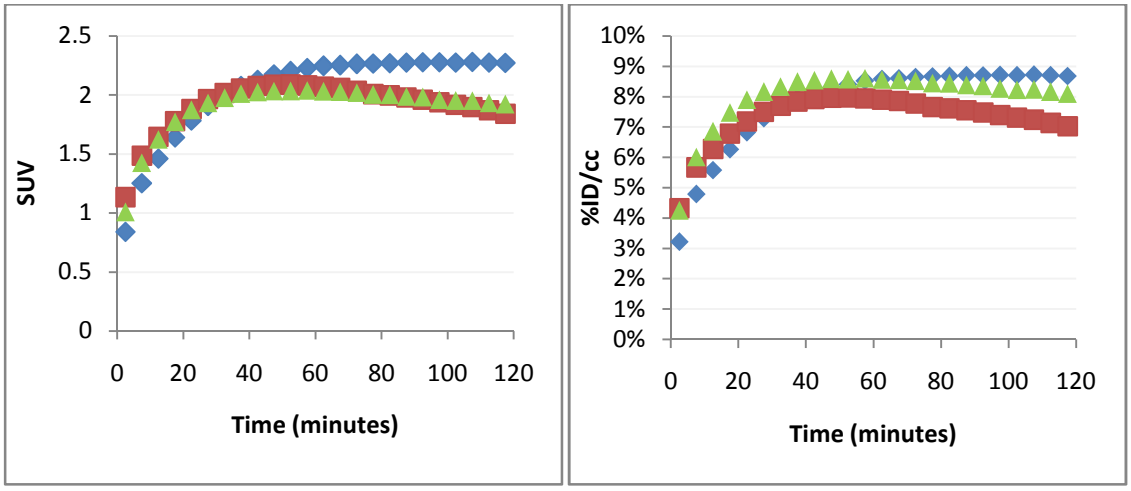

B. [^{18}F]FLT

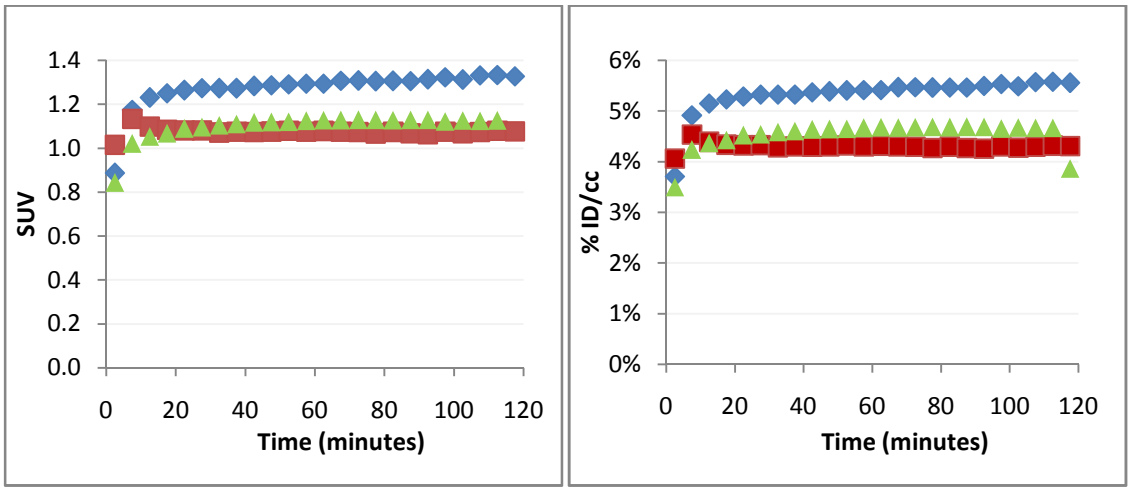

C. [^{11}C]PK11195

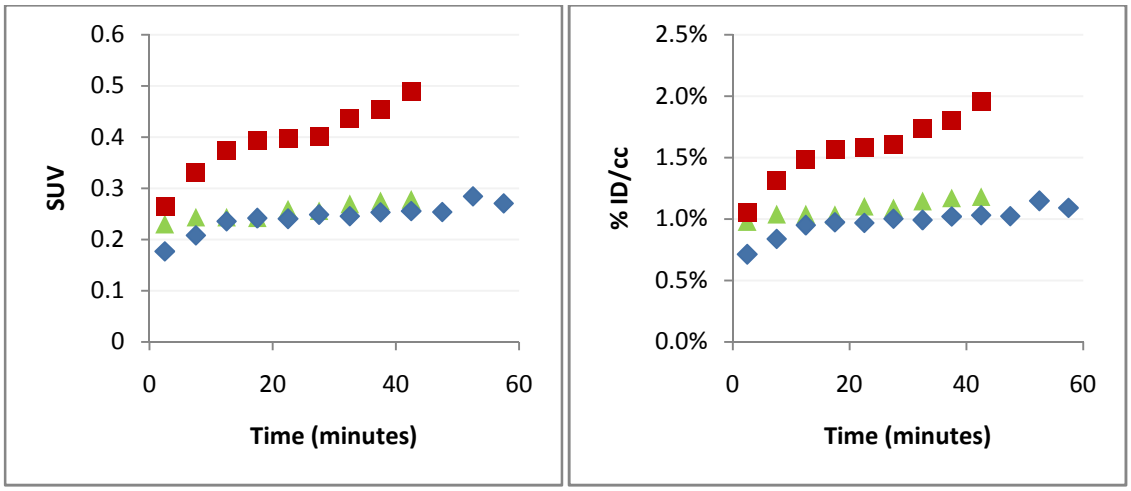

Figure 6: MicroPET time-activity curves for 3 mice with 9L tumors implanted at the nape and imaged with (A) [^{18}F]FDG, (B) [^{18}F]FLT, and (C) [^{11}C]PK11195. SUV (left) and %ID/cc (right) values are displayed. Regions of interest were drawn on the axial plane images in ASIPRO to quantify tumor localization of radioligand.

For [^{18}F]FLT, *ex vivo* data demonstrates good tumor localization with a peak at the 30 minutes (9.10±0.68 %ID/g), and slight washout at 60 minutes (7.03±1.15). The data from the images provides a similar trend, with uptake increasing to approximately twenty minutes (4.5% ID/cc), then stabilizing.

[^{11}C]PK11195 has a moderate increase in uptake at one hour compared to earlier points (3.50±1.10 at 60 minutes vs. 1.52±0.52, 5 minutes and 2.70±1.84, 30 minutes) and the greatest variation within each group *ex vivo*. The trend is seen in the *in vivo* data as each mouse has distinct uptake pattern. However, [^{11}C]PK11195 tumor localization was determined to be poor by SUV (less than 0.5).

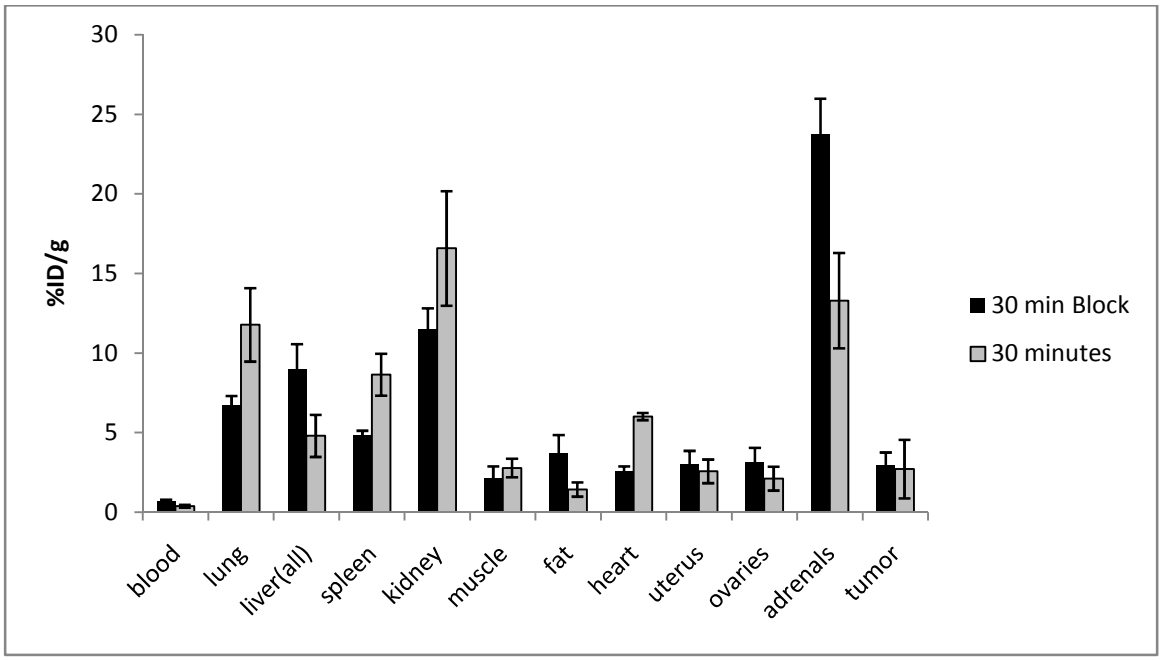

Figure 7: *Ex vivo* data comparing the distribution of [^{11}C]PK11195 at 30 minutes post-injection and 30 minutes post-injection with blocking dose. [^{11}C]PK11195 was co-injected with cold PK11195 at 5 mg/kg. Blocking is seen in organs that express PBR such as the lungs and heart. Tumor uptake in not altered by the blocking dose suggesting that uptake is non-specific.

In Figure 7, the *ex vivo* data for 30 minutes (grey bars) and 30 minutes with a blocking dose of 5 mg/kg (excess) PK11195 are shown. The 9L tumor uptake is not altered by the block administration; however, the adrenals (positive control organs for PBR) increase in tracer localization with the block. Tissues that are considered to have moderate expression, such as the lung, kidney and heart display reduced uptake, as do low expressing tissues. The adrenals are known to have a high density of receptors, determined to have B_{max} values as high as 20,000 fmol/mg protein in rat adrenal tissue.[18] Therefore, as radioligand is blocked from other organs, the adrenal can still bind additional ligand.

Summary of Part III

[^{11}C]PK11195 is not blocked in tumor tissues, nor is uptake of the ligand higher than other tissues. The time-activity curves do confirm that PK11195 imaging session can be limited

to one hour after injection without loss of meaningful data, and that data taken at 20 minutes post-injection is characteristic of the localization of [^{11}C]PK11195 in tumors. The time-activity curves for [^{18}F]FLT validate our conditions for these tracers as well. However, the site of implantation for tumor model selected presented a challenge for [^{18}F]FDG validation, and the *in vivo* tumor data cannot be separated from the adjacent brain activity.

IV. Comparison of PK11195 to FEDAA1106

Having demonstrated that our PET methodology for characterization of PBR expression is valid, the limitations of PK11195 are also evident. As it is the established ligand for PBR due to the lack of species variations in affinity characteristic of Ro5-4864 and was a prominent tool in the understanding of PBR, it was a reasonable choice for initial investigations. However the half-life of [^{11}C]PK11195 limits its utility in PET. Fortunately, many alternative PBR ligands have been developed based on SAR analyses of PK11195 and Ro5-4864. So there are available lead compounds, a diverse group of structures which have high affinity values and selectivity for binding to PBR.

Of these, [^{18}F]FEDAA1106 is a particularly promising radiopharmaceutical for targeting PBR. With the generous assistance of Dr. Robert Mach, Dr. Zhude Tu and Shihong Li, we compared [^{11}C]PK11195 to [^{18}F]FEDAA1106 in tumor-bearing mice.

Study Design

For the study, three cell lines were implanted in nude mice. The 9L glioma cell line was selected as well as two human breast cancer cell lines (MDA-MB-231 clones) due to their overexpression of PBR. In our experience, the MDA-MB-231 tumor line displays drastically different *in vivo* growth depending on the cell culture conditions. When the MDA-MB-231 cell

line available for purchase from ATCC (Manassas, VA) was cultured in CO_2-free incubators, transplanted tumors grew slowly in nude mice. When this cell line was maintained in a 5% CO_2 incubator, the transplanted cells developed more quickly into tumors. A second cell line clone was MDA-BGL2. This cell line was selected by techniques for metastatic potential and was used with the permission of Dr. Kathy Weilbaecher at Washington University.

(R)-N-desmethyl PK11195 (ABX GmbH, Germany) is methylated by $[^{11}C]CH_3I$ produced on the GE PETtrace MeI MicroLab in a method based on Camsonne et al. Substrate was dissolved in DMSO with 15% KOH added prior to $[^{11}C]CH_3I$ delivery. After $[^{11}C]CH_3I$ has been trapped, the reaction mixture is heated at 90°C (3 minutes). Reverse phase HPLC preparative separation is used with ACN/ ammonium formate buffer mobile phase. Product was reformulated in 10% ethanol in normal saline. Overall synthesis time is 60 minutes from the end of bombardment, and batch yields were 0.37 to 0.74 GBq (10-20 mCi) with radiochemical purity greater than 99% and specific activity exceeding 50 TBq/mmol (1,350 Ci/mmol).

N-(5-fluoro-2-phenoxyphenyl)-N-(2-tosylethyl-5-methoxybenzyl), synthesized by Shihong Li and Zhude Tu, is dissolved in DMSO and fluorinated by $[^{18}F]$fluoride produced by the $^{18}O(p,n)^{18}F$ reaction through proton irradiation of enriched ^{18}O water to produce N-(5-fluoro-2-phenoxyphenyl)-N-(2-$[^{18}F]$fluoroethyl-5-methoxybenzyl). Overall synthesis time is 60 minutes, and had radiochemical purity greater than 99% and specific activity exceeding 54 TBq/mmol (1,450 Ci/mmol).

Tumor-bearing mice were imaged on two sequential days, receiving one radiopharmaceutical each day. MDA-BGL2 tumor-bearing mice were imaged on the first day with $[^{11}C]$PK11195, and imaged on the next day with $[^{18}F]$FEDAA1106. For quantification of localization, biodistribution was performed. *Ex vivo* analysis compared the distribution of

radiopharmaceutical at 30 minutes to a blocking group also at 30 minutes. The 9L tumor-bearing mice were used for a blocking dose response study to look at the 30 minute time-point with [^{11}C]PK11195. For [^{18}F]FEDAA1106, the 9L tumor-bearing mice were used to observe the localization and washout of the radiotracer using 5, 30, and 60 minute time points.

Results

The studies were designed to address several aspects of PBR ligand localization. The first question asked was: could we see a dose response in [^{11}C]PK11195 uptake with increasing block? To answer that 9L tumor-bearing mice were given cold PK11195 at concentrations of 1, 5, and 10 mg/kg and groups were compared at 30 minutes post injection *ex vivo*. In Figure 8, the data shows that there is a reduction in localization to moderate PBR expressing organs such as lung and heart. Tumor uptake is not altered by any quantity of excess PK11195. Adrenals do not block, rather increased uptake of [^{11}C]PK11195 is seen.

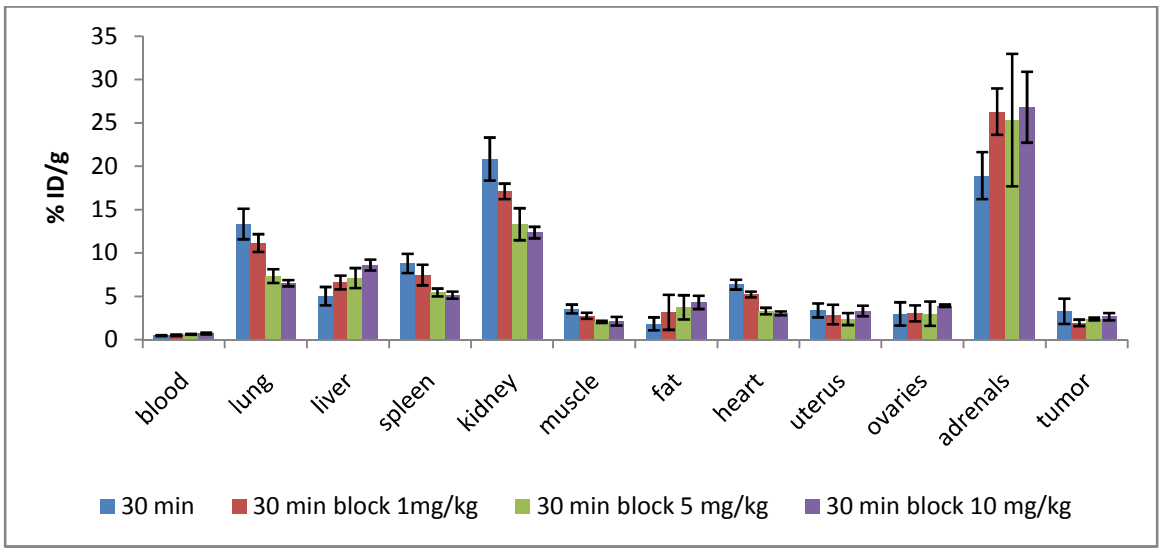

Figure 8: Dose Response Blocking study *ex vivo* with [^{11}C]PK11195. Block doses were administered 30 minutes prior to radiopharmaceutical, at doses of 1 mg/kg, 5 mg/kg and 10 mg/kg cold PK11195. 9L Tumor-bearing mice were killed 30 minutes post-injection. There is a dose response in PBR expressing organs, with reduction in lung, kidney and heart. The tumor uptake does not decrease with increasing unlabeled PK11195.

Our previous data indicate that [^{11}C]PK11195 will not be a useful ligand for peripheral tumor imaging. [^{18}F]FEDAA1106 distribution was also assessed *in vivo* and *ex vivo*. In Figures 9, 10 and 11, the distribution profile of [^{18}F]FEDAA1106 is shown. Figure 9 illustrates results of *ex vivo* analysis of MDA-MB-231 tumor-bearing mice at 30 minutes post-injection and compares [^{18}F]FEDAA1106 and [^{11}C]PK11195, including brain. Figure 10 shows ASIPro projection of the summed images for MDA-BGL2 tumor bearing mice administered [^{11}C]PK11195 and [^{18}F]FEDAA1106. In Figure 11, the distribution of [^{18}F]FEDAA1106 at 5,30 and 60 minutes is shown. The profile is distinct from that of [^{11}C]PK11195 (Figure 9). Lung uptake is higher for [^{18}F]FEDAA1106, washing out slowly, and heart has the second highest localization. Adrenal uptake is lower for [^{18}F]FEDAA1106 than for [^{11}C]PK11195. Kidney and spleen are also organs with substantial uptake.

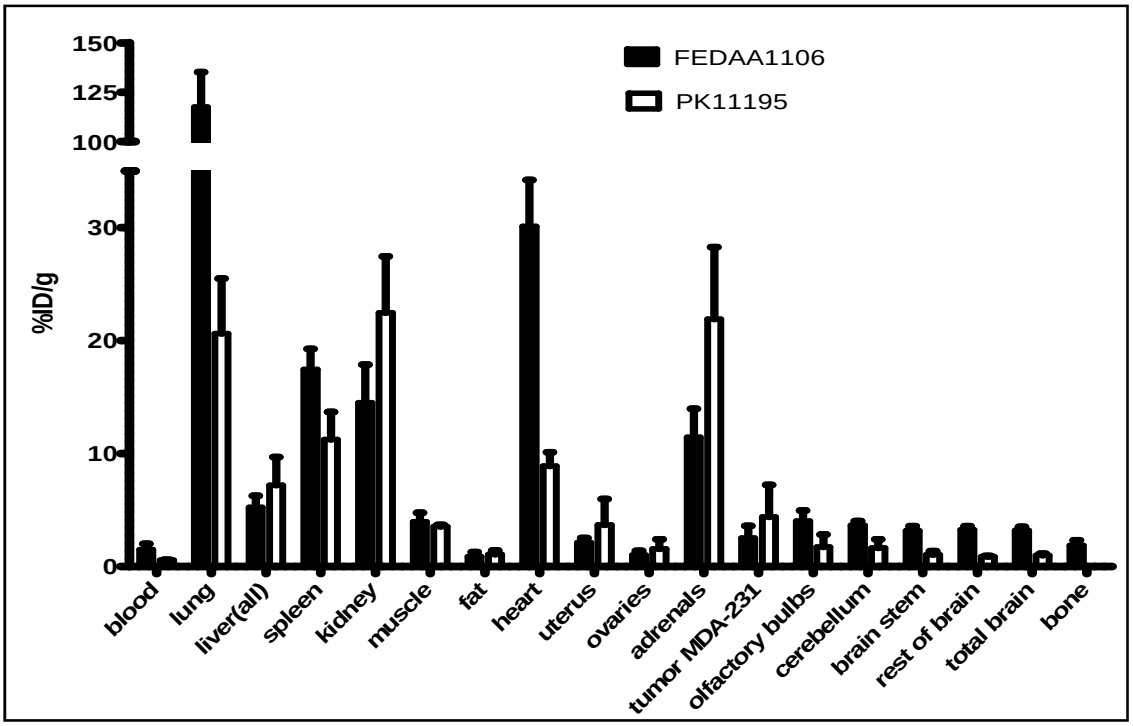

Figure 9: Direct comparison *ex vivo* PBR ligands distribution in MDA-MB-231 tumor-bearing mice at 30 minutes post injection. The two PBR ligands possess distinct localization patterns. FEDAA1106 predominantly localizes the lung, in greater quantities than PK11195. PK11195 has a more homogenous distribution. FEDAA1106 also crosses the blood-brain barrier more than PK11195, increasing approximately three-fold in uptake at 30 minutes post-injection.

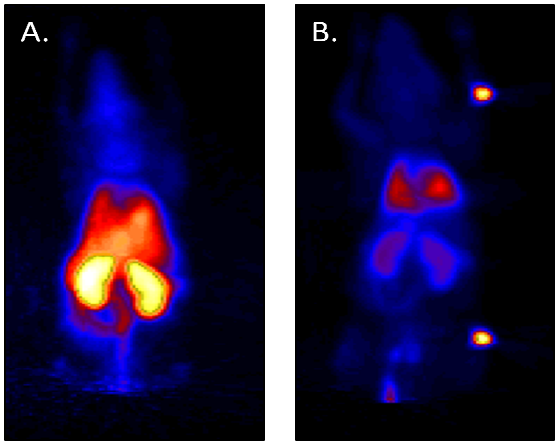

Figure 10: 9L tumor-bearing mice ASIPro summed projection images with (A) [^{11}C]PK11195 and [^{18}F]FEDAA1106. When PK11195 is administered there is homogenous distribution in the torso with increased localization in the kidneys. FEDAA1106 has a distinct distribution, with the greatest uptake in lung and kidney can be visualized in summed two hour scan shown above.

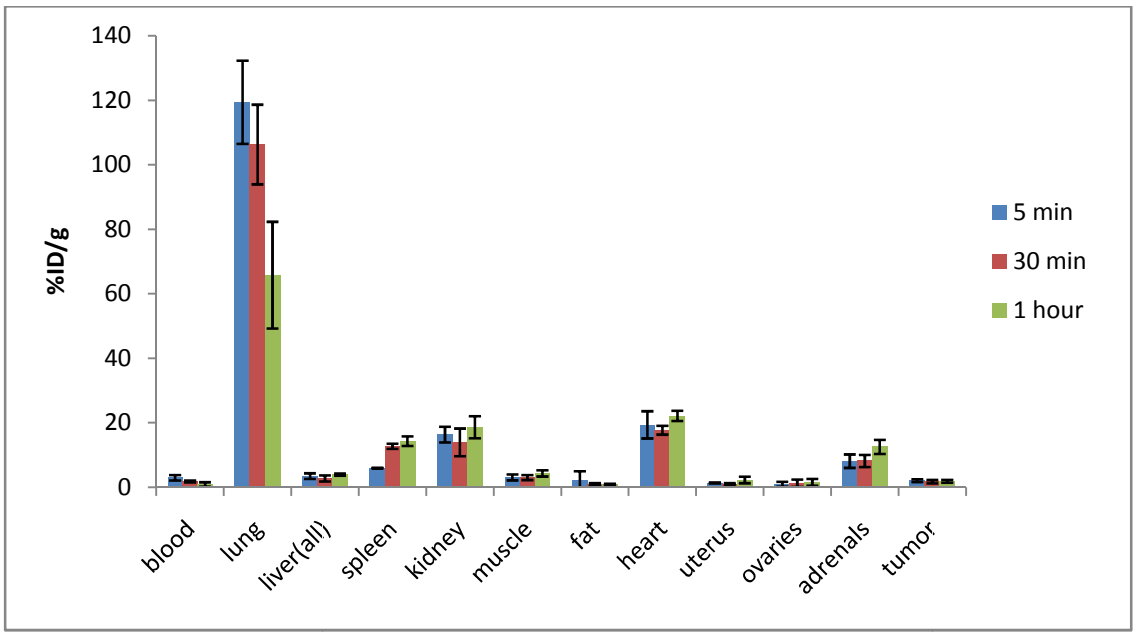

Figure 11: *Ex vivo* data comparing the distribution of [^{18}F]FEDAA1106 at 5,30, and 60 minutes post-injection in 9L tumor-bearing mice. Lung uptake predominates and slowly washes out, to approximately half of the initial uptake at 60 minutes. Adrenal, heart and kidney have similar localization at all time points.

A blocking study was performed using excess PK11195 at 5 mg/kg (Figure 12). One group was given a blocking dose of excess cold PK11195 (5 mg/kg) at 30 minutes prior to the injection of the radiopharmaceutical [^{18}F]FEDAA1106. Mice were killed 30 minutes after the radioactivity was given for *ex* vivo analysis. A large reduction of lung localization by [^{18}F]FEDAA1106 occurred when the animals were given cold PK11195. Heart uptake was slightly reduced, and adrenal had an increase in radiotracer.

These observations led us to perform a second dose-response study in non-tumor bearing mice. In this study cold, excess FEDAA1106 was co-administered with [^{18}F]FEDAA1106 at 100 µg/kg, 1 mg/kg, and 10 mg/kg. Data from this study is shown in Figure 13, plotting tissue versus %ID/g, and Figure 14, plotting %ID/organ versus tissue. We see a dose-dependent decrease in lung uptake, with a >50% reduction with 1 mg/kg and >80% reduction with 10 mg/kg. The heart does not decrease with doses of 100 µg or 1 mg/kg, indicating that lung uptake during oxygenation of blood was the limiting factor in heart uptake, which would be the next major organ for uptake.

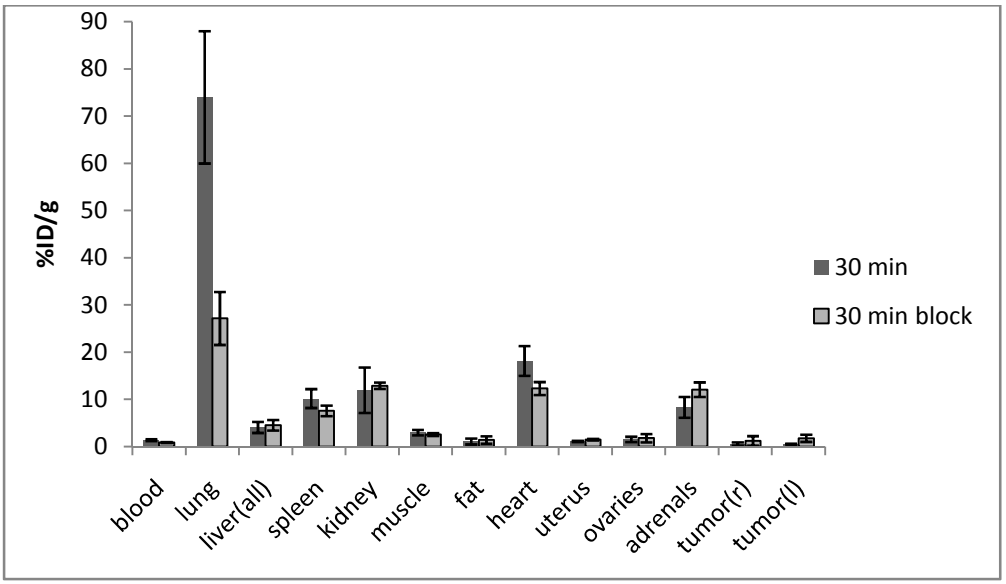

Figure 12: Blocking study with PK11195 to measure [^{18}F]FEDAA1106 localization 30 minutes post injection in MDA-BGL2 tumor bearing mice. The largest difference is seen in the lung with 60% block of [^{18}F]FEDAA1106 localization with a 5 mg/kg unlabeled PK11195 dose.

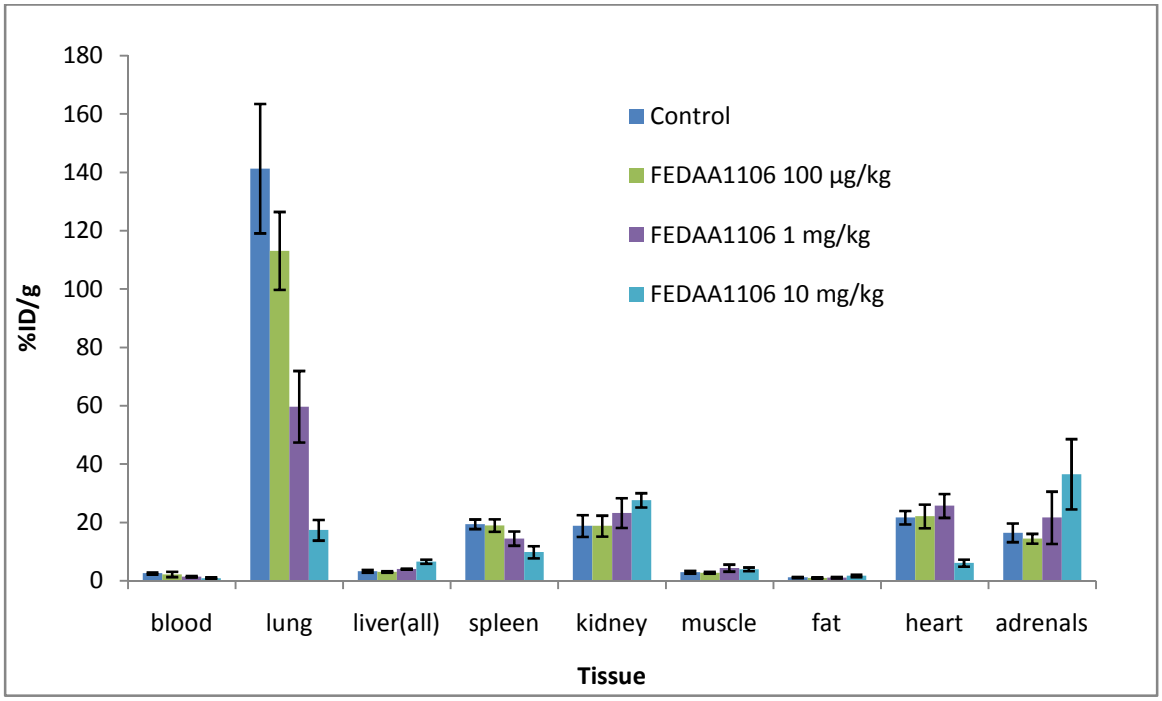

Figure 13: Blocking dose response curve (% ID/ g) for non-tumor bearing mice with [^{18}F]FEDAA1106 with coadministration of cold FEDAA1106. Mice were killed at 30 minutes post-injection. Lung decrease in [^{18}F]FEDAA1106 localization is dose-dependent. Blocking is also seen in heart at the unlabeled dose of 10 mg/kg.

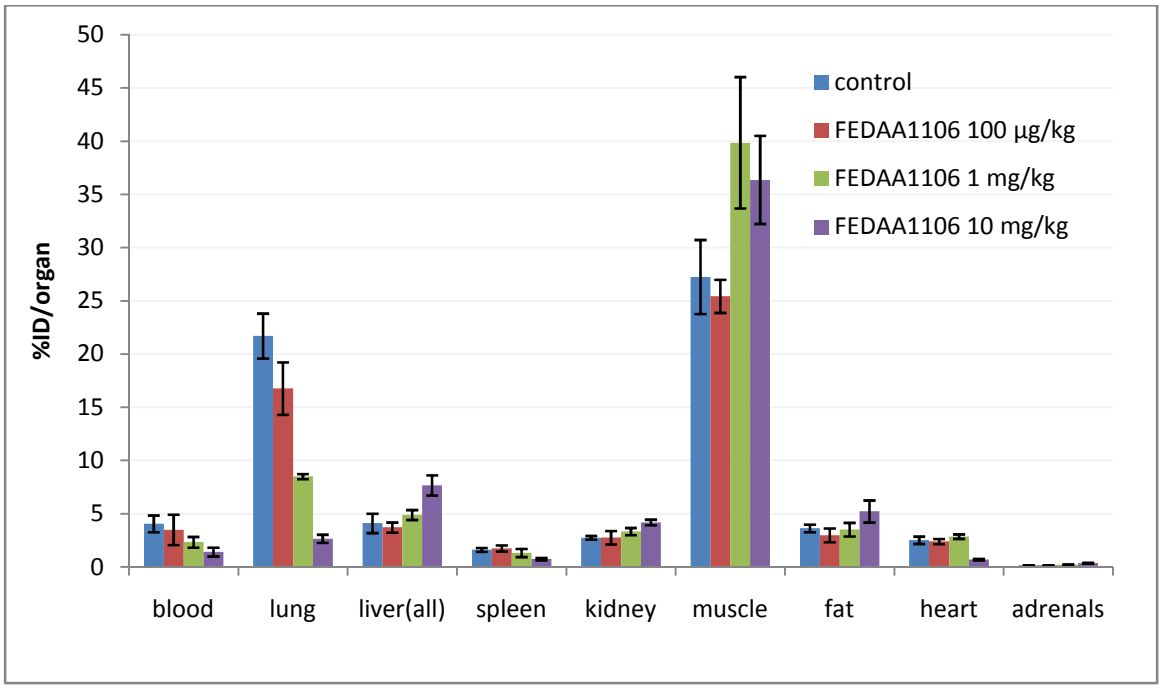

Figure 14: Blocking dose response curve (% ID/ organ) for non-tumor bearing mice with [^{18}F]FEDAA1106 co-injected with unlabeled FEDAA1106. Mice were killed at 30 minutes post-injection. Lung localization decreases by 23% with 0.1 mg/kg and 65% when 1 mg/kg is given. When 10 mg/kg is administered the specific localization is blocked and uptake has been significantly reduced (88% block).

The localization within lung was demonstrated to be receptor-specific by the capacity of cold PK11195 and FEDAA1106 to prevent uptake in a dose-specific fashion. To satisfy ourselves, the blocking data was analyzed to account for PBR binding sites. Using reported values for PBR expression in lung and protein levels in lung tissue, we estimate a total quantity of 47.3 picomoles of PBR in the mouse lung.[18,19] By injecting 100 µg/kg of FEDAA1106 we were administering 5.4 picomoles total dose of FEDAA1106 and a limited reduction of 23% was seen. With the 1 mg/kg dose of cold FEDAA1106 there was a total of 54 picomoles of receptor antagonist given, and this resulted in a further decrease in [^{18}F]FEDAA1106 localization to 8.50% ID/organ. A 10 mg/kg (540 picomoles) injection of FEDAA1106 reduced the radiopharmaceutical localization by 88% (2.66%). This low level of [^{18}F]FEDAA1106 uptake which can be attributed to non-specific binding by lipophilic FEDAA1106 (logP=3.7).[20]

Figure 14 illustrates two significant findings. The first is that *in vivo* localization of [^{18}F]FEDAA1106 predominates in the lungs, an organ rich in PBR. The second important finding is that the *in vivo* localization to the lung bed can be prevented by administering excess FEDAA1106 in a dose dependent manner. When sufficient FEDAA1106 is given to fully occupy the number of PBR receptor sites in the lungs, localization of the radioligand is negligible. Taken together, these results indicate that [^{18}F]FEDAA1106 localization to the lung is receptor-specific. This conclusion has major implications in the use of radiolabeled PBR ligands as radiopharmaceuticals in tumor imaging.

Summary of Part IV

Comparing the distribution of [^{11}C]PK11195 to [^{18}F]FEDAA1106, we observe a distribution in which with the lungs retain a large amount of the injected radiopharmaceutical. Because the lungs are the first major PBR containing organ intraveneously administered radiolabeled PBR ligands encounter, the lungs act as a reservoir that prevents distribution of radiopharmaceutical to tissues downstream. The data from the dose-response study with excess FEDAA1106 proves that the utility of PBR as a target for PET imaging is limited. Ligands with improved affinity will not provide peripheral tumor localization due to expression of PBR in lung beds.

Chapter summary

PET provides a method to non-invasively analyze tumors for characteristics such as metabolism and proliferation. Its strength lies in the potential for longitudinal imaging of tumors such as initial and follow-up scans to assess changes in tumor properties. It also allows for multiple tracers to be used as biomarkers to tease out distinct tumor features. We wanted to compare tumor localization of [^{18}F]FDG, [^{18}F]FLT and [^{11}C]PK11195 in the same animals to

determine the viability of measuring glucose, proliferation by Thymidine Kinase 1, and proliferation by PBR, respectively.

In this chapter, the radioligand distributions *in vivo* and *ex vivo* were compared. We previously observed that breast cancer cell lines displayed differential levels of [^{11}C]PK11195 uptake in vitro and characterized cell lines. To build on these findings, tumors were implanted from these breast cancer cell lines and studied using [^{18}F]FDG, [^{18}F]FLT, and [^{11}C]PK11195. Imaging data was compared to *ex vivo* biodistribution measurements. In preliminary studies, we found similar tumor localization of FDG and FLT, and good tumor localization for PK11195.

These investigations confirmed some expectations and revealed disappointments in others. As expected, tumors that established quickly with implantation of cells showed a greater glucose utilization rate as measured with [^{18}F]FDG than cell lines that developed into solid tumors more slowly. Tumors that took longer to establish their microenvironment had increasing uptake of [^{18}F]FLT. Despite the observed *in vitro* differences between cell lines in PBR expression, the results of *in vivo* studies were disappointing, with similar low uptake in tumors regardless of level of PBR.

The results forced us to reevaluate the methods employed. Since PBR has been investigated in glioma models more extensively, we selected a glioma cell line that was utilized in the lab of a collaborator for a study to validate the technique. In the study comparing the 9L tumor line with [^{18}F]FDG, [^{18}F]FLT and [^{11}C]PK11195, we implanted cells in the nape of the neck, following the standard practice for imaging studies with 9L. This proved to be problematic for the [^{18}F]FDG data, as tumor grew towards the high background brain tissue. *In vivo* data therefore had large spillover activity that resulted in inconsistency between the *ex vivo* and *in vivo* imaging data. The *in vivo* and *ex vivo* data for [^{18}F]FLT was in agreement. SUV data indicates an above background uptake of [^{18}F]FLT in the tumors and they could be visualized.

[^{11}C]PK11195 data correlates, but the relative uptake compared to [^{18}F]FLT and [^{18}F]FDG was poor, as was the calculated SUV time activity curve. Additionally, excess cold PK11195 was not able to block tumor uptake of [^{11}C]PK11195. Other organs known to express PBR were blocked by the excess compound, such as lung and heart, indicating little specific uptake of the radiopharmaceutical in the tumor.

The studies performed, taken together, demonstrate poor tumor localization of the PBR ligand, [^{11}C]PK11195. This compound has been used extensively since its identification in 1983 as a specific ligand for PBR.[21,22] In the intervening years, as applications for PET imaging of PBR have developed, so have additional ligands that display improved affinity values. One is [^{18}F]FEDAA1106, and this compound was made by collaborators.

We designed studies to evaluate the distribution of [^{18}F]FEDAA1106 and compare the distribution profile to that of [^{11}C]PK11195. Our data found that the most uptake was seen in the lungs, and this uptake was significantly increased compared to PK11195. In a dose-response study with cold FEDAA1106, lung uptake decreased as the dose increased. Heart remains consistent at low blocking doses, blocked only at the maximum dose of unlabeled FEDAA1106 (10 mg/kg). Adrenal uptake is not affected at low doses and slightly increased at 10 mg/kg. Taken together, these observations suggest that increasing the affinity for PBR is not useful in targeting to tumors. Additionally, it suggests that the expression of the protein in the lungs results in a dramatic decrease in the bioavailability of the radioligand for tumor localization. Peripheral tumor visualization of PBR by PET imaging of PBR ligands thus holds little promise.

BIBLIOGRAPHY

1. Broet, P.; Romain, S.; Daver, A.; Ricolleau, G.; Quillien, V.; Rallet, A.; Asselain, B.; Martin, P. M.; Spyratos, F., Thymidine kinase as a proliferative marker: clinical relevance in 1,692 primary breast cancer patients. *J Clin Oncol* **2001,** 19, (11), 2778-87.

2. Braestrup, C.; Squires, R. F., Specific benzodiazepine receptors in rat brain characterized by high-affinity [3H]-diazepam binding. *Proceedings of the National Academy of Sciences of the United States of America* **1977,** 74, (9), 3805-9.

3. Hardwick, M.; Fertikh, D.; Culty, M.; Li, H.; Vidic, B.; Papadopoulos, V., Peripheral-type benzodiazepine receptor (PBR) in human breast cancer: correlation of breast cancer cell aggressive phenotype with PBR expression, nuclear localization, and PBR-mediated cell proliferation and nuclear transport of cholesterol. *Cancer Res* **1999,** 59, (4), 831-42.

4. Ferrarese, C.; Pierpaoli, C.; Linfante, I.; Bobo, R.; Guthrie, B.; Kufta, C.; Duhaney, M.; Melisi, J.; Fulham, M., Peripheral benzodiazepine receptors and glucose metabolism in human gliomas. *Journal of Neuro-oncology* **1994,** 22, (1), 15-22.

5. Vlodavsky, E.; Soustiel, J. F., Immunohistochemical expression of peripheral benzodiazepine receptors in human astrocytomas and its correlation with grade of malignancy, proliferation, apoptosis and survival. *J Neurooncol* **2007,** 81, (1), 1-7.

6. Galiegue, S.; Casellas, P.; Kramar, A.; Tinel, N.; Simony-Lafontaine, J., Immunohistochemical assessment of the peripheral benzodiazepine receptor in breast cancer and its relationship with survival. *Clin Cancer Res* **2004,** 10, (6), 2058-64.

7. Black, K. L.; Ikezaki, K.; Toga, A. W., Imaging of brain tumors using peripheral benzodiazepine receptor ligands. *Journal of Neurosurgery* **1989,** 71, (1), 113-8.

8. Miyazawa, N.; Hamel, E.; Diksic, M., Assessment of the peripheral benzodiazepine receptors in human gliomas by two methods. *Journal of Neuro-oncology* **1998,** 38, (1), 19-26.

9. Groom, G. N.; Junck, L.; Foster, N. L.; Frey, K. A.; Kuhl, D. E., PET of peripheral benzodiazepine binding sites in the microgliosis of Alzheimer's disease. *J Nucl Med* **1995,** 36, (12), 2207-10.

10. Vowinckel, E.; Reutens, D.; Becher, B.; Verge, G.; Evans, A.; Owens, T.; Antel, J. P., PK11195 binding to the peripheral benzodiazepine receptor as a marker of microglia activation in multiple sclerosis and experimental autoimmune encephalomyelitis. *J Neurosci Res* **1997,** 50, (2), 345-53.

11. Han, Z.; Slack, R.; Li, W.; Papadopoulos, V., Expression of peripheral benzodiazepine receptor (PBR) in human tumors: relationship to breast, colorectal, and prostate tumor progression. *Journal of Receptors and Signal Transduction* **2003,** 23, (2&3), 225-38.

12. Katz, Y.; Eitan, A.; Gavish, M., Increase in peripheral benzodiazepine binding sites in colonic adenocarcinoma. *Oncology* **1990,** 47, (2), 139-42.

13. Beinlich, A.; Strohmeier, R.; Kaufmann, M.; Kuhl, H., Specific binding of benzodiazepines to human breast cancer cell lines. *Life Sciences* **1999,** 65, (20), 2099-2108.

14. Batra, S.; Alenfall, J., Characterization of peripheral benzodiazepine receptors in rat prostatic adenocarcinoma. *Prostate* **1994,** 24, (5), 269-78.

15. Venturini, I.; Zeneroli, M. L.; Corsi, L.; Avallone, R.; Farina, F.; Alho, H.; Baraldi, C.; Ferrarese, C.; Pecora, N.; Frigo, M.; Ardizzone, G.; Arrigo, A.; Pellicci, R.; Baraldi, M., Up-regulation of peripheral benzodiazepine receptor system in hepatocellular carcinoma. *Life Sciences* **1998,** 63, (14), 1269-1280.

16. Maaser, K.; Grabowski, P.; Sutter, A. P.; Hoepfner, M.; Foss, H.-D.; Stein, H.; Berger, G.; Gavish, M.; Zeitz, M.; Scheruebl, H., Overexpression of the peripheral benzodiazepine receptor is a relevant prognostic factor in stage III colorectal cancer. *Clinical Cancer Research* **2002,** 8, (10), 3205-3209.

17. Rae, J. M.; Creighton, C. J.; Meck, J. M.; Haddad, B. R.; Johnson, M. D., MDA-MB-435 cells are derived from M14 melanoma cells--a loss for breast cancer, but a boon for melanoma research. *Breast Cancer Res Treat* **2007,** 104, (1), 13-9.

18. Mercer, K. A.; Weizman, R.; Gavish, M., Ontogenesis of peripheral benzodiazepine receptors: demonstration of selective up-regulation in rat testis as a function of maturation. *J Recept Res* **1992,** 12, (4), 413-25.

19. Upreti, GC; Ratcliff, RA; Riches, PC., Protein estimation in tissues containing high levels of lipid: modifications to Lowry's method of protein determination. *Analytical Biochemistry* **1988,** (168), 421-7.

20. Zhang MR, Maeda J, Furutsuka K, Yoshida Y, Ogawa M, Suhara T, Suzuki K., [^{18}F]FMDAA1106 and [^{18}F]FEDAA1106: two positron-emitter labeled ligands for peripheral benzodiazepine receptor (PBR). Bioorganic and Medicinal Chemistry Letters **2003**, (13), 201-4.

21. Le Fur, G; Guilloux, F; Rufat, P; Benavides, J; Uzan, A; Renault, C; Dubroeucq, MC; Guérémy, C. Peripheral benzodiazepine binding sites: effect of PK 11195, 1-(2-chlorophenyl)-N-methyl-(1-methylpropyl)-3 isoquinolinecarboxamide. I. In vitro studies. *Life Sciences* **1983,** 33, (16), 1837-47.

22. Le Fur, G; Guilloux, F; Rufat, P; Benavides, J; Uzan, A; Renault, C; Dubroeucq, MC; Guérémy, C. Peripheral benzodiazepine binding sites: effect of PK 11195, 1-(2-chlorophenyl)-N-methyl-(1-methylpropyl)-3 isoquinolinecarboxamide. Ii. In vivo studies. *Life Sciences* **1983**, 33, (16), 1849-56.

Chapter 4

Conclusions and Future Directions

Conclusions

This dissertation presents the results of studies undertaken to characterize peripheral benzodiazepine receptors (PBR) in breast cancer cell lines *in vitro* and *in vivo*. Literature suggests that the protein holds promise as a biomarker for a range of diseases including cancers and neuroinflammatory disorders, and as such has been a target for development of novel PET radiopharmaceuticals in the last decade. However, prior to our beginning this work, research had focused on the central nervous system, with studies of PBR expression in peripheral disease states limited to *in vitro* studies. The desired endpoint of this research was the application of imaging technology of PET for non-invasive measurement of PBR expression in peripheral tumors.

In Chapter 2, breast cancer cell lines were characterized. PBR expression was the first cellular property that was addressed. Our initial plan was to measure and quantify PBR with Western blot analysis. However, lack of detectable bands in loaded samples and significant non-specific background signals hampered the utility of this method. Indirect and direct ELISA were attempted next. For the indirect ELISA, the low absorbance values resulted in a limited capacity to measure protein levels below a concentration of 10 pmoles/mg total protein. A positive control cell line that is considered to be a high expressing cell line has a density estimated to be at this level. Therefore this method could quantify a range of PBR expression. In the direct or "sandwich" ELISA, the signal was detectable but did not vary across a standards curve. The issue was identified as cross-reactivity between the primary antibodies, and thus this method could not be applied. PBR measurements could be assessed using the uptake of [^{11}C]PK11195 in whole cell studies, and the data show that breast cancer cell lines have differing levels of PBR.

The second element of focus was the proliferation potential measured as population doubling time. To measure this value, cells were counted by hemocytometer at 24 hour intervals to create a growth curve and calculate PDT. Due to the low number of cells being counted during early log-phase growth, the accuracy of this method is less than at ideal cell numbers per 1 mm^2 on the hemocytometer. The MTS assay was selected for this purpose. It does have the disadvantage of a narrow range of quantitative use, but that overlapped log-phase growth in these studies so the method was applied. The cells were measured to have population doubling times that varied from 14 to 40 hours.

Cell aggression was also measured using the "wound-healing" assay and the soft agar assay. In the "wound-healing" assay, cell migration into the "wound tract" was measured. In the soft agar assay, the growth capacity of cells in an anchorage-independent environment is determined. The cell lines analyzed displayed varied capacities to migrate and establish colonies.

The data were compared to determine if there was a correlation between the expression of PBR and either proliferation or aggression *in vitro*. There was no correlation seen between PBR and proliferation. There was a positive correlation for PBR and aggression; both "wound-healing" and number of cell colonies increased when the cell line displayed higher levels of PBR. These data are consistent with literature and indicate that peripheral benzodiazepine receptor expression could provide a useful biomarker in tumor characterization *in vivo*.

In Chapter 3, the potential of PET for *in vivo* detection and characterization of breast cancer tumors was explored. In our initial studies, the tumor-bearing mice were imaged with [^{18}F]FDG, [^{18}F]FLT and [^{11}C]PK11195. Each animal was imaged with one of the radiopharmaceuticals and immediately killed for *ex vivo* biodistribution to quantify uptake of the

tracer in the xenograft. It was found in the *in* vivo images and the *ex* vivo data that each of the radiopharmaceuticals localized to the tumor.

For more detailed PET studies, the breast cancer cell lines were chosen to select differential PBR expression, based on our *in vitro* data from Chapter 2. The goal of this selection was to determine whether we could observe image contrast with [^{11}C]PK11195, as well as any correlation with [^{18}F]FDG or [^{18}F]FLT localization to the tumor. Unfortunately, [^{11}C]PK11195 displayed poor tumor uptake, regardless of the *in vitro* expression of PBR. It was observed that there was the expected trend of elevated uptake of [^{18}F]FDG in tumors which grew more rapidly, and that tumors with more established microenvironments have greater uptake of [^{18}F]FLT .

The lack of significant tumor uptake of [^{11}C]PK11195 called to question our methods. To address the issue, we applied our study parameters to a validated brain tumor model. We selected a glioma cell line (9L) which is used in the lab of a collaborator and matched their conditions when employing the cells. In 9L tumor-bearing mice, [^{18}F]FDG, [^{18}F]FLT , and [^{11}C]PK11195 were sequentially imaged. *Ex vivo* biodistribution was performed to quantify tracer distribution and compare to *in vivo* data by image analysis. The location of the xenograft at the nape resulted in confounding results for the [^{18}F]FDG data. Due to tumor growth onto the skull, and therefore proximity to high glucose consuming brain tissue, there was a large amount of spillover into the tumor ROI. This resulted in an image artifact that resulted in a PET overestimation of tumor [^{18}F]FDG uptake that exceeded *ex vivo* data. For [^{18}F]FLT and [^{11}C]PK11195, the uptake of tracer in brain was not a concern, and showed close agreement between the *in vivo* and *ex vivo* data.

These data on [^{11}C]PK11195 indicated that the radiopharmaceutical would not be useful for detection of PBR on peripheral tumors. However, novel ligands have been designed in

recent years with improved affinity for PBR, and we compared one of these, [^{18}F]FEDAA1106, against [^{11}C]PK11195 in studies with 9L and MDA-MB-231 (a PBR positive control breast cancer cell line). The biodistribution differed significantly for the two PBR-binding radioligands. [^{18}F]FEDAA1106 had predominant lung uptake that was demonstrated to be due to specific binding to PBR in studies with competitive binding with unlabeled PK11195 and in receptor saturation studies with increasing doses of unlabeled FEDAA1106. From this we conclude that PBR has limited potential as a PET biomarker of peripheral tumor sites. The high concentration of PBR in the lungs, limits the amount of intravenously-injected radioligand that reaches PBR sites in the periphery, including those targeted tumors.

Despite these disappointing results, these data are nonetheless exciting in that they suggest unexpected new opportunities for research and development of PBR ligands as PET radiopharmaceuticals. The very high localization of PBR-binding radioligands within the lung compartment makes them obvious candidates for evaluation as potential radiopharmaceuticals for PET study of pulmonary disease. PBR numbers are altered in interstitial lung disease, and PBR ligands have therapeutic effects in pulmonary inflammatory processes. Receptors in the lung may mediate the inhibition of various airway responses, such as smooth muscle contraction, microvascular leakage, brochospasm and cough. Because such responses are common in respiratory diseases like asthma, evaluation of pathological changes in PBR may identify targets for drug development. Optimization of PET methodologies that noninvasively measure PBR binding in vivo would thus be useful for not only for increased understanding of lung pathology, but also for longitudinal studies that evaluate drug and other therapeutic interventions to improve lung function.